OPERA

Definition of the future boundary conditions for the near-field model_2

OPERA-PU-TNO421_2

Radioactive substances and ionizing radiation are used in medicine, industry, agriculture, research, education and electricity production. This generates radioactive waste. In the Netherlands, this waste is collected, treated and stored by COVRA (Centrale Organisatie Voor Radioactief Afval). After interim storage for a period of at least 100 years radioactive waste is intended for disposal. There is a world-wide scientific and technical consensus that geological disposal represents the safest long-term option for radioactive waste.
Geological disposal is emplacement of radioactive waste in deep underground formations. The goal of geological disposal is long-term isolation of radioactive waste from our living environment in order to avoid exposure of future generations to ionising radiation from the waste. OPERA (OnderzoeksProgramma Eindberging Radioactief Afval) is the Dutch research programme on geological disposal of radioactive waste.
Within OPERA, researchers of different organisations in different areas of expertise will cooperate on the initial, conditional Safety Cases for the host rocks Boom Clay and Zechstein rock salt. As the radioactive waste disposal process in the Netherlands is at an early, conceptual phase and the previous research programme has ended more than a decade ago, in OPERA a first preliminary or initial safety case will be developed to structure the research necessary for the eventual development of a repository in the Netherlands. The safety case is conditional since only the long-term safety of a generic repository will be assessed. OPERA is financed by the Dutch Ministry of Economic Affairs and the public limited liability company Electriciteits-Produktiemaatschappij Zuid-Nederland (EPZ) and coordinated by COVRA. Further details on OPERA and its outcomes can be accessed at www.covra.nl.

This report concerns a study conducted in the framework of OPERA. The conclusions and viewpoints presented in the report are those of the author(s). COVRA may draw modified conclusions, based on additional literature sources and expert opinions. A .pdf version of this document can be downloaded from www.covra.nl

OPERA-PU-TNO421_2
Title: Definition of the future boundary conditions for the near-field model_2
Authors: Hanneke Verweij (TNO), Susanne Nelskamp (TNO), Johan Valstar (Deltares), Joan Govaerts (SCK-CEN)
Date of publication: April 2016
Keywords: future boundary conditions, Boom Clay, Rupel Clay

Summary

This report describes the execution and results of the second part of Task 4.2.1 of the OPERA research project. The research concerns the future hydraulic boundary conditions and properties of host rock for geological disposal of radioactive waste, around a generic repository in that host rock. The Boom Clay (also known as Rupel Clay Member) is studied as a potential host rock.
Three different 1D-3D modelling approaches are used in Task 4.2.1 to obtain information on the boundary conditions and properties. The modelling approaches include 1D-3D basin modelling, 2D and 3D groundwater flow modelling. Results include maps and cross-sections showing variation in time of temperature and hydraulic conditions of the Rupel Clay Member for different climatic conditions, including moderate climate, cold climate without ice cover (permafrost), cold climate with ice cover (glaciation) and warm climate. These regional modelling results were used to derive future changes in boundary conditions and properties for a generic repository in the Rupel Clay Member at a generic depth of 500 m for the studied climatic scenarios.

Samenvatting

Dit rapport beschrijft de uitvoering en resultaten van het tweede deel van Taak 4.2.1 van het OPERA onderzoeksprogramma. Taak 4.2.1 is gericht op het uitvoeren van onderzoek betreffende de randvoorwaarden en eigenschappen rond een potentiële opbergfaciliteit voor radioactief afval in een gastgesteente in de toekomst. De Boomse Klei (ook bekend als Rupel Klei) wordt hierbij onderzocht als potentieel gastgesteente.

In Taak 4.2.1 is gebruik gemaakt van 1D, 2D en 3D modelleringen van de ondergrond van Nederland, te weten 1D-3D bekkenmodellering en 2D en 3D grondwater modellering. Deze modelleringen hebben geresulteerd in kaarten en profielen betreffende de veranderingen in de tijd in temperatuur en grondwaterstromingscondities in de Rupel Klei en eigenschappen van de Rupel Klei voor de volgende klimaatscenario's: gematigd klimaat, koud klimaat zonder ijsbedekking (permafrost), koud klimaat met ijsbedekking (glaciaties) en warm klimaat. De regionale resultaten van de modelleringen zijn vervolgens gebruikt om toekomstige veranderingen in de randvoorwaarden en eigenschappen rond een potentiële opbergfaciliteit voor berging van radioactief afval in de Rupel Klei op een diepte van 500m, af te leiden voor de bestudeerde klimaatscenarios.

1. Introduction

1.1. Background

The five-year research programme for the geological disposal of radioactive waste – OPERA- started on 7 July 2011 with an open invitation for research proposals. In these proposals, research was proposed for the tasks described in the OPERA Research Plan (Verhoef and Schröder, 2011).

In OPERA a first preliminary or initial safety case will be developed to structure the research necessary for the eventual development of a repository in the Netherlands. The safety case is conditional since only the long term safety of a generic repository in Boom Clay at a generic depth of 500 m will be assessed (Verhoef and Schröder, 2011). Task 4.2.1 is part of the safety assessment component 'Description of the Disposal system'. It provides input to the 'Formulation and implementation of assessment models' step in the safety assessment.

1.2. Objectives

The research proposed for Task 4.2.1 is described in the Research Plan with the following title: *Definition of boundary conditions for near-field model*.

The main objective of this task is to provide top, lateral and bottom boundary conditions for the near-field area, the undisturbed part of the Boom Clay at present-day and in the future. Thermal and hydraulic boundary conditions for modelling transport processes through the Boom Clay and the overburden are basic conditions defining the OPERA Safety Case.

The proposed modelling and calculations build on findings of Tasks 4.1.1 (*Description of the present geological and geohydrological properties of the geosphere*) and 4.1.2 (*Future evolution of geological and geohydrological properties of the geosphere*) and will serve as direct input to Tasks 6.1.5 (*Non-diffusion related transport processes of solutes in Boom Clay*), 6.2.1 (*Modelling approach for hydraulic transport processes*) and 7.2.5 (*Parameterization of PA models*).

This report describes the execution and results of the research concerning the boundary conditions for the near field area, the undisturbed part of the Boom Clay in the future. The Boom Clay in the Netherlands is also known as Rupel Clay Member (Vandenberghe et al., 2014).

1.3. Realization

This report has been compiled by TNO, Deltares and SCK-CEN. TNO performed a literature study and 1D and 3D basin modelling simulations to investigate variations in thermal and hydraulic boundary conditions for the near field area in the Rupel Clay Member in response to changing climatic conditions. Deltares performed 3D gravity-induced groundwater flow simulations to investigate changing hydraulic conditions in the Rupel Clay Member in response to a selection of the normal evolution scenarios and altered evolution scenarios defined in Task 421. Building on their study of permafrost development carried out in Task 412, SCK-CEN focussed in this Task on modelling the mutual influence of permafrost development and groundwater flow.

1.4. Explanation contents

The research aimed to increase the understanding of possible future variations in thermal and hydraulic conditions for the near field area in the Rupel Clay Member at a generic depth of about 500 m. For this purpose different modelling approaches were applied to a selection of glacial and interglacial conditions that prevailed during the past 1 million years as analogues for future conditions.

The focus of chapter 2 is on the investigation by basin modelling of the impact of glacial-interglacial variation in surface temperature conditions on: 1) the magnitude of temperature fluctuations in the Rupel Clay Member, and 2) the depth variations of the °C isotherm as proxy for variations in depth of the permafrost front. Additional modelling scenarios that are presented in this chapter concern the impact on temperature conditions in the Rupel Clay Member of long-time constant surface temperatures and increasing surface temperatures due to global warming.

Chapter 3 concerns the application and results of gravity-induced ground water flow modelling to investigate the changes in hydraulic conditions in the Rupel Clay Member for a selection of normal evolution scenarios and altered evolution scenarios. The different scenarios and the associated hydraulic boundary conditions used for the groundwater flow modelling are described. The selected normal evolution scenarios include the following climatic conditions; moderate climate (present-day conditions); cold climate without ice cover (permafrost conditions); cold climate with ice cover (glaciation); warm climate. The selected altered scenarios are the deep well, glacial valley, and fault scenario. The groundwater flow modelling covers the entire area of onshore Netherlands.

Chapter 3 includes the description of modelling results concerning the influence of permafrost conditions on hydraulic heads above and below the Rupel Clay Member. Chapter 4 is focussed entirely on a detailed study of the mutual influence of groundwater flow and permafrost growth and degradation. The chapter includes detailed information on the physical background of processes involved and on the modelling set-up for the numerical modelling of coupled groundwater flow and permafrost. The modelling is executed along a W-E cross section through the central part of the Netherlands. Modelling results concern the evolution of permafrost for conductive and advective heat transfer conditions during the last 120 kyrs. In addition attention is paid to the evolution of flow velocities in layers overlying the Rupel Clay Member during this same time interval.

The last chapter describes a basin modelling study of the impact of vertical ice-sheet loading on the evolution of pressures and overpressures in the Rupel Clay Member.

2. Future thermal boundary conditions

2.1. Introduction

The results of literature and modelling studies concerning present-day temperature conditions of the Rupel Clay Member described in Verweij and Nelskamp (2015; Task 241-1) indicate that present-day temperatures in the Rupel at a depth of ca 500 m vary between 22 °C and 26 °C and are still in a transient state. The transient state results from previous surface temperature fluctuations and, especially in the southern part of the Netherlands, also from deeper reaching paleo groundwater flow conditions.

The time it takes for changes in temperature boundary conditions to propagate through the subsurface depends on its thermal diffusivity:

$K = (\lambda/\rho c)$

where,

K = *thermal diffusivity* (m^2s^{-1})
λ = *bulk thermal conductivity* ($Wm^{-1}K^{-1}$)
c = *bulk specific heat capacity of a medium, i.e. the amount of heat energy required to raise the temperature 1°K of 1kg of that medium*
ρc = *volumetric heat capacity* = $ø\rho_w c_w + (1- ø)\rho_r c_r$ ($Jm^{-3}K^{-1}$)
$ø$ = *porosity*
c_w = *specific heat capacity of water* ~ 4200 $Jkg^{-1}K^{-1}$
c_r = *specific heat capacity of rock* ~ 1000 $Jkg^{-1}K^{-1}$
ρ_w = *density of water* (kgm^{-3})
ρ_r = *density of rock matrix* (kgm^{-3})

For a sedimentary basin fill of porosity ($ø$=10%), *bulk thermal conductivity* (λ = 2.5 $Wm^{-1}K^{-1}$), *density of the rock matrix* (ρ_r = 2300 kgm^{-3}), *density of pore water* (ρ_w = 1000 kgm^{-3}), *the volumetric heat capacity* = ρc = 0.1 $\rho_w c_w$ + 0.9 $\rho_r c_r$ = 2.5*106 $Jm^{-3}K^{-1}$, *and the thermal diffusivity* = 10^{-6} m^2s^{-1} ~ 32 km^2My^{-1}.

Ter Voorde et al. (2014) investigated the effect of the three major climatic (Milankovitch) cycles, with periods of 23, 42 and 100 kyr on subsurface temperatures using analytical and numerical solutions for cyclic temperature variations. The calculations clearly showed that the magnitude, duration and penetration depth of the effect of changes in surface temperature depend on its amplitude and especially the wavelength of the temperature variations (Figures 2.1 and 2.2).

Recent studies in offshore and onshore Netherlands showed that glacial-interglacial temperature fluctuations affect subsurface temperatures with magnitudes that decrease with depth (Verweij et al., 2013; Ter Voorde et al., 2014, respectively).

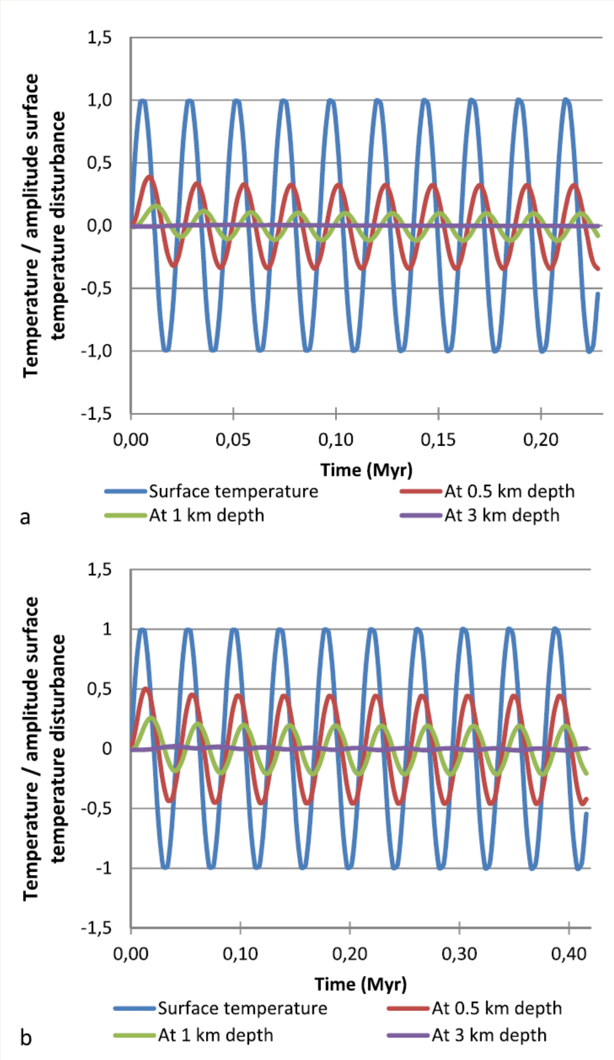

Figure 2.1: The relative response to cyclic surface temperature fluctuations for assumed thermal diffusivity of 10-6 m2s-1 (a) with a period of 23 kyr and (b) with a period of 42 kyr. The amplitudes of the cycles are scaled to 1 (From Ter Voorde et al., 2014).

Ter Voorde et al. (2014) used a numerical model to study the effect of the surface temperature history of the past 130000 years on present-day subsurface temperatures in Onshore Netherlands assuming conductive heat flow conditions. The modelling indicated that this paleo temperature history resulted in a decreased geothermal gradient in the upper kilometer of the Dutch subsurface, and a slightly increased gradient at depths between 1 and 3 km.

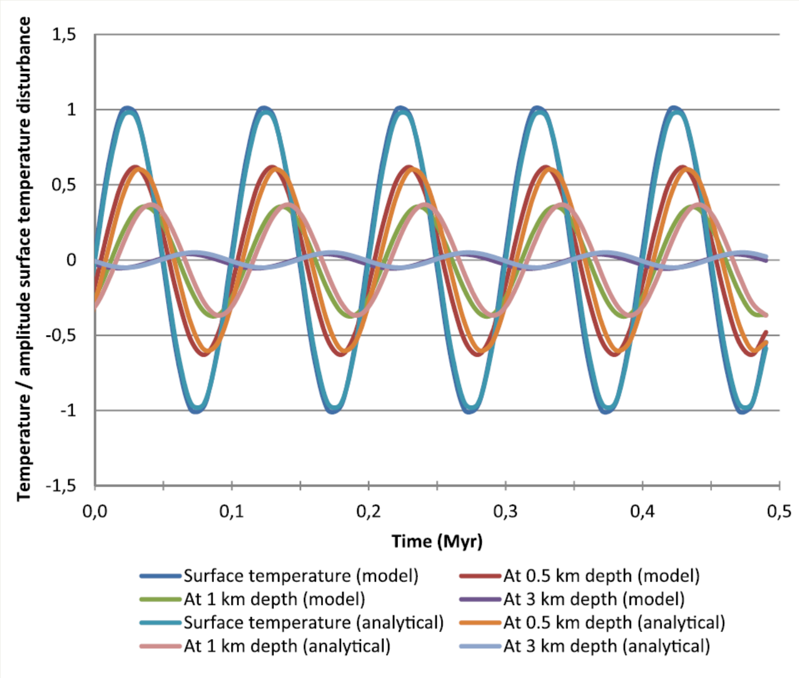

Figure 2.2: The relative response to cyclic surface temperature variations for a thermal diffusivity of 10-6 m2s-1 with a period of 100 kyr and an amplitude scaled to 1; calculated both analytically and numerically (From Ter Voorde et al., 2014).

In order to study the effect of surface temperature fluctuations on the thermal conditions of the Rupel Clay Member over a period of 1 Myrs, we used detailed 1D basin modelling with surface temperature fluctuations of the past 1 Myrs as an analogue for future surface temperature conditions.

2.2. Basin modelling: input data and boundary conditions

The basin modelling software PetroMod (v.2014.1 of Schlumberger) was used to simulate the 1D burial and temperature history at the 17 locations in onshore Netherlands (Figure 2.3). These locations coincide with those used by Govaerts et al., 2015 in their simulations of permafrost depth in the Netherlands. Information on the general background of basin modelling is given by Verweij and Nelskamp (2015) in the report of Task 421_1.

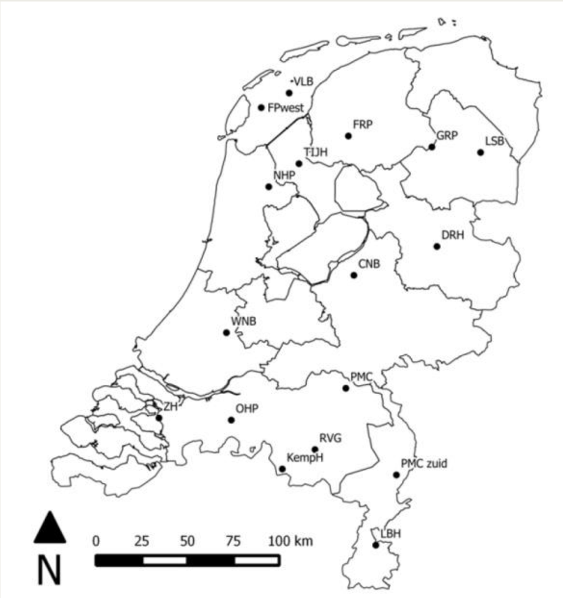

Figure 2.3: map showing locations of 1D basin modelling (from Govaerts et al., 2015).

The geological input consists of 1D extractions at locations shown in Figure 2.3 from the static Digital Geological Model (DGMv2; www.dinoloket.nl/ondergrondmodellen); this model input has been extended to greater depth and older stratigraphic units (until Triassic) with 1D extractions from the deep geological model (DGM deep v4). The geological input also includes new depth and thickness information of the Rupel Clay Member published by Vis and Verweij (2014).

The lithological composition of the stratigraphic units was taken from the 3D basin model of the northern part of the Netherlands (Nelskamp et al., 2015). The 1D basin modelling was executed by using newly derived porosity-depth relations for sand and clay derived by using a combination of porosity data from shallow depths (3800 porosity data; depths 0-30 m from DINO database), the Rupel Clay Member (Vis and Verweij, 2014) and porosity data from oil and gas boreholes (Nelskamp et al., 2015; Verweij et al., 2015).

The boundary conditions include water depth, basal heat flow and surface temperature history. The paleo water depth was taken from the 3 existing 3D basin models. The basal heat flow boundary condition was extracted from these 3D basin models at the depth of the Triassic. The surface temperature boundary condition before 1 Ma are also similar to the ones used in the 3D basin models. Three new scenarios for detailed surface temperature boundary conditions during the last 1 Myrs were implemented in the basin modelling:

- Scenario I: Average temperature variations based on temperature reconstructions published by Bintanja and Van de Wal (2008) (Figure 2.4);
- Scenario II: Detailed temperature variations based on temperature reconstructions published by Bintanja and Van de Wal (2008) (Figure 2.4);
- Scenario III: Scenario 1 of average temperature variations with the last 120 kyrs replaced by three temperature scenarios derived from the ones used in permafrost study of Govaerts et al. (2015) (Figure 2.5).

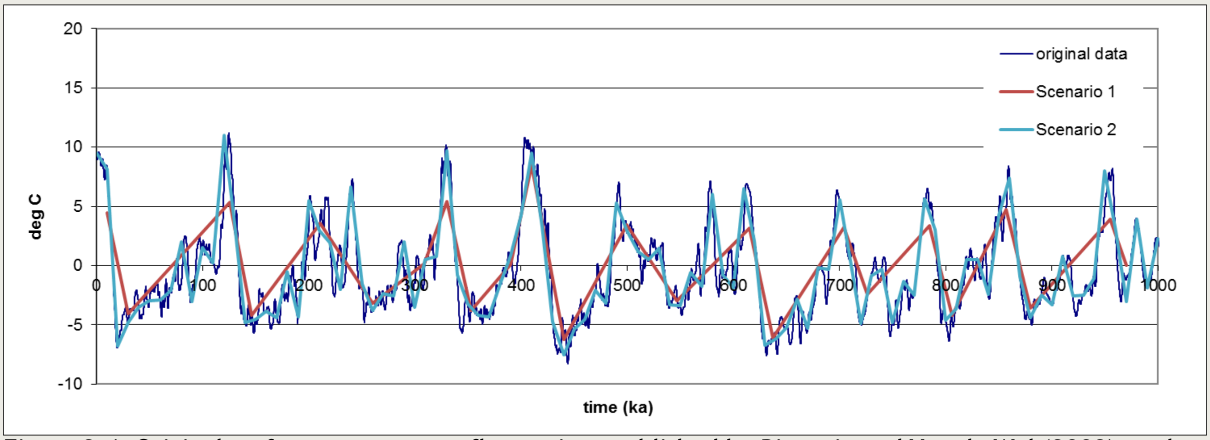

Figure 2.4: Original surface temperature fluctuations published by Bintanja and Van de Wal (2008), and the simplified temperature curves representing the temperature boundary conditions of scenarios I and II.

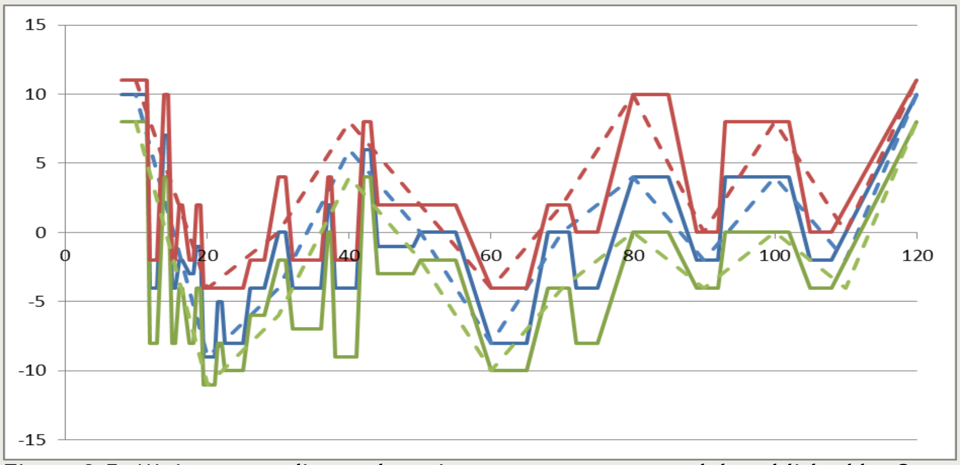
Figure 2.5: Minimum, median and maximum temperature models published by Govaerts et al. (2015) (solid lines) and the temperature boundary conditions used in scenario III (dashed lines).

2.3. Burial history of the Rupel Clay Member

Figure 2.6 shows the change in burial depth of the Rupel Clay Member from 1.5 Ma to present-day at the 17 locations shown in Figure 2.3. The change in burial depth varies laterally: both increases in burial depth (e.g at RVG, TYH, NHP, FRP, FPwest) and decreases of burial depth occur. The decrease in burial depth is most clear for the Rupel Clay Member in southeastern most part of the Netherlands at LBH. The changes in burial depth are less than 100m.

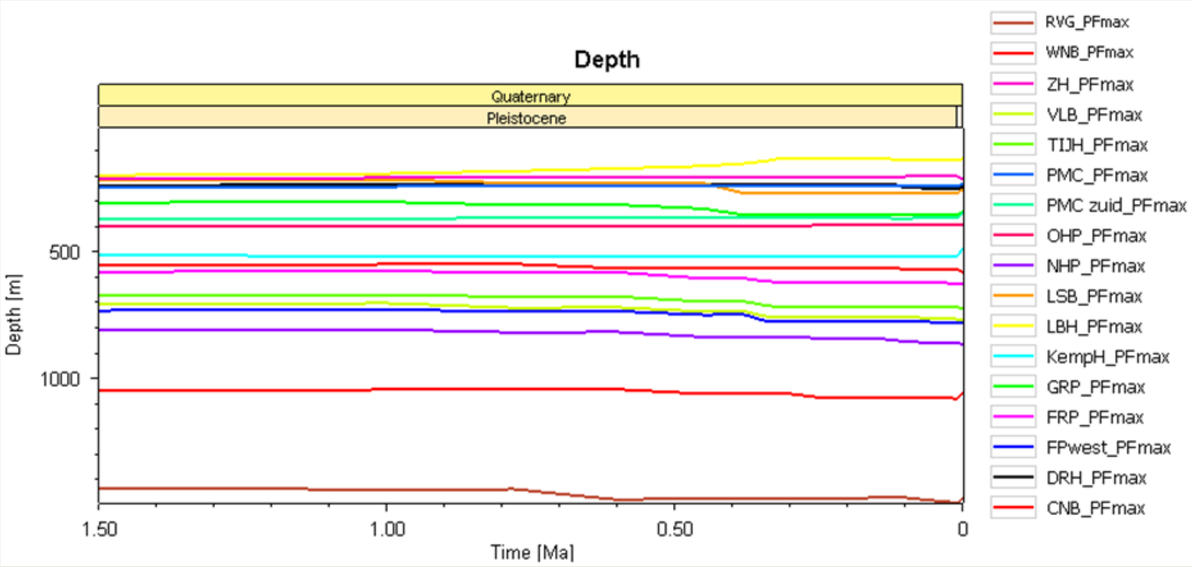

Figure 2.6: Burial history of the Rupel Clay Member from 1.5 Ma to present day at 17 locations shown in Figure 2.3.

2.4. Basin modelling of impact surface temperature variations on temperature evolution in Rupel Clay Member

The 1D basin modelling of the location in the West Netherlands Basin has been selected to show the main relevant results of running the different temperature boundary scenarios Figure 2.7).

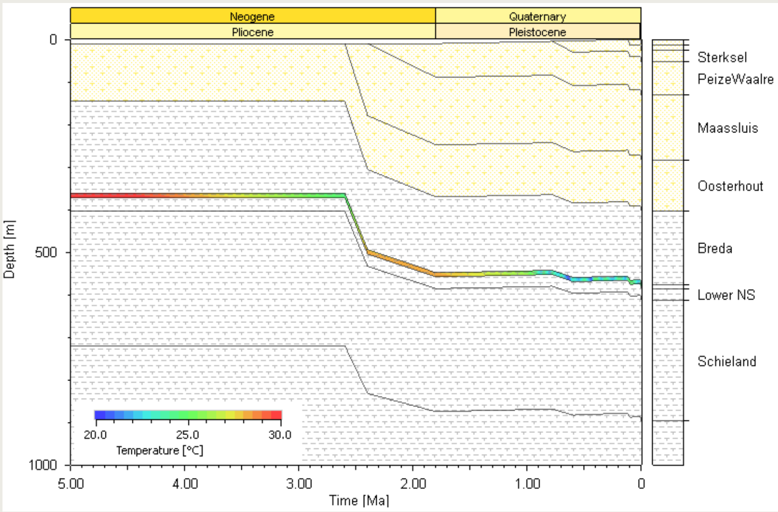

Figure 2.7: Burial history of the Rupel Clay Member in the West Netherlands Basin (see Figure 2.3 for location). The location of the Rupel Clay Member is indicated by the temperature overlay.

The first simulation step involved the comparison of the impact of scenario I and II of the surface temperature boundary condition on the development of the temperature in the subsurface at different depths. The simulated temperature variations in the shallow layers close to the surface (e.g. in the Peize Waalre Formation) can reach up to 15 °C, showing all details of the two surface temperature boundary conditions (Figure 2.8).

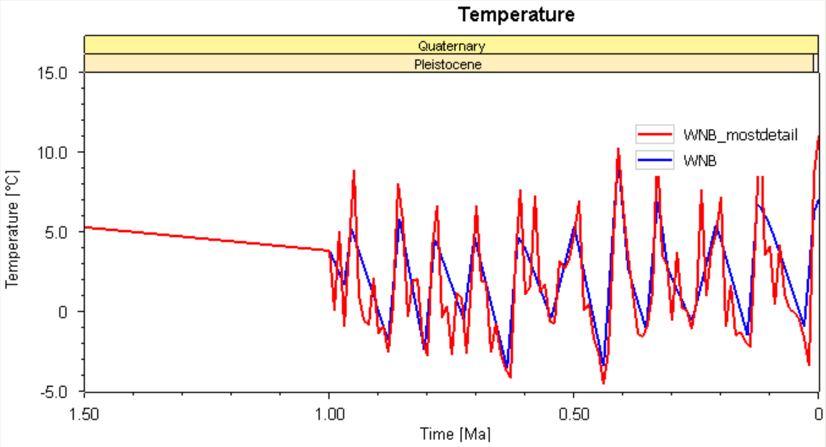

Figure 2.8: Comparison of the temperature evolution of the Peize Waalre Formation at shallow depth in the West Netherlands Basin from 1.5 Ma to present-day; results of 1D basin model simulations using scenario I (blue) and scenario II (red).

The surface temperature fluctuations of scenario I and II influence the temperature evolution at greater depth of 2km (Triassic) (Figure 2.9).

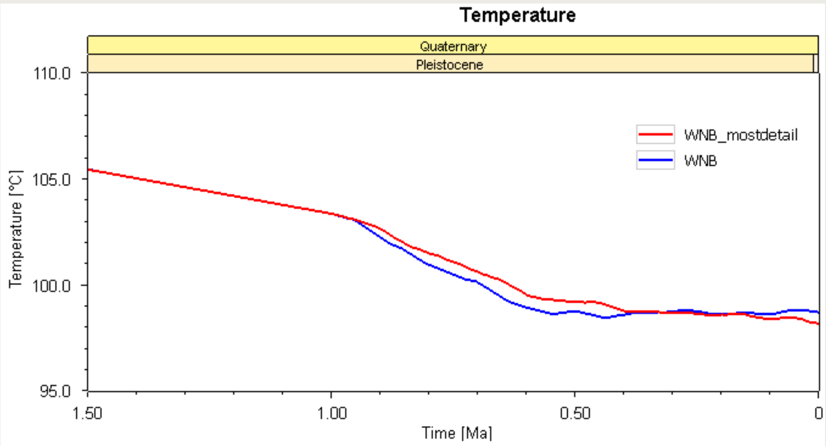

Figure 2.9: Comparison of the temperature evolution of the Triassic at 2 km depth in the West Netherlands Basin from 1.5 Ma to present-day; results of 1D basin model simulations using scenario I (blue) and scenario II (red).

The surface temperature fluctuations between glacial and interglacial times cause clearly visible temperature changes of up to 5 °C in the Rupel Clay Member at ca 600 m depth (Figure 2.10). Figure 2.10 also shows that the smaller temperature peaks in the most detailed scenario 2 are not reflected in the temperature evolution in the Rupel: the temperature evolution in the Rupel resulting from scenario 2 of the thermal boundary condition closely resembles the temperature evolution induced by scenario 1. Clear temperature fluctuations of about 2°C are visible down to a depth of about 1000 m. The maximum depth of the Rupel Clay Member in the Netherlands is about 1600m. At this depth the basin modelling simulations show temperature variations of less than 1 °C. It can therefore be assumed that future surface temperature variations, typical for glacial and interglacial periods will influence the temperature evolution in the Rupel Clay Member.

The differences between the simulation results of scenario I and scenario II are only minor at the depth of the Rupel Clay Member.

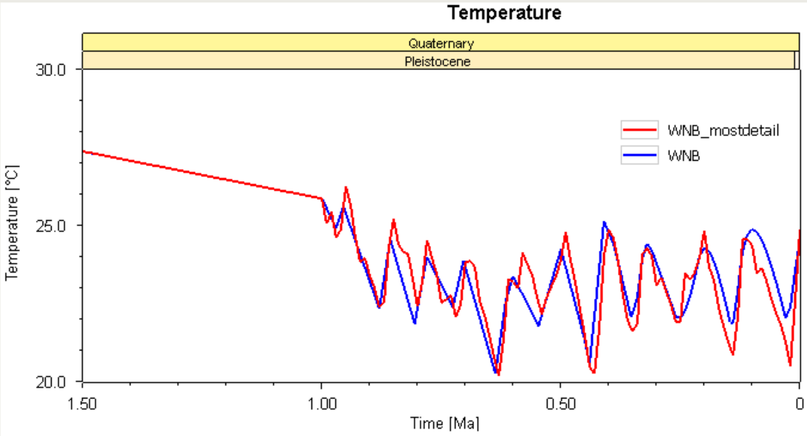

Figure 2.10: Comparison of the temperature evolution of the Rupel Clay Member at ca 500 m depth in the West Netherlands Basin model using scenarios I (blue) and II (red).

The influence of using a detailed surface temperature model for the last 120 kyrs on the temperature evolution in the Rupel Clay Member was investigated by basin modelling Scenario III (thermal boundary condition Scenario I of average temperature variations with the last 120 kyrs replaced by three temperature scenarios derived from the ones used in permafrost study of Govaerts et al., 2015; Figure 2.5). Figure 2.11 shows the resulting temperature evolution of the Rupel Clay Member for the West Netherlands Basin. The present-day difference in temperature in the Rupel Clay Member between the minimum and maximum scenario is around 3.5 °C.

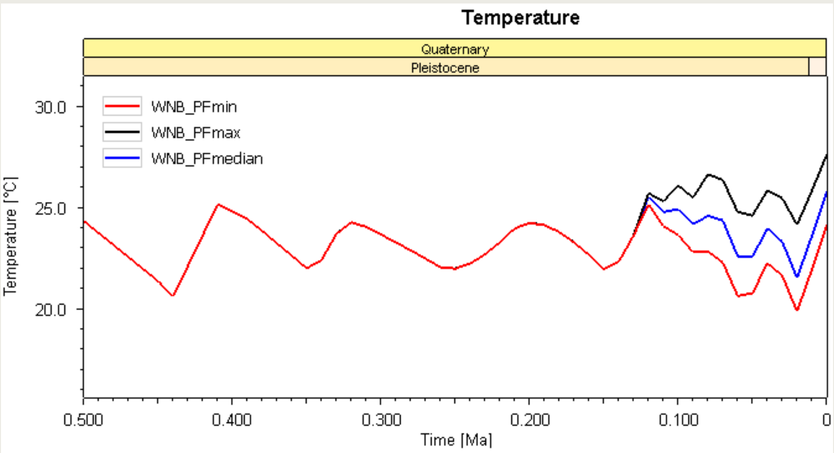

Figure 2.11: Temperature evolution of the Rupel Clay Member in the West Netherlands Basin using the minimum, median and maximum thermal boundary conditions of scenario III (Figure 2.5).

2.5. Basin modelling: impact of glacial-interglacial surface temperature variations on depth variations of the 0°C isotherm

The minimum, median and maximum thermal boundary conditions of scenario III are used to investigate the impact of these surface temperature variations for the last 120 Ma on the variations in depth of penetration of the 0.5°C, 0°C and -0.5 °C isotherms at 17 locations in the Netherlands (Figure 2.3). The fluctuation of the isotherms through time in the West Netherlands Basin (Figure 2.12) clearly show the influence of the different cold periods. For the last glacial period the 0°C isotherm reaches a depth of 80 m for the minimum thermal boundary condition of scenario 3, 160 m for the median case and 200 m for the maximum case. The location where the temperature reaches 0°C and the subsurface is 50% frozen is indicative of the permafrost progradation front (Govaerts et al., 2015). The 0°C isotherm can be considered to be a proxy for the depth of occurrence of permafrost. The numerical modelling result of the permafrost progradation front of 154 m for the same location in the West Netherlands Basin presented by Govaerts et al (2015; table 12) corresponds very well with the basin modelling result of the depth of the 0 °C isotherm of 160 m.

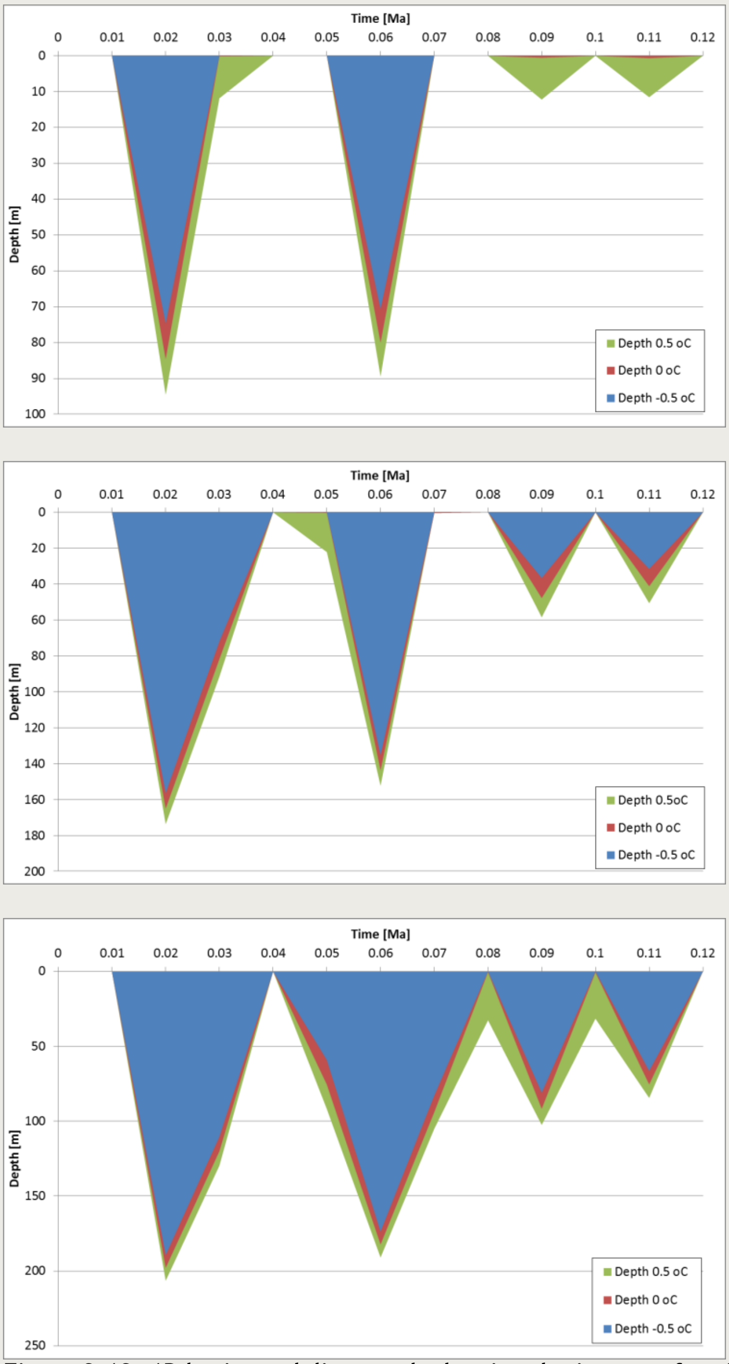

Figure 2.12: 1D basin modeling result showing the impact of surface temperature boundary condition scenario 3 on the depth of penetration of the 0.5°C, 0°C and -0.5 °C isotherms. From top down: impact of the minimum, median and maximum surface temperature evolution.

The 1D basin modelling results of the evolution of the penetration depth of the 0 °C isotherm at the 17 locations were used to create maps of the lateral variation of the depth of the 0 °C at different times during the past 120 kyrs. Figures 2.13 and Figure 2.14 present examples of such maps for the Elsterian and Weichselian ice age, respectively.

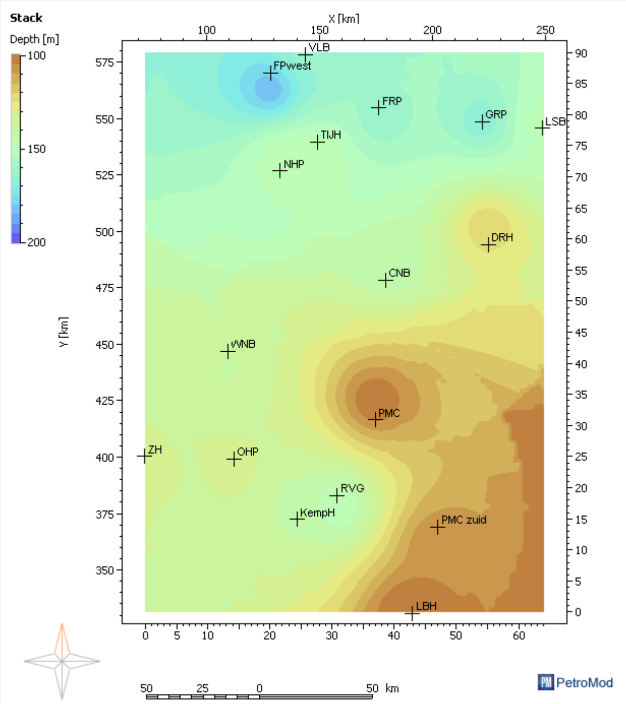

Figure 2.13: Depth of 0°C isotherm during the Elsterian ice age (~0.44 Ma) based on 1D modelling and interpolation.

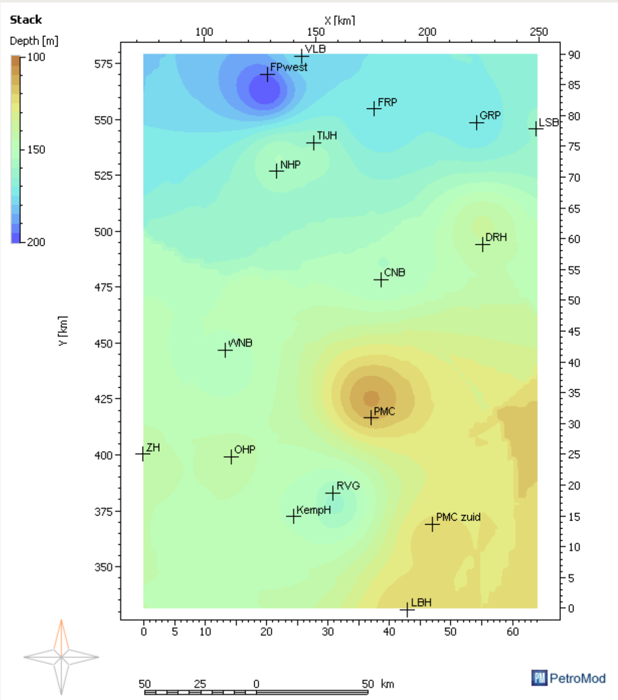

Figure 2.14: Depth of 0°C isotherm during the Weichselian ice age (~0.02 Ma) based on 1D modelling and interpolation.

2.6. Basin modelling: impact of glacial-interglacial surface temperature variations on future temperature evolution Rupel

The depth of the Rupel Clay Member did not vary much over the last 1 Ma (Figure 2.6): the temperature history of the Rupel Clay Member from 1 Ma to present-day can be considered as an analogue for future temperature evolution. Paleo temperature maps created by interpolation of the modelled temperatures of the Rupel Clay Member at 0.44 Ma, 0.41 Ma, 0.11 Ma and 0.02 Ma are presented in Figures 2.15, 2.16, 2.17 and 2.18, respectively. The maps show that the greatest temperature variations in the Rupel Clay member are related to burial depth: temperatures are lower where the Rupel is closer to the surface for all time intervals. These shallow locations also show the greatest effect of surface temperature variations (compare temperature maps related to cold surface temperatures at 0.02 Ma and 0.44 Ma with those associated with interglacial relatively warm surface temperatures at 0.11 ma and 0.41 Ma). This confirms the findings described in Sections 2.1 and 2.4 and shows that future surface temperature variations will have a greater impact on the temperature in the Rupel Clay Member the closer the Rupel is located near the ground surface.

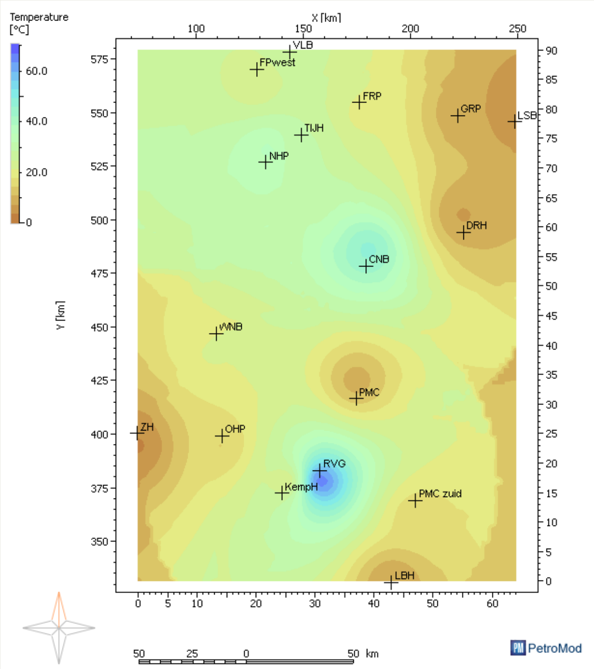

Figure 2.15: Paleo temperature map of the Rupel Clay Member at 0.44 Ma. Map based on 1D modelling and interpolation of temperatures at 17 locations.

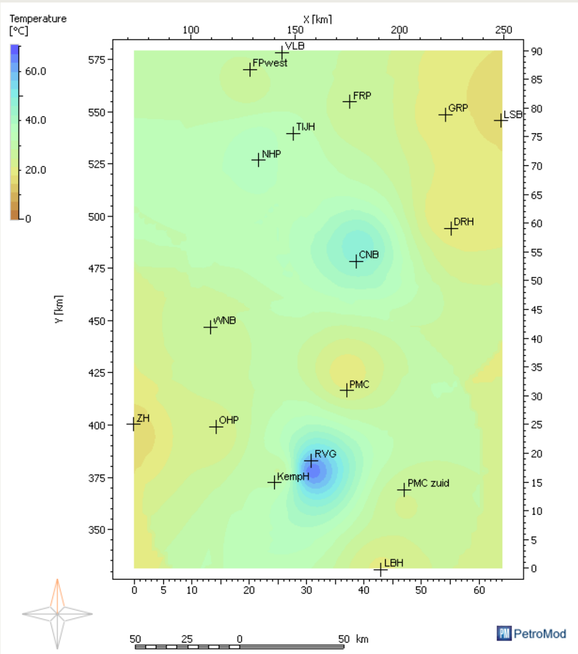

Figure 2.16: Paleo temperature map of the Rupel Clay Member at 0.41 Ma. Map based on 1D modelling and interpolation of temperatures at 17 locations.

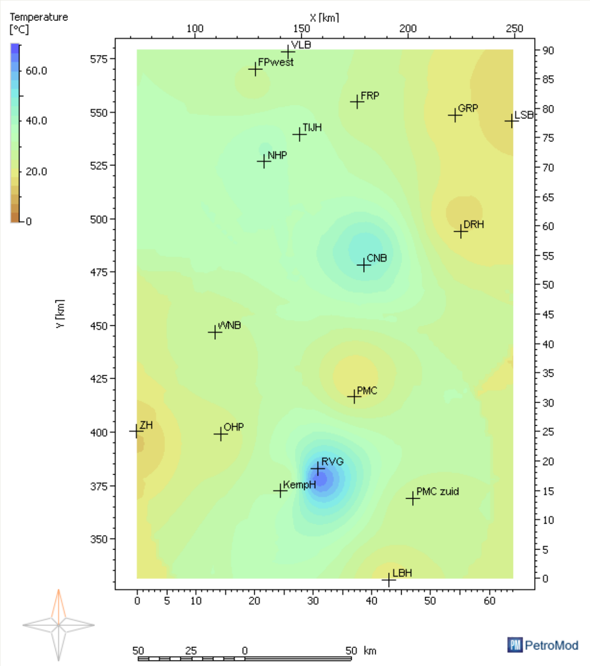

Figure 2.17: Paleo temperature map of the Rupel Clay Member at 0.11 Ma. Map based on 1D modelling and interpolation of temperatures at 17 locations.

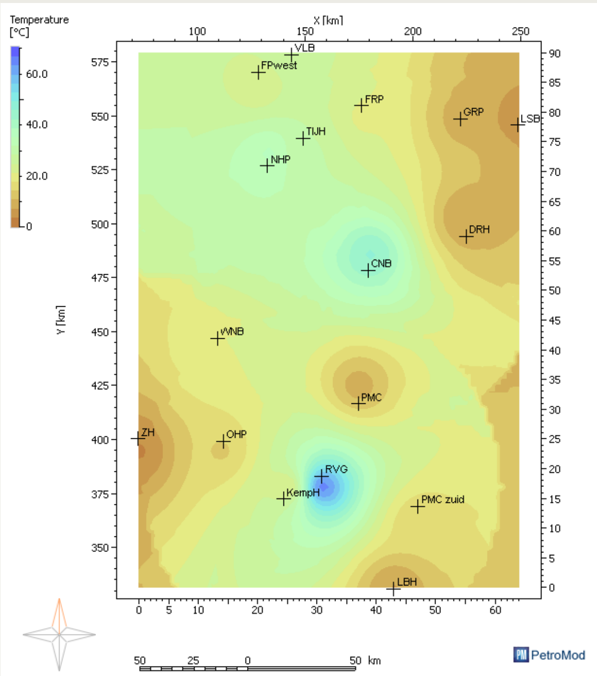

Figure 2.18: Paleo temperature map of the Rupel Clay Member at 0.01 Ma. Map based on 1D modelling and interpolation of temperatures at 17 locations.

2.7. Basin modelling: impact of global warming on future temperature evolution Rupel

The impact of increasing surface temperatures due to global warming is investigated for climate scenario Csb (Mediterranean, warm/dry summer) described by Ten Veen et al. (2015). Ten Veen et al. present the area south of Porto in Portugal with an annual average temperature of 15.4 °C as a representative analogue for this climate. This average annual temperature is approximately 6 °C warmer than current average temperatures for the Netherlands.

The 1D basin model of the West Netherlands Basin was used to study the impact of the global warming. Initially the surface temperature at present-day was increased by 6 °C (Figure 2.19) and compared with the modelling result for surface thermal boundary condition scenario II (i.e. average surface temperature variations based on temperature reconstructions published by Bintanja and Van de Wal, 2008; shown in Figure 2.4) (Figure 2.20).

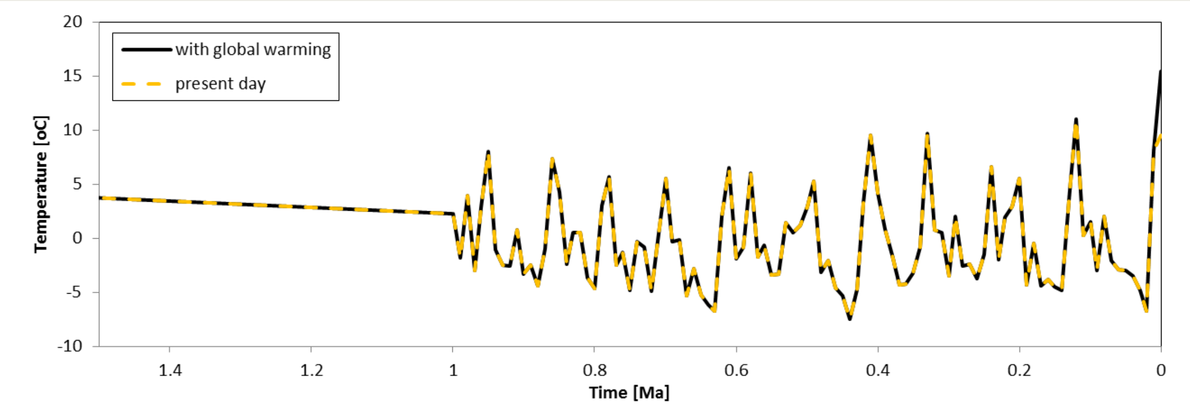

Figure 2.19: Surface temperature boundary conditions for scenario 2 (yellow line) and for scenario 'global warming' with current temperature increased with 6 °C (black line).

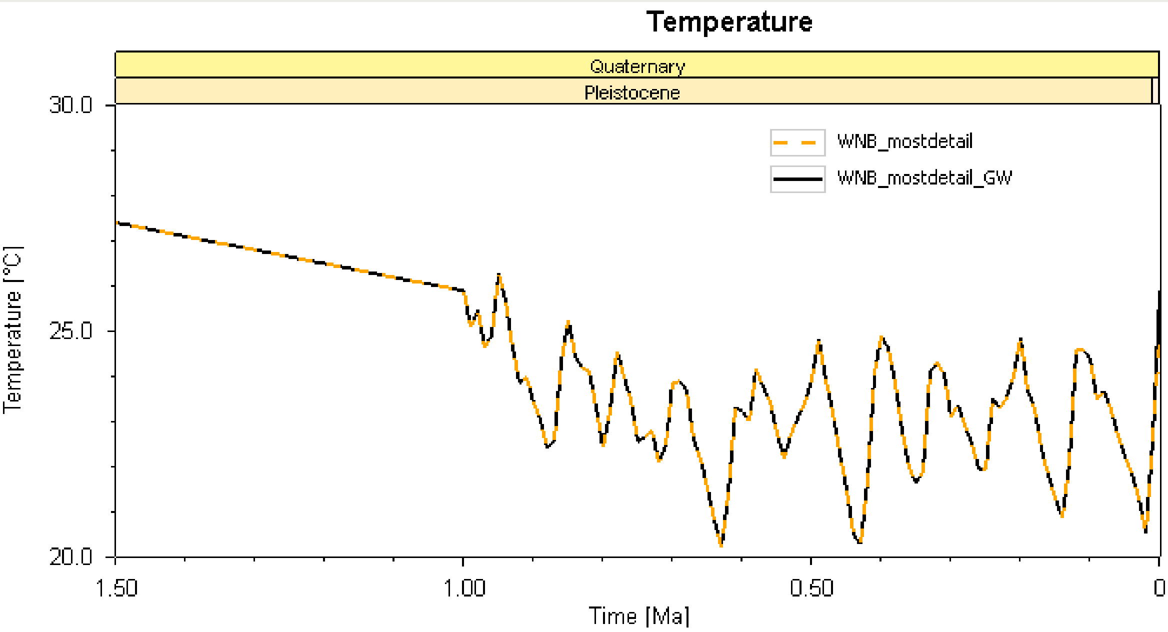

Figure 2.20: Modelled evolution of temperature in the Rupel Clay Member from 1. 5 Ma to present-day for two surface temperature boundary conditions shown in Figure 2.19 (yellow line shows modelling result for scenario II and black line for global warming scenario).

The surface temperature increase after the last ice age occurs very rapidly for both scenarios. The additional 6 °C increase in surface temperature takes place in the last 10 kyrs (Figure 2.19). Comparison of the modelling results (Figures 2.19 and 2.20) show that the surface temperature increase of 6 °C results in an increase of 1 °C in the Rupel Clay Member in the West Netherlands Basin (at depth of ca 600 m). Figure 2.21 shows the impact of the additional increase in temperature on the change of temperature with depth. The increase in subsurface temperature gradually diminishes with depth.

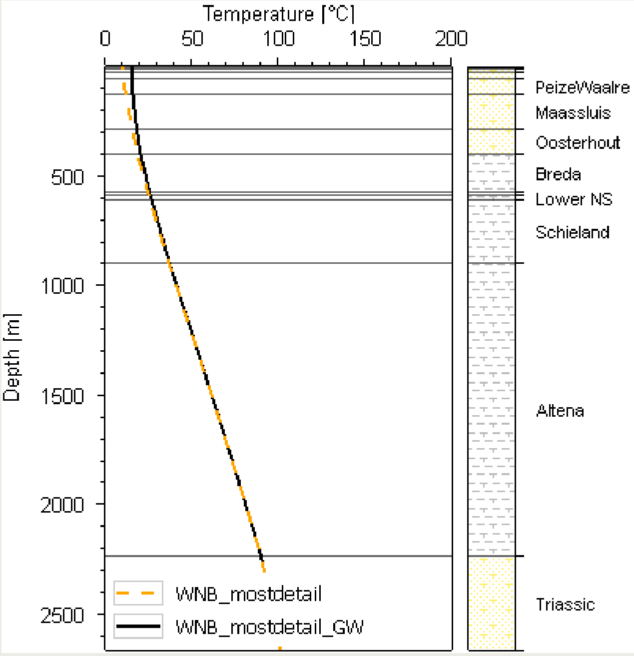

Figure 2.21: Modelled present-day change in temperature with depth in the West Netherlands basin for two surface temperature boundary conditions shown in Figure 2.19 (yellow line shows modelling result for scenario I and black line for global warming scenario).

It takes time for changes in temperature boundary conditions to propagate through the subsurface (Section 2.1). Rapid changes in surface temperature such as the increase in surface temperature after the last ice age and the more so for the additional increase in present-day temperature in the global warming scenario will result in subsurface temperatures that are not in equilibrium with these thermal boundary conditions. If the surface thermal boundary conditions stay constant over longer periods of time the subsurface temperatures will eventually reach a steady state (see e.g. Ter Voorde et al., 2014).

The long term effects of the surface temperature increase were studied by giving the model one million years to equilibrate without adding further sedimentation and burial for two different thermal boundary conditions: 1. the surface temperature is constant at present-day temperature of 9.5 °C; 2. the surface temperature gradually increases from 9.5 °C to 15.5 °C (Figure 2.22).

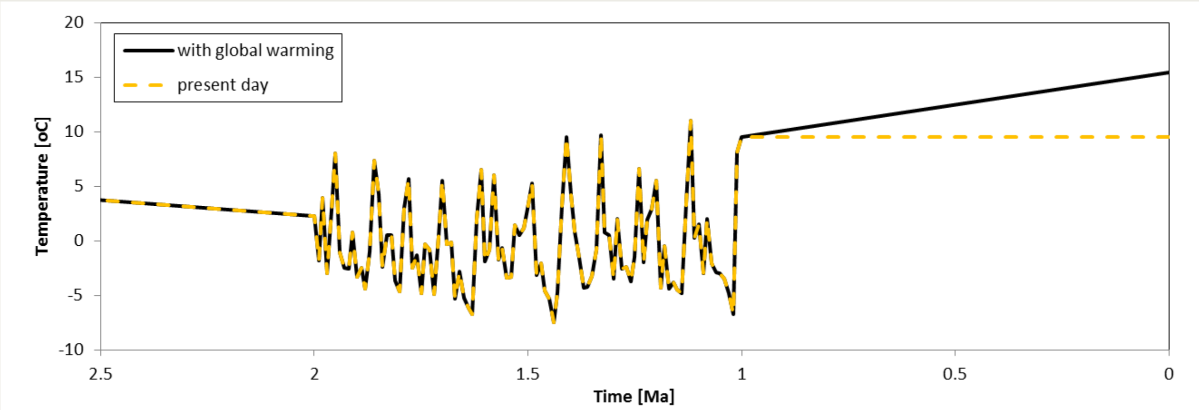

Figure 2.22: Surface temperature boundary conditions for 1) surface temperature boundary condition scenario 2 plus 'future' constant surface temperature of 9.5 °C during 1Myr (yellow line), and for 2) surface temperature boundary condition scenario II plus 'future' gradually increasing surface temperature from 9.5 °C to 15.5 °C during 1 Myr.). The boundary condition at 1 Ma represents the present-day situation, while the period from 1Ma to 0 Ma represents 1 million year into the future.

The modelling results indicate that the temperature of the Rupel Clay Member will increase the coming hundred thousands of years even if the surface temperature does not increase (Figure 2.23). After 1 million years the simulated temperature of the Rupel Clay Member has increased 8 °C. For the gradually increasing surface temperature from 9.5 °C to 15.5 °C the temperature of the Rupel increases with 13 °C over the period of 1 million year. Figure 2.24 shows the modelling results for the temperature change with depth after 1 million years from now.

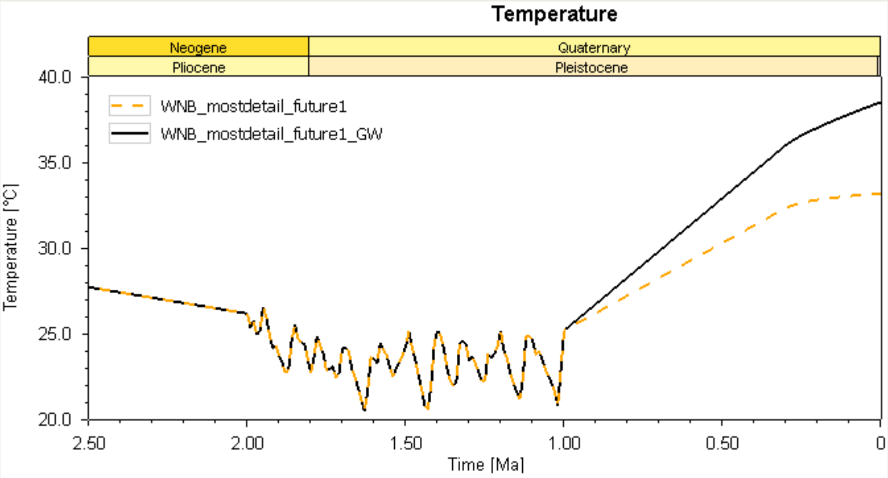

Figure 2.23: Modelled evolution of temperature in the Rupel Clay Member for the 'future'1 million years (from 1 Ma to 0 Ma in this figure) using the two surface temperature boundary conditions given in Figure 2.22. The temperature at 0 Ma represents the temperature after 1 million year from now.

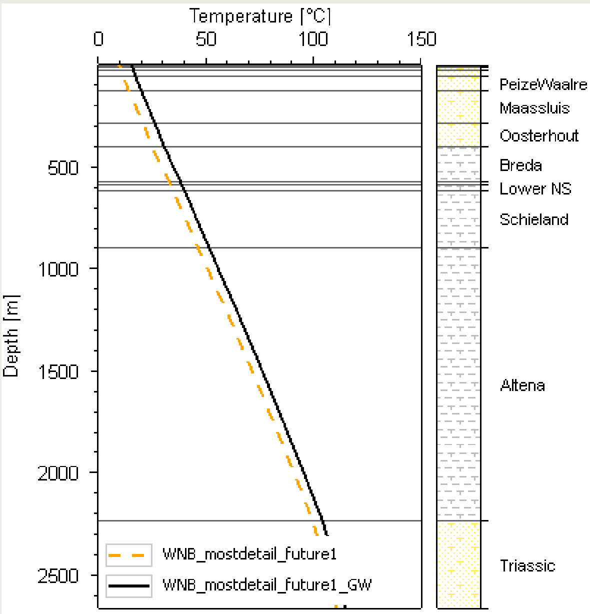

Figure 2.24: Modelled change in temperature with depth in the West Netherlands basin after 1 million year from now for the two 'future' surface temperature boundary conditions shown in Figure 2.22 (yellow line shows modelling result for constant surface temperature and black line for increasing surface temperature for the next 1 million years).

2.8. Conclusion

Basin modelling studies have been executed for different surface temperature scenarios, including glacial-interglacial conditions comparable to those in the previous 1 Myr as well as increasing surface temperatures due to global warming. All basin modelling are based on the assumptions that heat is transported by thermal conductivity only.

The results of 1D basin modelling using surface temperature fluctuations published by Bintanja and Van de Wal (2008) for the last 1 Myrs indicate that surface temperature fluctuations between past glacial and interglacial times cause clearly visible temperature changes of up to 5 °C in the Rupel Clay Member at ca 600 m depth. Clear temperature fluctuations of about 2°C are visible down to a depth of about 1000 m. The maximum depth of the Rupel Clay Member in the Netherlands is about 1600m. At this depth the basin modelling simulations show temperature variations of less than 1 °C.

The impact of glacial-interglacial temperature variations on the depth variation of the 0.5 °C, 0°C and -0.5 °C isotherms was studied by 1D basin modelling at 17 locations using surface temperature fluctuations published by Bintanja and Van de Wal (2008) replaced by 3 detailed temperature scenarios for the last 120 000 years published by Govaerts et al. (2015). Maps of the lateral variation of the depth of the 0ºC isotherm for different times during the past 120 kyrs based on these 1D basin modelling results show that maximum depth of penetration of the 0oC isotherm is about 200m. Assuming that the 0ºC isotherm can be considered to be a proxy for the depth of occurrence of permafrost, the permafrost will not reach the generic depth of 500 m in the Rupel Clay Member for similar future glacial-interglacial surface temperature conditions.

A gradual surface temperature increase from present-day temperature of 9.5 ºC to 15.5 ºC at 1 Ma in the future increases the temperature of the Rupel Clay Member at an assumed constant 500 m depth by 13 ºC.

At present-day the temperature in the Rupel Clay Member is not in steady state , i.e. not in equilibrium with the present-day surface temperature conditions. Keeping the surface temperature constant for a prolonged period of time allows the temperature in the Rupel to reach a steady state. The 1D basin modelling results indicate that for a constant surface temperature boundary condition of 9.5 ºC during the next 1 million year the temperature of the Rupel Clay at 500 m depth reaches a steady state and increases with 8 ºC in comparison with present-day temperature.

3. Future hydraulic boundary conditions

Deltares performed 3D gravity-induced groundwater flow simulations to investigate changing hydraulic conditions in the Rupel Clay Member in response to a selection of the normal evolution scenarios and altered evolution scenarios defined in Task 421 (e.g. Ten Veen et al. 2015). The impact of these scenarios on the hydrogeological system in a general sense is discussed briefly in section 3.1. The translation of these scenarios into the hydrogeological model is discussed in section 3.2. Sections 3.3 and 3.4 presents the results and conclusions, respectively.

3.1. Geohydrological scenarios

The normal evolution scenarios are defined as a sequence of the following different climate conditions:
Scenario 1: Moderate climate (present day)
Scenario 2: Cold climate without ice cover (permafrost)
Scenario 3: Cold climate with ice cover (glaciation)
Scenario 4: Warm climate

The selected altered scenarios include:
Scenario 5: Deep well
Scenario 6: Glacial valley
Scenario 7: Fault

3.1.1. Moderate climate

For this climate, the existing hydrogeological situation with the present human impact is used.

3.1.2. Cold climate without ice cover (permafrost)

In the permafrost climate, the moisture in the soil and subsoil freezes to a considerable depth (Figure 3.1). It may thaw in summer but only for a few surface feet at maximum (Ten Veen et al., 2015). In general, precipitation will not be able to reach the deeper groundwater and will be discharged as overland flow to reach surface waters.

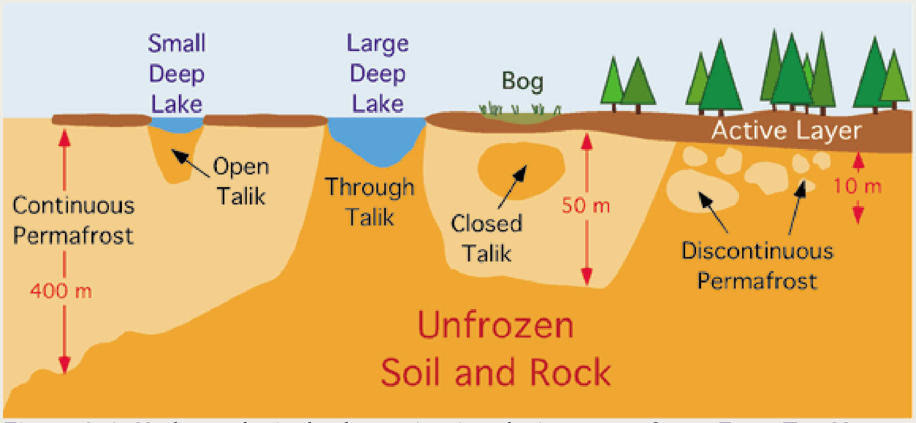

Figure 3.1: Hydrogeological schematization during permafrost. From Ten Veen et al. (2015) and retrieved from website: http://www.physicalgeography.net/fundamentals/10ag.html.

A potential connection between the biosphere and the deeper groundwater may be present in active river systems with considerable seepage whose heat flux prevents the soil to get frozen. If this potential connection is not present, the groundwater flow can be expected to be much lower as it is driven from higher groundwater tables in areas without permafrost (far away in the hinterland) towards the lowered sea level or towards active river systems.

Hence, on a larger scale the groundwater flow is expected to be dominated by recharge somewhere in the hinterland, where no permafrost conditions exists. Hydraulic heads in the hinterland are possibly also influenced by draining surface water streams, resulting in a water table in the hinterland that is close to the drainage levels of the surface water. Through the subsurface, the hinterland is hydrogeologically connected with the Netherlands. Seepage can only take place into open river systems or eventually into the sea.

The sea level can drop more than 120 m during an intense glacial cycle (Ten Veen et al., 2015; chapter 8). The sea would retreat far away from the present coast line. The hydraulic heads will drop by far less than this 120m at the present coast line (i.e. at the boundary of the groundwater model). Ten Veen et al. (2015) also report that the range of expected fluvial incision over Dutch territory does not exceed 20 m in the Southern North Sea Delta. It is assumed that river stages would drop by a few of tens of meters at most and groundwater heads near these river systems can be expected to drop by the same amount. Hydraulic heads along the present coast line will drop as well, but also not with the same amount as the drop of the sea level. When no groundwater recharge is present, the hydraulic gradient in the deeper aquifers in the direction towards the river system is likely to be small and the deeper groundwater will flow into the same direction as the active river systems.

During permafrost conditions without ice cover in the Netherlands a forebulge can develop in the Netherlands due to an ice sheet loading north of the Netherlands. A maximum forebulge uplift of 18 m is assumed for an assumed ice sheet thickness of 1500 m (proposal for the maximum ice sheet thickness in Scandinavia by Follestad and Fredin, 2011; Table 6.1 in Ten Veen et al., 2015). River systems can incise to a greater depth below ground surface due to this forebulge uplift.

Permafrost depth model calculations by Govaerts et al. (2015) indicate that the average permafrost front would reach depths of 140 and 180 m below ground surface for Weichselian temperature conditions.

3.1.3. Cold climate with ice cover (glaciation)

During a period with ice cover, additional water fluxes are expected to be present.
When air temperatures are above zero, the ice will melt at its surface. Surface melting rates in the ablation area of the ice sheet are reported to be in the order of 1000 to 10,000 mm/year (Boulton and Curle, 1997). These authors also report that this surface meltwater can flow into the glacier through moulins but that this meltwater is discharged as surface water at the glacial surface of the ice further downstream, with the exception for a narrow marginal zone.
At the base of the glacier, water also melts due to the geothermal heat flux and by shear heating at the ice-bed interface. The rate of this basal meltwater is unlikely to exceed the range of 1 – 100 mm/year (Boulton and Curle, 1997). This water may infiltrate into the subsurface if the transmissivity in the subsurface is enough to drain this water. Otherwise, it may flow in a thin layer between the ice bed interface or through channels. The assumption in model calculations in Boulton and Curle (1997) is 25 mm/year.

Another flux is caused by consolidation of the subsurface due to the load of the ice sheet. The porosity will decrease and a volume of water equal to the decrease in the porosity is squeezed out. Depending on the soil type and the extent to which the groundwater will find its way out, this consolidation process can act as a fast or slow process. This process will cease when the soil matrix becomes able to withstand the glacial load and a new equilibrium is reached. During the retreat of the ice cap, the subsurface will rebound partially. Although this process is described in (Boulton and Curle, 1997) it has been neglected in the modelling in this chapter. The locations of the ice cover during the last Elsterian, Saalian and Weichselian periods are shown in Figure 3.2.

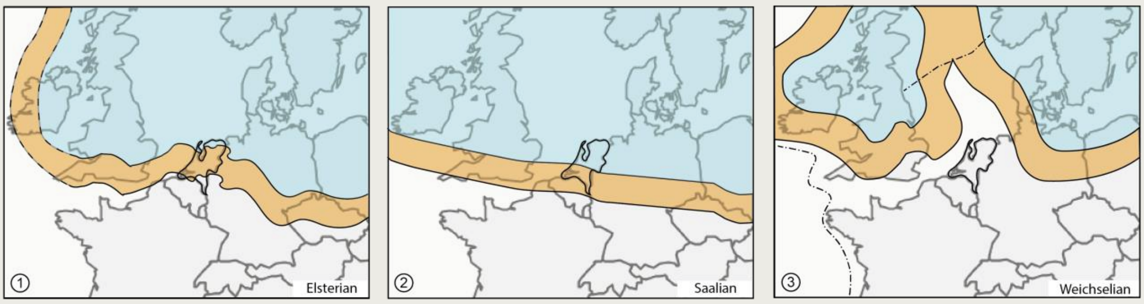

Figure 3.2: Location of the ice cover (blue) and the forebulge (orange) for three different ice-advance scenarios with analogy to the Elsterian, Saalian and Weichselian ice-sheet configurations (from Ten Veen et al., 2015).

Ten Veen et al. (2015) report in Table 4.2, third scenario, a maximum ice cover thickness of 195 m for an ice cover in the northern half of the Netherlands.

In front of the ice cover, permafrost conditions can be present resulting in an impermeable upper part of the subsurface in the permafrost regions and permeable upper part related to active surface water systems.

3.1.4. Warm climate

For a warm scenario, different predictions for different time scale have been made:

1. For the climate change due to CO_2 increase in the atmosphere, KNMI (http://www.climatescenarios.nl/images/Brochure_KNMI14_EN.pdf) made 4 different scenarios for the periods around 2050 (between 2036 and 2065) and around 2085 (between 2071 and 2100). In the most extreme scenario W_H (warm with a large change in air circulation pattern), the average temperature increases with 3.7 ºC; the sea level rises with 45 to 80 cm, the average rainfall increases with 7% (from 851 to 911 mm/year) and the potential evaporation (Makkink) increases with 10% (from 559 to 615 mm/year).

2. On the longer term climate change can even be more severe. In Ten Veen et al. (2015; Chapter 12) sea level rises of a few meters to 10 m are reported for a Mediterranean type of climate and up to 60 m as an extreme case if all ice on earth will melt. In ten Veen et al. (2015) an analogue for the Mediterranean climate is given: south of Porto in Portugal with an average annual precipitation of 1236 mm/year. In http://www.stadtklima.de/cities/europe/pt/porto/porto.htm an annual average potential evapotranspiration of 716 mm/year is given for Porto, which is probably close to the value for the region south of Porto.

In the second scenario, it seems unlikely that the present coast line in the Netherlands will still be present and large parts of the Netherlands will have been reclaimed by the sea.

3.1.5. Deep well

A deep well can influence the water fluxes near the interface of the Rupel Clay as well as increase the hydraulic gradient over the Rupel Clay. This deep well could be anywhere in the country at depth where an attractive aquifer is present. The effect of such well is expected to be highest close to the well location.

3.1.6. Glacial valley

During a period of deglaciation, melt water may erode the subsurface below the ice coverage locally. In a later stage these valleys are filled up with new deposits. Tunnel valleys created during the Elsterian ice age reach depths of about 500 m below the present land surface in the Northern part of the Netherlands (Ten Veen et al., 2015). Tunnel valleys can have lengths of up to more than a hundred kilometers and width of a few kilometers (Ten Veen et al., 2015).

3.1.7. Fault

Bense et al. (2003) describe fault properties for faults in the Roer Valley Graben. They report a fault width of 5 m, a reduction in horizontal hydraulic conductivity of more than 2 orders of magnitude for a fault zone crossing a sandy aquifer, and an increase in vertical hydraulic conductivity in the fault zone. They also report that effects of clay smearing or juxtaposition of aquitards and aquifers may be an important reason for increased flow resistance. Although not mentioned in Bense et al. (2003), it is assumed here that for clayey layers no increase in the vertical hydraulic conductivity takes place.

3.2. Set up groundwater flow model

The above scenarios were translated into the subsurface flow model.
A model of the present day situation was developed in OPERA WP 621 and reported in detail in Valstar and Goorden (2016). This model used the NHI model as a starting point and the model was extended in the vertical direction to include the Rupel Clay Member and relevant geological layers above and below. The model describes the groundwater flow in the onshore part of the Netherlands. For each scenario, all adaptations from the model are described below.

3.2.1. Scenario 1: Moderate climate (present situation)

The model set up of the present situation is exactly equal to the model reported in Valstar and Goorden (2016).

3.2.2. Scenario 2: Cold climate without ice cover (permafrost)

River stages and bottom elevations
In the permafrost groundwater model, a drop of hydraulic heads of 30 m is assumed at the fixed model boundaries at the North Sea and at the river stages of the main river systems (Rhine and Meuse and Scheldt systems). The hydraulic head drop of 30 m is an assumption for the fluvial incision due to sea level drop and the forebulge uplift.
All other surface water and drainage systems, including the Wadden Sea, that are active in the moderate climate model are inactive in this scenario.

Groundwater recharge
In areas with permafrost all precipitation is drained by surface runoff and groundwater recharge is zero. In areas with active rivers the groundwater flow is dominated by the river levels and not by recharge which thus is also assumed to be zero.

Hydraulic heads at model boundary with Germany and Belgium
During permafrost conditions hydraulic heads in Belgium and Germany are likely to drop as well but it is hard to make an estimate how large this drop will be. It is probably controlled by the river levels (that have may have declined as well) and by the groundwater levels somewhere in a far hinterland where no permafrost conditions are present.

As a worst case assumption, the boundary heads in all model layers are set equal to heads that mimic best the larger scale flow systems with minimal influences of present recharge based on present data. For the Belgium and German borders south of the entrance of the river Rhine, a fixed head boundary is set, with a hydraulic head that is 30m lower than the present hydraulic head of the lowest layer of the model in the present situation. At the German border north of the entrance of the Rhine, a no flow boundary has been implemented. In that region the hydraulic boundary heads in the present model are strongly affected by recharge and implying a similar boundary condition as for the other borders did result in unrealistic groundwater flow patterns.

Hydraulic conductivity
The hydraulic conductivity in the upper 160 m (average of the permafrost front (140-180 m) in the permafrost model) are set to zero for the entire model with an exception below river systems of the Rhine, Meuse and Scheldt.

Abstractions
All groundwater abstractions in the present model are not present in this model scenario.

3.2.3. Scenario 3: Cold climate with ice cover (glaciation)

Ice cover
The glacial extent in the model is set north of the present Rhine, Nether Rhine and Lek rivers and the maximum ice cover thickness is set to 195 m (see Ten Veen et al., 2015, table 6.2: third scenario) at the northern edge of the Netherlands diminishing to zero at the ice sheet margin (3.3). Its melt water flux is 25 mm/year for the entire area and this flux is forced into the upper layer as long as the groundwater pressure does not exceed the ice pressure.

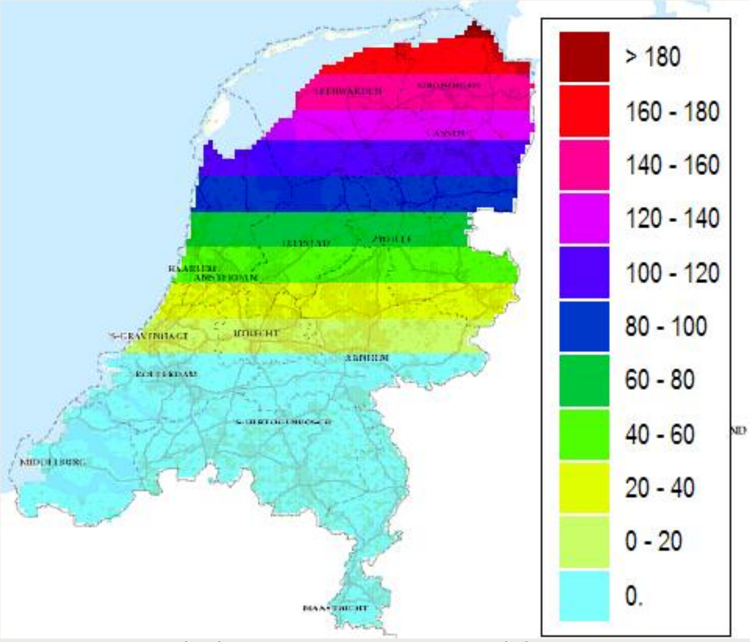

Figure 3.3: Ice thickness (m) in scenario model.

The boundary conditions in the part with the ice cover are not known beforehand and depend on how well the melt water is drained by the subsurface. It is to be expected that part of the meltwater from the area north of the Netherlands enters the subsurface and flows south toward the Netherlands. As a worst case the hydraulic heads at the northern boundary are set equal to the pressure of the ice cover for all model layers. The eastern and western boundaries in the area with the ice cover are set to no flow boundaries. These boundary conditions are based on a north-south flow direction that can be expected for the Saalian analogy in Figure 3.2.

The pressure of the ice cover forces a flux of groundwater out of the pores. The amount of water that is replaced during a period with ice coverage is calculated using the porosity-depth relationships described in Valstar and Goorden (2016).This amount is translated into a source flux of each individual model cell, by dividing this amount of water with an assumed period of the ice coverage of 20,000 year. The porosities and hydraulic conductivities in this region are also updated using the relationships given in Valstar and Goorden (2016).

Permafrost region
The other part of the model domain is assumed to be a permafrost region with the exception of the Rhine (without the IJssel), Maas and Scheldt river systems
This region of the model has the same changes as the permafrost model.

3.2.4. Scenario 4: Warm climate

Both warm climate scenarios are modelled:

Scenario 4a: Climate Change prediction W_H of KNMI
In this scenario, the sea level is assumed to increase with 0.80 m, the groundwater recharge is assumed to increase with 4 mm/year (based on the increase in precipitation minus the increase in the potential evaporation). River levels in the major river systems (Rhine, Meuse, Scheldt) as well as in the IJssel lake are increased with 0.8 m. The other surface water levels are not changed. All other model input is not changed.

Scenario 4b: Mediterranean Climate
In this scenario, the sea level rise is assumed to be 10 m, based on the upper margin for the Mediterranean Climate. The part of the model domain with an elevation below 10 m above the present mean sea level is modelled with a constant head boundary of 10 m above the present mean seal level in the upper layer of the model. This area is shown in Figure 3.4. River and drain stages in all layers which are lower than 10 m are set equal to 10 m. All groundwater abstractions in the flooded area are turned off.

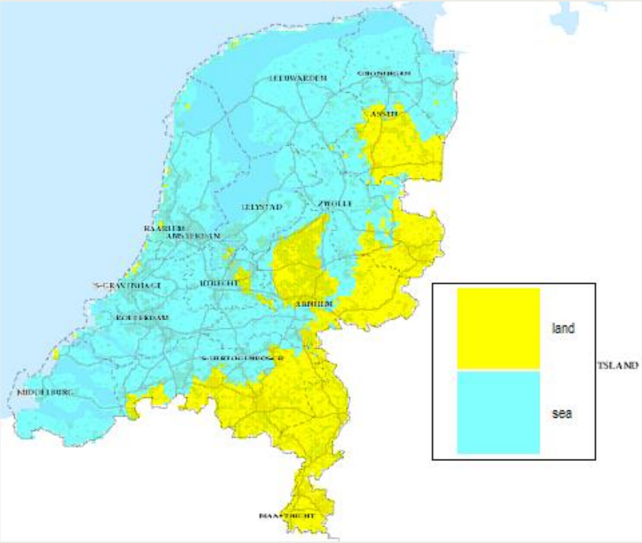

Figure 3.4: Area reclaimed by the scenario in model scenario 4b.

For groundwater recharge we assume a value of 520 mm/year based on an average annual precipitation of 1236 mm/year and an actual evaporation that is equal to the potential evapotranspiration of 716 mm/year.
The boundary condition in Germany and Belgium are set equal to 10 m above the present mean sea level in case the value in the reference model was lower; otherwise the boundary head remains unchanged.
Other input parameters remain unchanged.

3.2.5. Scenario 5: Deep well

This scenario includes a well in the center of the country at a depth of 500 m with a maximum drawdown in the model of 10 m. The well location is selected in a region where path line calculations were started in Valstar and Goorden (2014). This because the effect on travel times of path lines starting near such well is expected to be large.
The deep well location is shown in Figure 3.5.

Figure 3.5: Location of the well in the deep well scenario.

3.2.6. Scenario 6: Glacial valley

In this model scenario a glacial valley of 500 m depth, 5 km wide, 50 km long oriented north to south in the Northern part of the Netherlands is added. Two different scenarios for this glacial valley are modelled: (a) the valley is filled up with ice with a melt water rate of 25 mm/year and other conditions similar as in the glacial scenario and
(b) the valley is filled up with coarse sand and other conditions are similar to the present day moderate climate model. The location of the modelled glacial valley is shown in Figure 3.6.

Figure 3.6: Location of glacial valley in the model scenario.

3.2.7. Scenario 7: Fault

One fault was added to the model. The width of the fault is assumed to be 5 m, which is smaller than the resolution of the model grid. The location of the simulated fault is shown in Figure 3.7.

Figure 3.7: Location of the simulated fault.

The horizontal hydraulic conductivity in the fault $k_{h,fault}$ is decreased by a factor 100 compared to its original value $k_{h,original}$. The effective horizontal conductivity $k_{h,eff}$ is obtained with the upscaling equation for serial flow:

$$\frac{250m}{k_{h,eff}} = \frac{5m}{k_{h,\,fault}} + \frac{245m}{k_{h,original}}$$

Using a reduction factor for the fault hydraulic conductivity of a factor 100, the effective horizontal hydraulic conductivity perpendicular to the fault becomes approximately 33% of its original value.

The vertical hydraulic conductivity at the fault is set at 10 times its original value for all layers except for clayey layers (Veldhoven Clay Member and Rupel Clay). The effective vertical hydraulic conductivity is obtained with the upscaling equation for parallel flow:

$$k_{v,effective} = \frac{5m}{250m} k_{v,\,fault} + \frac{245m}{250m} k_{\mathrm{v,original}}$$

The effective value for the vertical hydraulic conductivity in the model cells with the fault is 18% larger than its original value.

3.3. Results groundwater flow modelling

In this chapter, the results of the model with respect to the boundary condition for flow models through the Rupel Clay are reported. Results for transport through the entire geosphere will reported in the final OPERA report of WP 6.2.

3.3.1. Results scenario 1: Moderate climate

The hydraulic heads in the layer above and below the Rupel Clay and the hydraulic gradients over the Rupel Clay are shown in Figure 3.8.

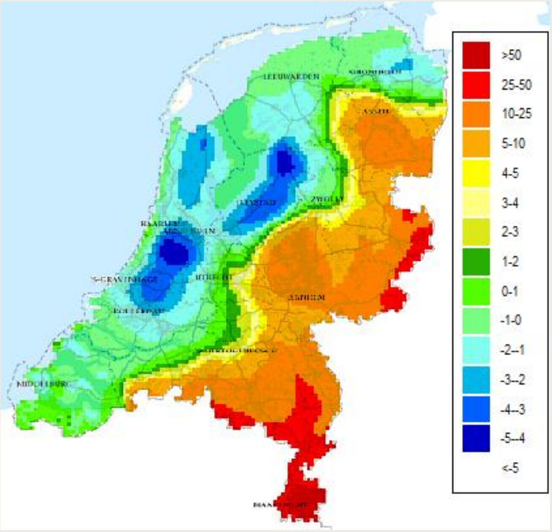

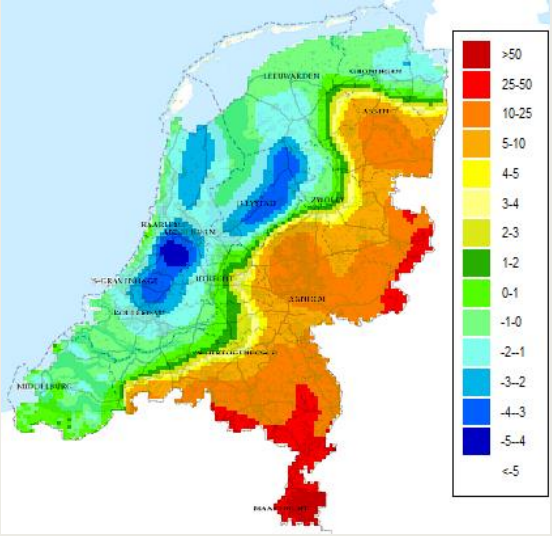

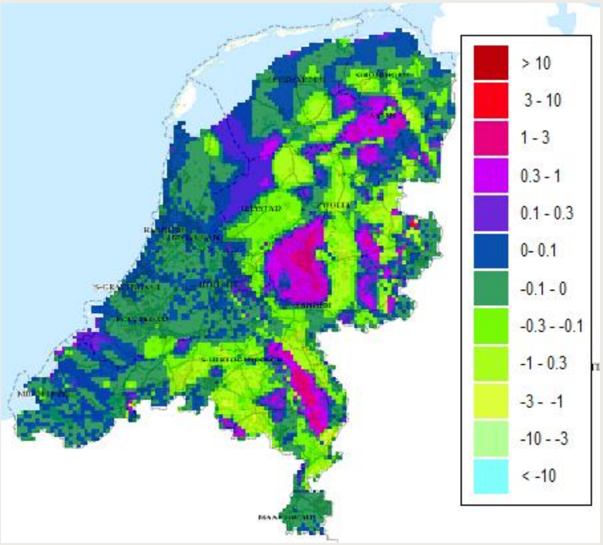

Figure 3.8: Hydraulic heads (in m) in the layer above (upper left) and below (upper right) the Rupel clay, the vertical hydraulic gradients over the Rupel Clay model layer (lower) from the moderate climate model.

3.3.2. Results scenario 2: Cold climate without ice cover (permafrost)

The hydraulic heads in the layer above and below the Rupel Clay, the hydraulic gradients over the Rupel Clay are shown in Figure 3.9.

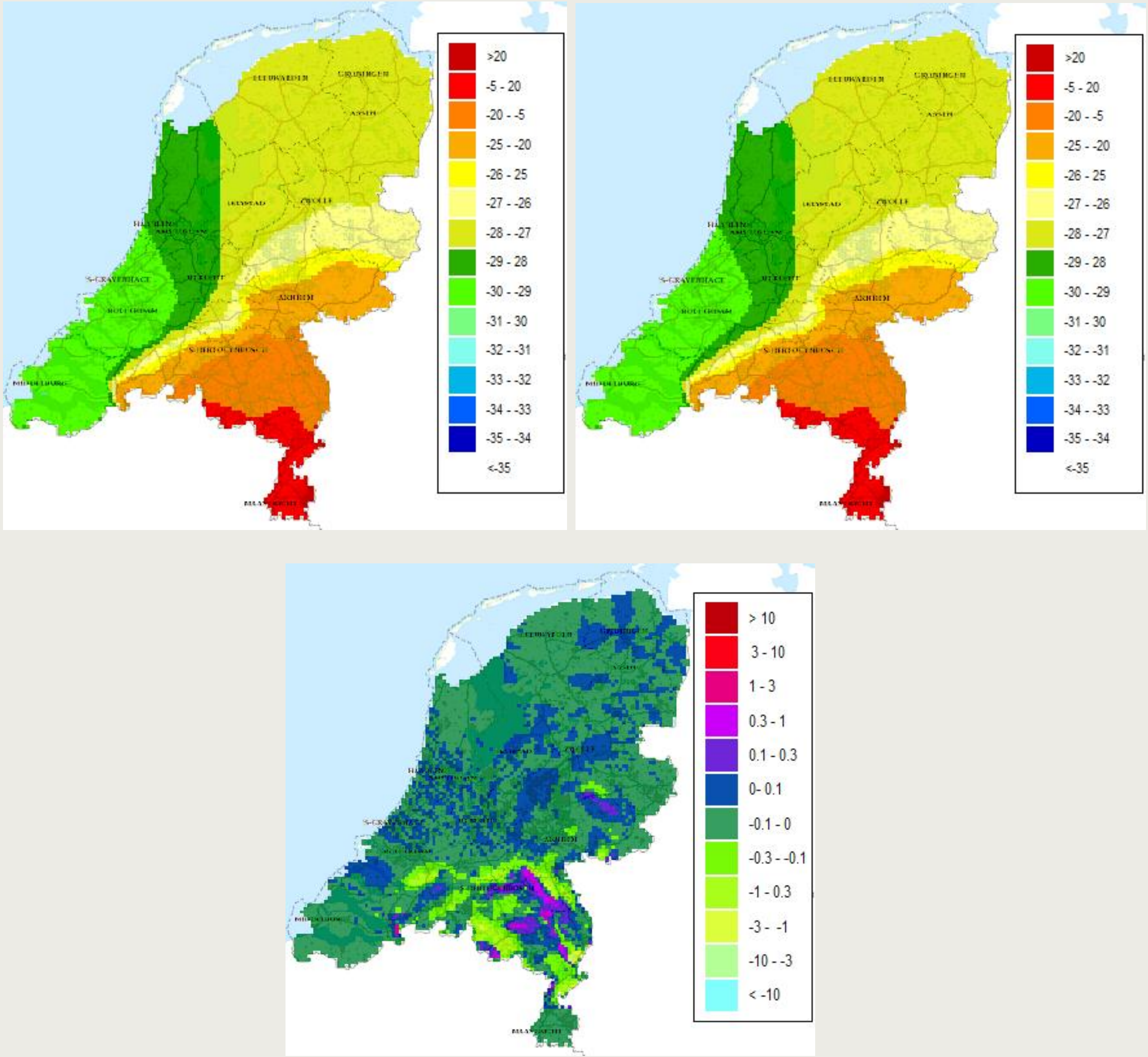

Figure 3.9: Hydraulic heads (m) in the layer above (upper left) and below (upper right) the Rupel Clay, the vertical hydraulic gradients over the Rupel Clay model layer (lower) from the cold climate without ice cover (permafrost) model.

In comparison with the model for the present situation the hydraulic gradient over the Rupel Clay has predominantly decreased.

3.3.3. Results scenario 3: Cold climate with ice cover (glaciation)

The hydraulic heads in the layer above and below the Rupel Clay, the hydraulic gradients over the Rupel Clay are shown in Figure

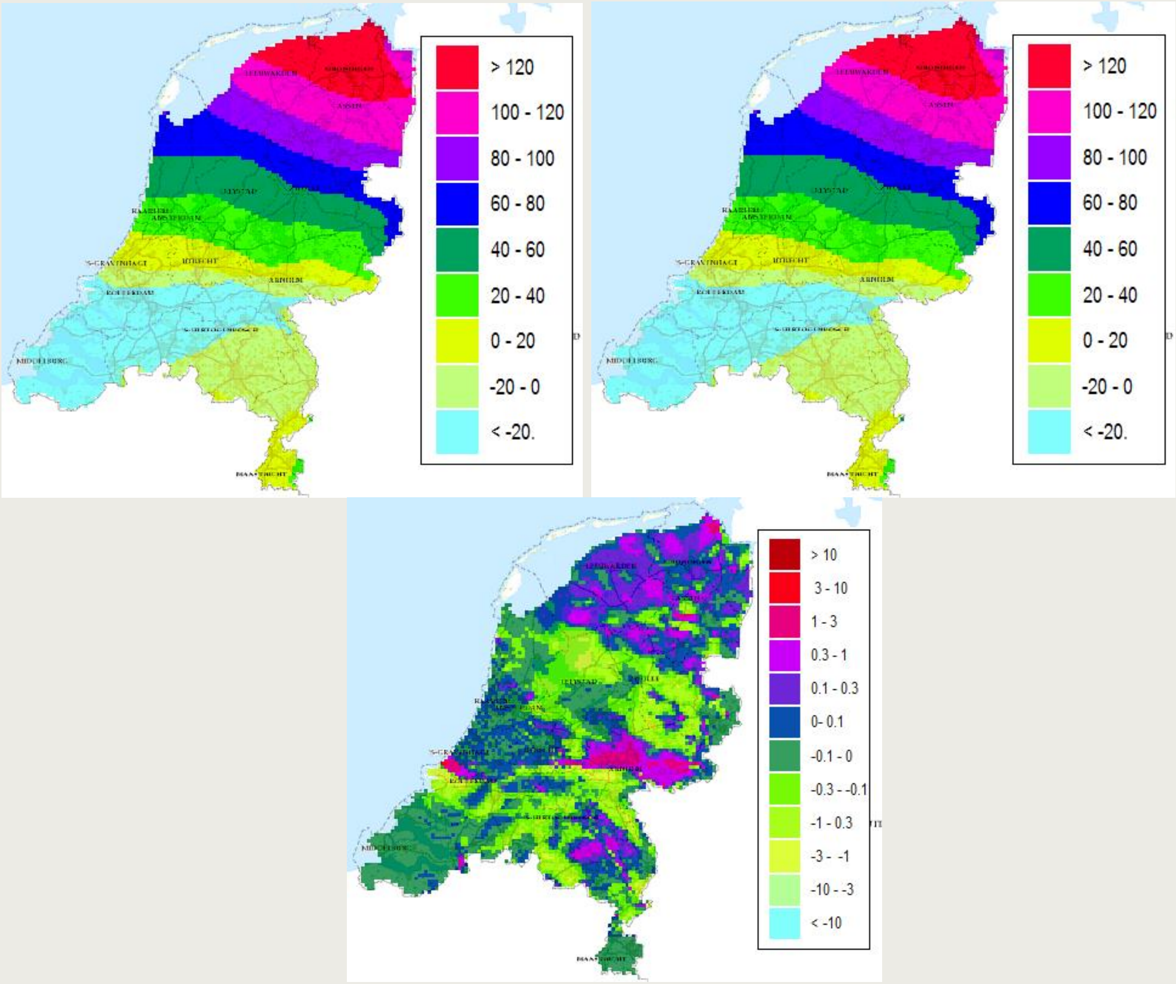

Figure 3.10: Hydraulic heads (m) in the layer above (upper left) and below (upper right) the Rupel Clay, the vertical hydraulic gradients over the Rupel Clay mode layer (lower) from the cold climate with ice cover (glaciation) model.

In comparison with the model for the present situation the hydraulic gradients over the Rupel Clay has changed considerably. In the northern part of the country, larger positive (= downward) head gradients are clearly visible. Also just north of the ice cover boundary large positive gradients are visible, whereas south of this boundary larger negative (= upward) gradients are simulated. This effect close to the boundary of the ice cover is due to the fact that just south of the ice cover, permafrost conditions are prescribed. There, the upper 160 m of the subsurface have zero conductivity and the groundwater flow originating from below the ice cover is forced to move downward near the edge of the ice cover. Further south the flow is upward again in the area of the Rhine river system where locally no permafrost conditions are prescribed.

In some other areas, such as the northern part of the Veluwe, downward gradients over the Rupel Clay in the moderate climate model have changed to upward gradient in this glaciation scenario.

3.3.4. Results scenario 4: Warm climate

Climate Change prediction W_H of KNMI)

The hydraulic heads in the layer above and below the Rupel Clay, the hydraulic gradients over the Rupel Clay for the climate change prediction W_H of the KNMI are shown in Figure

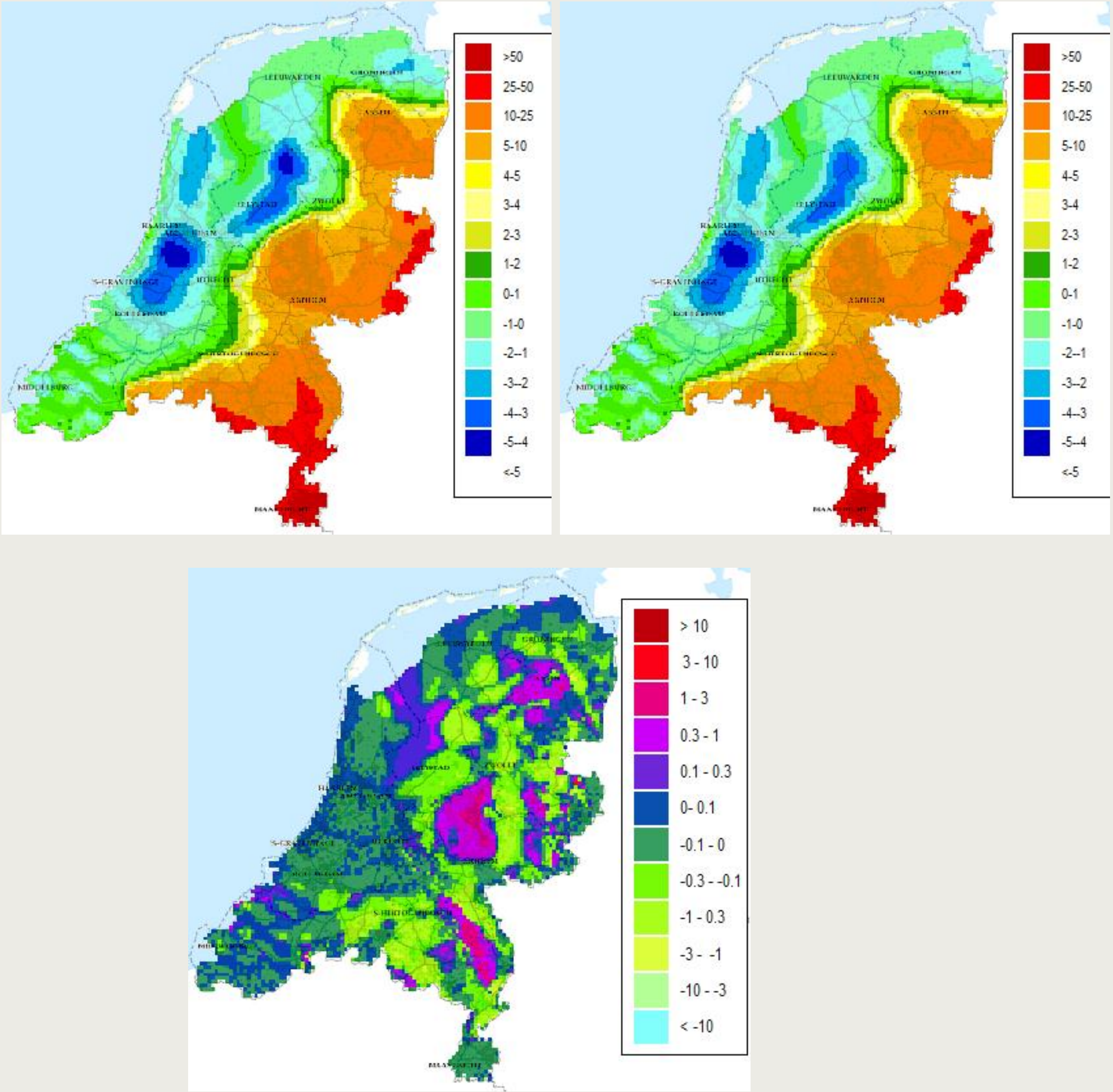

Figure 3.11: Hydraulic heads (m) in the layer above (upper left) and below (upper right) the Rupel Clay, the vertical hydraulic gradients over the Rupel Clay model layer (lower) from the warm climate model (*Climate Change prediction W_H of KNMI*).

In comparison with the model for the present situation the hydraulic gradient over the Rupel Clay are very similar.

Mediterranean

The hydraulic heads in the layer above and below the Rupel Clay, the hydraulic gradients over the Rupel Clay for the Mediterranean climate are shown in Figure 3.12.

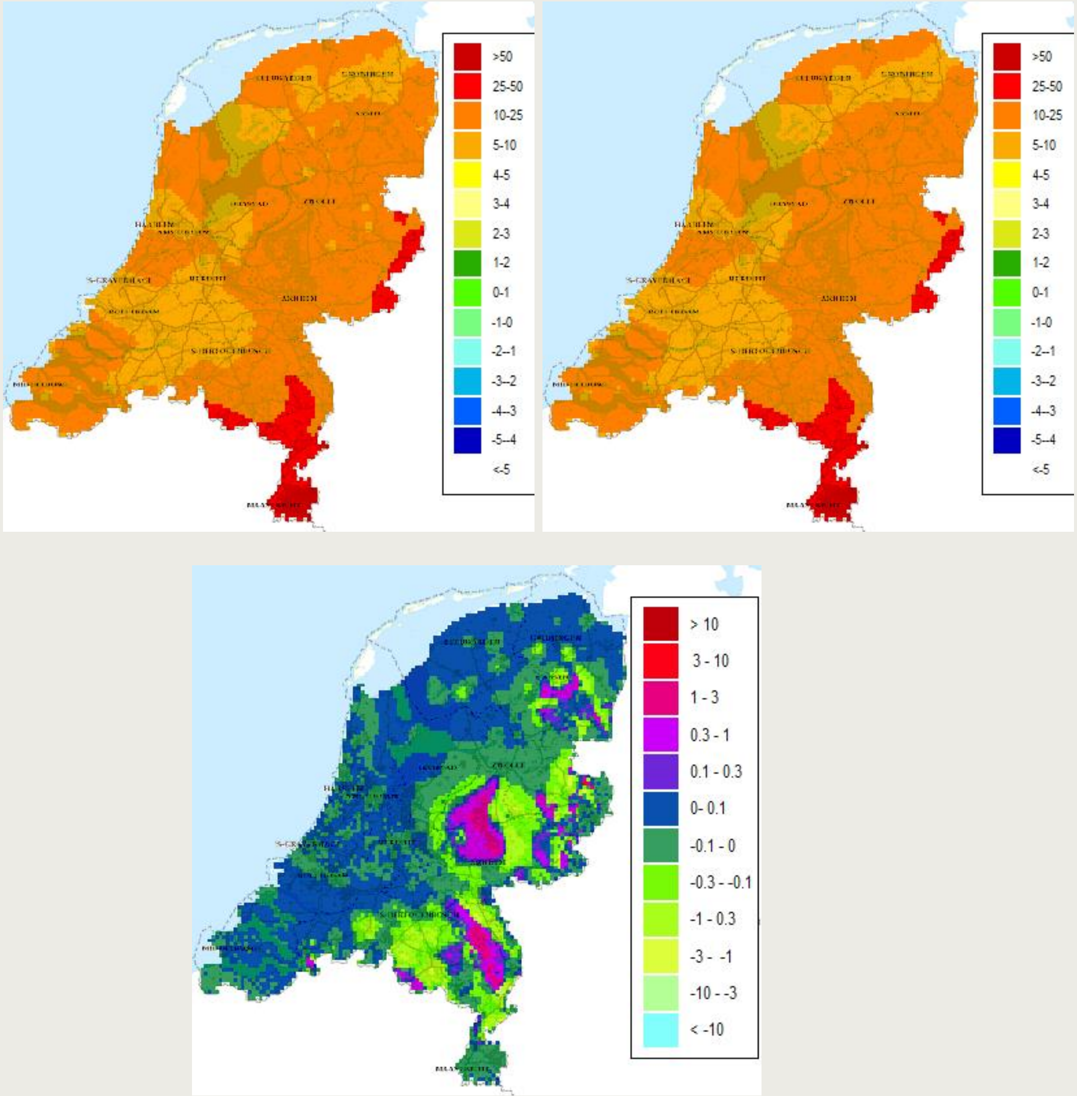

Figure 3.12: Hydraulic heads in the layer above (upper left) and below (upper right) the Rupel clay, the vertical hydraulic gradients over the Rupel Clay mode layer (lower) from the warm (*Mediterranean*) model.

In comparison with the model for the present situation the hydraulic gradient over the Rupel Clay has decreased, mainly in the areas that have been flooded in this scenario.

3.3.5. Results scenario 5: Deep well

The hydraulic heads in the layer above and below the Rupel Clay and the hydraulic gradients over the Rupel Clay are shown in Figure

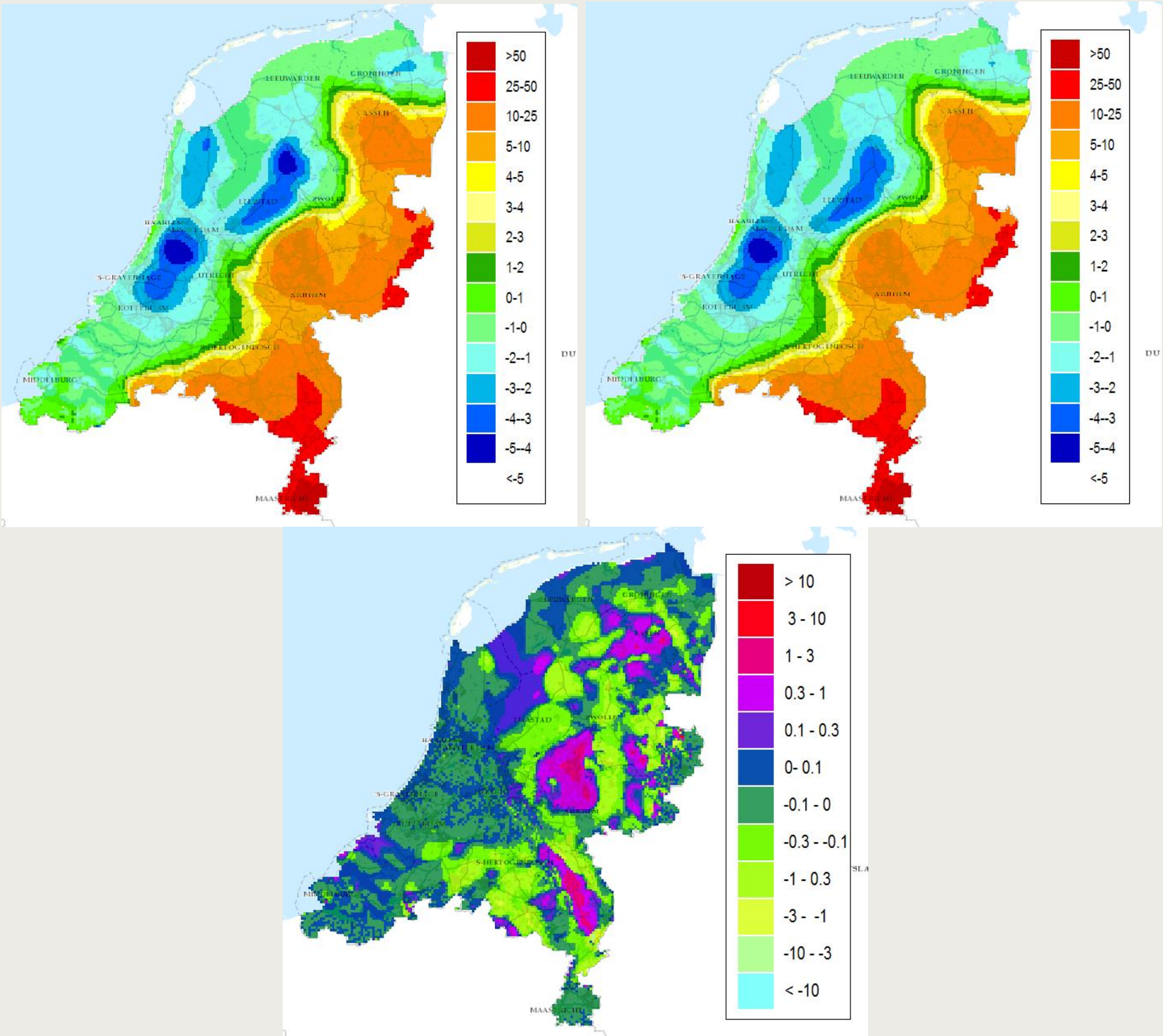

Figure 3.13: Hydraulic heads (m) in the layer above (upper left) and below (upper right) the Rupel Clay, the vertical hydraulic gradients over the Rupel Clay model layer (lower) from the deep well scenario model.

In comparison with the model for the present situation the hydraulic gradient over the Rupel Clay is only slightly changed in the vicinity of the simulated deep well at the western edge of the Veluwe. There, locally the gradient is now upward instead of downward.

3.3.6. Results scenario 6: Glacial valley

Ice-filled glacial valley

The hydraulic heads in the layer above and below the Rupel Clay and the hydraulic gradients over the Rupel Clay are shown in Figure

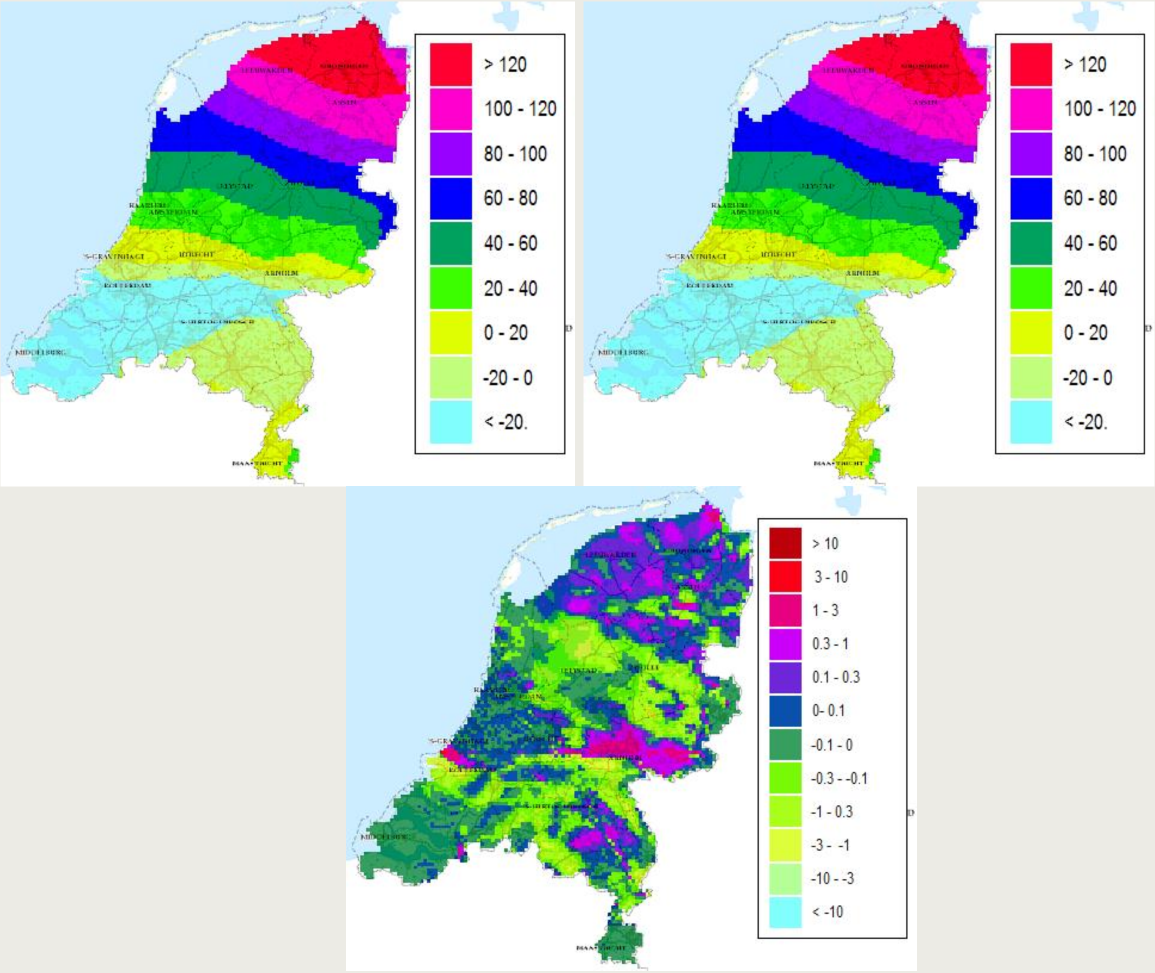

Figure 3.14: Hydraulic heads (m) in the layer above (upper left) and below (upper right) the Rupel Clay, the vertical hydraulic gradients over the Rupel Clay model layer (lower) from the ice-filled glacial valley scenario model.

This scenario of the ice-filled glacial valley has very similar results as the scenario for the cold climate with glaciation from Figure

Coarse sand-filled glacial valley
The hydraulic heads in the layer above and below the Rupel Clay and the hydraulic gradients over the Rupel Clay are shown in Figure .

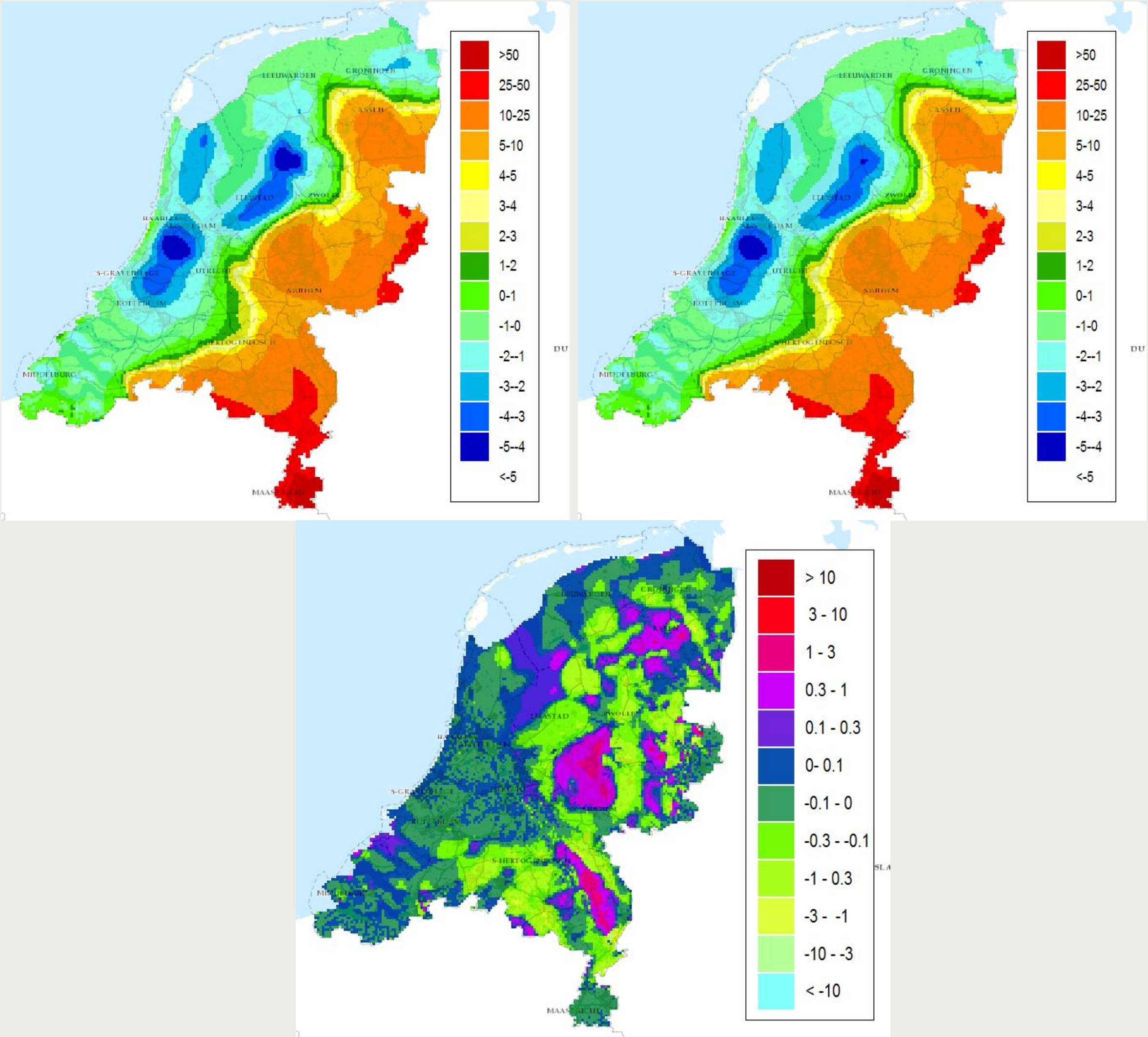

Figure 3.15: Hydraulic heads in the layer above (upper left) and below (upper right) the Rupel Clay, the vertical hydraulic gradients over the Rupel Clay model layer (lower) from the coarse sand-filled glacial valley scenario model.

In comparison with the model for the present situation the absolute hydraulic gradient over the Rupel Clay has locally increased in the vicinity of the simulated glacial valley. This increase is present for both upward and downward hydraulic gradients.

3.3.7. Results scenario 7: Fault

The hydraulic heads in the layer above and below the Rupel Clay and the hydraulic gradients over the Rupel Clay are shown in Figure .

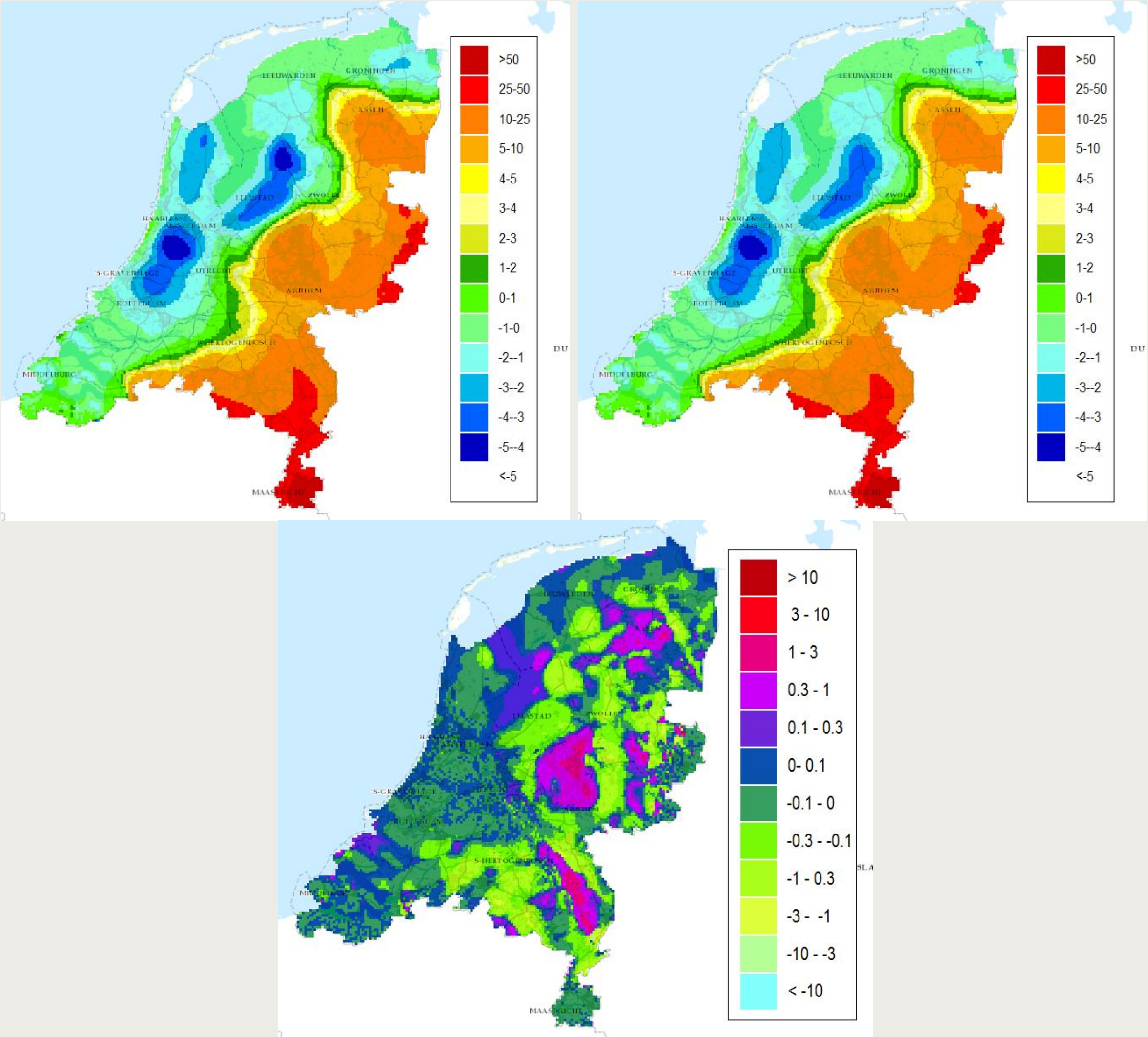

Figure 3.16: Hydraulic heads in the layer above (upper left) and below (upper right) the Rupel clay, the vertical hydraulic gradients over the Rupel Clay mode layer (lower) from the fault scenario model.

In comparison with the model for the present situation the hydraulic gradient over the Rupel Clay is only slightly changed in the vicinity of the simulated fault.

3.4. Conclusions and recommendations

3.4.1. Conclusions

From this study, the following conclusions can be drawn:

1. The groundwater flow model for the entire country has provided boundary conditions for local models for the Rupel Clay both for the present, moderate climate situation as well as for normal and altered evolution scenarios.

2. The impact of a cold period with glaciation on the hydraulic gradients over the Rupel Clay is larger than the other modelled scenarios.

3. For the different scenarios downward hydraulic gradients in the model for the present, moderate climate, situation can be reversed to upward hydraulic gradients.

4. Specific model scenario assumptions such as the location of the edge of the ice cover or the presence of active river systems in permafrost conditions are expected

to have a strong impact on the result for the hydraulic gradient over the Rupel Clay on a specific location.

3.4.2. Recommendations

From the experience gained in this study, the following recommendations can be made:

1. Validation of the model results for the present moderate climate and/or of the most sensitive model input parameters is needed.

2. For some geological scenarios, water fluxes over the boundaries of the present model are very important and they may be obtained from a model with a larger domain in future studies. An example is the cold climate without ice cover (permafrost) scenario in which the effect of rivers beyond the present model boundary such as the Ems in Germany and a river system north and west of the Netherlands over the present bottom of the North Sea is expected to influence the water flow near the present model boundaries considerably.

3. The effect of the interplay between the different geological conditions and their temporal variability should be analyzed in more detail. Examples are the depth of the permafrost in front of a slowly backward and forward moving ice cap, and the quantity and distribution of future erosion related to glaciation.

4. The translation from geological scenarios to hydrogeological models required many subjective choices. These choices required insight from many different disciplines. In this study, these choices were made from the viewpoint of the hydrogeologic modelling after gaining some insight into the other disciplines and these choices agreed upon by partners from other work packages within the OPERA program. Some of these choices needed to be adjusted by analyzing intermediate model results. For the future, a thorough review of the required and relevant model assumptions as well as the intermediate and final results by experts from the different disciplines is recommended.

4. Future groundwater flow and permafrost growth and degradation

4.1. Introduction

The permafrost depth modelling performed in OPERA Task 4.1.2 (Ten Veen et al., 2015; Govaerts et al., 2015) provided insight into the development of the permafrost depth in the Netherlands, using a best estimate temperature curve of the Weichselian as an analogue for the future. For Weichselian analogue conditions the modelling results indicated permafrost depths between 140-180 m for the Netherlands. Taking into account various sources of uncertainty, stochastic calculations point out that permafrost depth during the coldest stages of a glacial cycle such as the Weichselian, for any location in the Netherlands, would be between 120-200 m at the 2σ level. Govaerts et al. (2015) stated that in any case, permafrost would not reach depths greater than 270 m. They also found that most sensitive parameters in permafrost development are the mean annual air temperatures and porosity, while the geothermal flux is the crucial parameter in permafrost degradation once temperatures start rising again. These permafrost depth modelling studies did not take into account the interaction of groundwater flow and permafrost growth and degradation. This chapter describes the research executed by SCK-CEN concerning the mutual influence of groundwater flow and permafrost growth and degradation.

4.2. Theoretical background

4.2.1. Groundwater flow in freezing soils

Groundwater flow velocities are calculated using Darcy's law:

$$u = -\frac{K_h K_{res}}{\rho_w g} \nabla p \qquad (1)$$

With u the Darcy velocity (m/s), K_h hydraulic conductivity (m/s), K_{res} a multiplication factor which corrects the initial conductivity for the ice content of the soil, ρ_w is density of water (kg/m^3), g the gravitational acceleration (m/s^2), and p pressure (Pa).

When the pore fluids freeze, the hydraulic conductivity will be strongly reduced. This reduction factor K_{res} is implemented using a Heaviside function (S-shaped curve) depending on the water saturation. In order to ensure numerical stability, even a fully frozen soil is still assigned a so-called residual fraction of the initial hydraulic conductivity. The calculation has been done for different values of this residual conductivity in order to test the sensitivity of the flow field to this parameter.

Density and viscosity changes because of temperature changes are not taken into account (due to the relatively small temperature range).

4.2.2. Heat transfer in freezing soils

To describe heat transport in the subsoil of the Netherlands, the following two-dimensional enthalpy conservation equation is used with heat transport occurring by advection and conduction.

$$C_{eq} \frac{\partial T}{\partial t} + \nabla \cdot \left(-\lambda_{eq} \nabla T \right) + C_w u \cdot \nabla T = Q \qquad (2)$$

where C_{eq} is the effective volumetric heat capacity (J/K·m³), T is temperature (K), λ_{eq} is the effective thermal conductivity (W/m·K), C_w is the effective heat capacity of the fluid, and Q is a heat source (W/m³).

When modelling the thermal effects of freezing and thawing, equation (2) has to include three phases: rock matrix, fluid and ice. To achieve this, the following volume fractions are defined:

$$\theta_m = 1-\theta,\ \theta_f = \theta\cdot\Theta,\ \theta_i = \theta-\theta_f \tag{3}$$

The subscripts *f, i* and *m* account for the mixture between solid rock matrix (*m*), fluid-filled pore space (*f*) and ice filled pore space (i). This mixture is characterized by porosity θ and Θ denotes the fraction of pore space occupied by fluid. As a result of the complicated processes in the porous medium, melting cannot be considered as a simple discontinuity. Θ is generally assumed to be a continuous function of temperature in a specified interval.

To avoid numerical problems, the advective heat transfer is switched off in the cells where the pore fluids are fully frozen, however note that water flow is still possible in these locations as a residual hydraulic conductivity is allowed.

4.2.3. Equivalent heat capacity

When a material changes phase, for instance from solid to liquid, energy is added to the solid. This energy is the latent heat of phase change. Instead of creating a temperature rise, the energy alters the material's molecular structure. This latent heat of freezing/melting of water, *L*, is 333.6 kJ/kg (Mottaghy & Rath, 2006) which is more than one order of magnitude larger than the value used by Walravens (1996). C_{eq} is a volume average, which also accounts for the latent heat of fusion:

$$C_{eq} = \theta_m\rho_m c_m + \theta_f\rho_f\left(c_f + \frac{\partial\Theta}{\partial T}L\right) + \theta_i\rho_i\left(c_i + \frac{\partial\Theta}{\partial T}L\right) \tag{4}$$

where θ is the volumetric content, *ρ* equals density (kg/m³), and *c* is the specific heat capacity (J/(K·kg)). It includes additional energy sources and sinks due to freezing/melting using the latent heat of fusion *L* for only the normalized pulse around a temperature transition $\frac{\partial\Theta}{\partial T}$ (K^{-1}). The integral of $\frac{\partial\Theta}{\partial T}$ must equal unity to satisfy the condition that pulse width denotes the range between the liquidus and solidus [a] temperatures. This approach is similar to the one used by Mottaghy & Rath (2006), Bense et al. (2009), Noetzli & Gruber (2009), Holmén et al. (2011) and Kitover et al. (2013). Values for the porosity, density and specific heat of the different components are given in 4.1.

[a] During heating, solidus is that temperature at which a solid begins to melt. Between the solidus and liquidus temperatures, there will be a mixture of solid and liquid phases. Just above the solidus temperature, the mixture will be mostly solid with some liquid phases. Just below the liquidus temperature, the mixture will be mostly liquid with some solid phases.

Table 4.1: Properties of the different components of the subsoil.

Parameter	Water	Ice	Rupel Clay Matrix	Sand Matrix
Density [kg/m³]	997	918	2803	2358
Porosity	-	-	0.39	From TNO data sheet
Specific Heat [J/(kg K)]	4185	1835	820	800
Thermal conductivity [W/(m K)]	0.54	2.37	1.98[b]	3.00

The values of the specific heat of the Rupel Clay matrix are obtained from the ATLAS study (Cheng et al., 2010), where the Boom Clay was studied. The equivalent heat capacity then adds up to 1443 J/(kg K) and 981 J/(kg K) for the fully unfrozen and frozen state respectively. This is in the same range as the values used by Marivoet & Bonne (1988) 1400 and 960 J/(kg K), and Kömle et al. (2007), 1266 and 977 J/(kg K) for clay sediments.

The value of the sand matrix is set to a value inside the ranges which are found for quartz minerals and sands (see Mallants, 2006 and references therein). For sandy soils, the equivalent heat capacity adds up to 1319 J/(kg K) and 937 J/(kg K) for the fully unfrozen and frozen state respectively when a porosity of 30% is assumed.

4.2.4. Heat conductivity

In case of a phase change at a single temperature, thermal conductivity is not continuous with respect to temperature. However, considering the freezing range in rocks, we use equation (2) and (3) for taking into account the contributions of the fluid and the ice phase. Since the materials are assumed to be randomly distributed, the weighting between them is realized by the square-root mean, which is believed to have a greater physical basis than the geometric mean (Mottaghy & Rath, 2006).

$$\lambda_{eq} = \left(\theta_m \sqrt{\lambda_m} + \theta_f \sqrt{\lambda_f} + \theta_i \sqrt{\lambda_i} \right)^2 \qquad (5)$$

Values for the thermal conductivity of the different components are given in 4.1.
The values of the thermal conductivity of the rock matrix of Rupel clay and sand are chosen in the same order of magnitude of the values used by Bense et al. (2009) and Mottaghy & Rath (2006), who used respectively 4.0 W/(m K) and 2.9 W/(m K) for a generic sediment rock species.

For Rupel clay, the equivalent thermal conductivity then adds up to 1.31 J/(kg K) and 2.03 J/(kg K) for the fully unfrozen and frozen state respectively. The conductivity value of unfrozen Rupel Clay is thus equal to the thermal conductivity obtained for Boom Clay from the ATLAS 3 study (Cheng et al., 2010).

In sandy soils, the equivalent thermal conductivity is 2.05 W/(m K) and 2.80 W/(m K) for the fully unfrozen and frozen state respectively. The values are in the same range as the values found in Mallants (2006) and references therein. The value for the frozen state is significantely lower than the one used by Walravens (3.60 J/(kg K)).

[b] This value has been chosen so the effective thermal conductivity equals 1.31 J/(kg K), which is the vertical thermal conductivity of Boom Clay obtained during the ATLAS study.

4.3. Modelling approach

The heat transport equation is implemented in COMSOL multiphysics 4.4, Earth Science Module (2014), together with all the correlations for the thermal properties. Because the thermal properties differ between the frozen and unfrozen state, a variable Θ is created, which goes from unity to zero for fully unfrozen to frozen. Therefore, the effective properties switch with the phase through multiplication with Θ.

The switch in Θ from 0 to 1 occurs over the liquid-to-solid interval (0.5°C to -0.5°C) using a smoothed Heaviside function to ensure numerical stability. The model implements the Heaviside function with the expression Θ = flc2hs($T-T_{trans}$,dT); where the transition temperature is T_{trans} and the transition interval for the function is dT, which is set to 1K. The pulse is the derivative of Θ with respect to temperature. $\frac{\partial \Theta}{\partial T}$ is expressed with the COMSOL Multiphysics differentiation operator, d.

4.4. Parameters, initial and boundary conditions

4.4.1. Porosity and lithology

Table 4.1: Porosity and lithology per geological layer.

Geological layer	Porosity (%)	Sand%
Holocene	35.8	100
Boxtel	38.7	100
Eem	35.6	100
Kreften	35.6	100
Drente	35.0	100
Peelo	38.2	100
Urk	38.1	100
Sterksel	28.5	100
Stamproy	58.0	100
Waalre	40.0	100
Kiezeloöliet	40.0	100
Oosterhout	37.0	100
Breda	35.0	100
Rupel Clay	37.0	0

4.4.2. Hydraulic parameters

The hydraulic parameters (horizontal and vertical hydraulic conductivity, respectively K_h and K_v) along the profile were acquired from basin modelling results (Nelskamp, pers comm 2015). Values were initially given in log(mD) and were averaged and recalculated to m/d (1 mD = 8.6×10^{-9} m/s at 15°C). The adopted hydraulic parameters for each geological layer are given in

Table 4.2.

Table 4.2: Hydraulic parameters per geological layer.

Geological layer	K_h (m/d)	K_v (m/d)
Holocene	2075	13.2
Boxtel	16.7	0.0889
Eem	14.7	0.0856
Kreften	1.75×10^{8}	2.14×10^{7}
Drente	0.0544	4.03×10^{-4}
Peelo	1.04×10^{-6}	6.72×10^{-9}
Urk	5.67	0.0363
Sterksel	3.34	0.0213
Stamproy	0.0359	2.56×10^{-4}
Waalre	6.14×10^{6}	3.98×10^{4}
Kiezeloöliet	341	2.2
Oosterhout	333	2.17
Breda	64	0.417

The highlighted values were adapted as they introduced numerical problems due to their unrealistically high values.

The value of Kreften was set the same as. The value of Waalre was set equal to that of resp. the Drente formation and Kiezeloöliet. The value of the Holocene was divided by 100 to obtain a value which is more acceptable for sandy soils.

4.4.3. Initial condition

It is assumed that the initial temperature profile at the start of the calculations, which is 120 000 years ago, is equal to present day conditions.

4.4.4. Upper boundary condition: temperature evolution of a future glacial cycle

The upper boundary condition is the temperature evolution of a future glacial cycle for which the Weichselian glacial is taken as an analogue. The temperature curve from Beerten (2011) and Govaerts et al. (2011) was significantly modified to include better estimates of the mean annual air temperature. Moreover, a minimum and maximum temperature curve was produced as input for stochastic simulations.

Palaeoclimatic and palaeoenvironmental evidence is preserved indirectly in biotic and abiotic records in sedimentary sequences (Huijzer and Vandenberghe, 1998). In the multiproxy approach for climate reconstruction, evidence of different origin is collected, analysed and synthetised, and converted into climate parameter values. Proxy data relevant to the reconstruction of the Weichselian climate include aeolian, fluvial and glacial deposits and/or landforms. Periglacial structures (frost cracks, cryoturbations, ice-wedge casts) are important abiotic proxy data within these sediments and are often the primary source of evidence. Botanical (pollen and plant macrofossils) and faunal evidence (beetles, ostracods, molluscs and vertebrates) are used as biotic proxy data from these deposits.

The temperature curves and data used in this study are shown in Figure 4.3 and

Table 4.3. Best estimates for the mean annual air temperature (MAAT) during isotope stage 5 is based on pollen data from van Gijssel (1995), but replotted against a more recent chronostratigraphical framework for the Weichselian glaciation (see Busschers et al., 2007, and references therein). The main features of the MIS5 climate (marine isotope stage 5) is the relatively mild stadials 5b and 5d, with an MAAT of -2°C, and the relatively cold interstadials 5c and 5a, with an MAAT of +4°C. The first period with continuous permafrost development in the Netherlands is MIS4, with MAAT values dropping to as low as -4°C and even -8°C for the end of MIS4, based on periglacial deformation phenomena (Huijzer and Vandenberghe, 1998). The following MIS3 is characterised by a somewhat milder climate, showing less periglacial deformation of the subsoil. Analysis of flora and fauna preserved within MIS3 sediments, and the type and nature of periglacial deformation shows that some interstadials might have reached an MAAT between 0°C and +6°C (e.g., Upton Warren, Hengelo and Denekamp interstadials; Huijzer and Vandenberghe, 1998, Busschers et al., 2007 and van Gijssel, 1995), and several stadials would have reached an MAAT as low as -4°C (e.g., Hasselo stadial; Busschers et al., 2007). Subsequently, the climate evolves towards the Late Glacial Maximum, which is situated in MIS2. Data for this stage is mainly derived from Renssen and Vandenberghe (2003) and Buylaert et al. (2008), and is based on the presence and type of periglacial deformation phenomena. The MAAT for the period between 28 ka and 15 ka would not have exceeded 0°C, while some periods show MAAT values as low as -8°C to -9°C. Finally, the end of MIS2 is characterised by a stepwise trend towards global warming, reaching present-day MAAT values of around +10°C for MIS1.

As already mentioned, the temperature data presented here are used as soil input data, without taking into account any buffering from vegetation or soil. This means that the best estimate permafrost calculations are in fact conservative estimates, whereas the influence from vegetation and snow is implicitly accounted for in the stochastic calculations.

Furthermore, the model is conservative as well with respect to the following phenomena. Firstly, vadose zone hydrology is neglected, but during very cold stadials, infiltration would probably be so low as to lower the groundwater table significantly. Next, outfreezing of pore water salt would lower the speed of permafrost development because more latent heat is needed to freeze water with elevated salt concentrations.

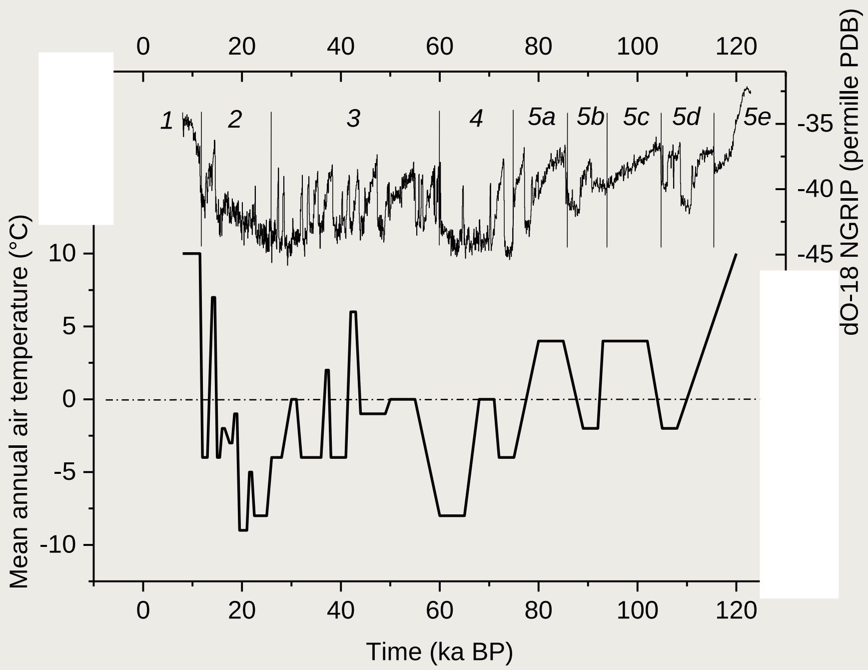

Figure 4.3: Best estimate temperature evolution for the Weichselian glaciation, which is taken as an analogue for a future glacial climate in permafrost calculations. The curve is based on data from van Gijssel (1995), Huijzer and Vandenberghe (1998), Renssen and Vandenberghe (2003), Busschers et al. (2007) and Buylaert et al. (2008). Marine isotope stages (numbering 1 to 5e) are taken from Busschers et al. (2007) and references therein. The oxygen isotope curve is reproduced from NGRIP (2004) data.

Table 4.3: Mean annual air temperature (MAAT) data for the Weichselian glacial. Based on Guiot et al. (1989), van Gijssel (1995), Huijzer and Vandenberghe (1998), Renssen and Vandenberghe (2003), Busschers et al. (2007) and Buylaert et al. (2008). Several stadials and interstadials are explicitly mentioned (Upton Warren, Hasselo, Hengelo, Denekamp, LGM, Bölling-Alleröd, Younger Dryas).

Time BP (ka)	Marine isotope stage	Best estimate (°C)
120	5e	10
108	5d	-2
105	5d	-2
102	5c	4
93	5c	4
92	5b	-2
89	5b	-2
85	5a	4
80	5a	4
75	4	-4
72	4	-4
71	4	0
68	4	0
65	4	-8
60	4	-8
55	3	0
50	3	0
49	3	-1
44	3	-1
43	3 (Upton Warren)	6
42	3	6
41	3 (Hasselo)	-4
38	3	-4
37.5	3 (Hengelo)	2
37	3	2
36	3	-4
32	3	-4
31	3 (Denekamp)	0
30	3	0
28	3	-4
26	3	-4
25	2	-8
22.5	2	-8
22	2	-5
21.5	2	-5
21	2 (Late Glacial Max.)	-9
19.5	2	-9
19	2	-1
18.5	2	-1
18	2	-3
17.5	2	-3
16.5	2	-2
16	2	-2
15.5	2	-4
15	2	-4
14.5	2 (Bölling-Alleröd)	7

14	2	7
13	2 (Younger Dryas)	-4
12	2	-4
11.5	1	10
8	1	10

4.4.5. Lower boundary condition: geothermal flux

At the base of the model a heat flow boundary of 0.06 W/m^2 is applied representing an average value for geothermal heat flow used in previous 1D calculations (Ten Veen et al., 2015).

4.5. Steady State groundwaterflow simulation benchmark

4.5.1. Objective

In order to benchmark the groundwater flow simulations done within COMSOL 4.4 (Comsol, 2014), a parallel model was built in MODFLOW2005 (Harbaugh, 2005), which is a modular groundwater flow model. The results will correspond to initial groundwater flow in absence of temperature effects.

4.5.2. Conceptual model

A cross section was selected from the Dutch geological model (Figure), extending from the east of the Netherlands (river IJssel) until the coast in the west. In the vertical direction, the geological model extends from the topography at the top to the top of the Rupel Formation. The geological model is given in Figure 4.4.

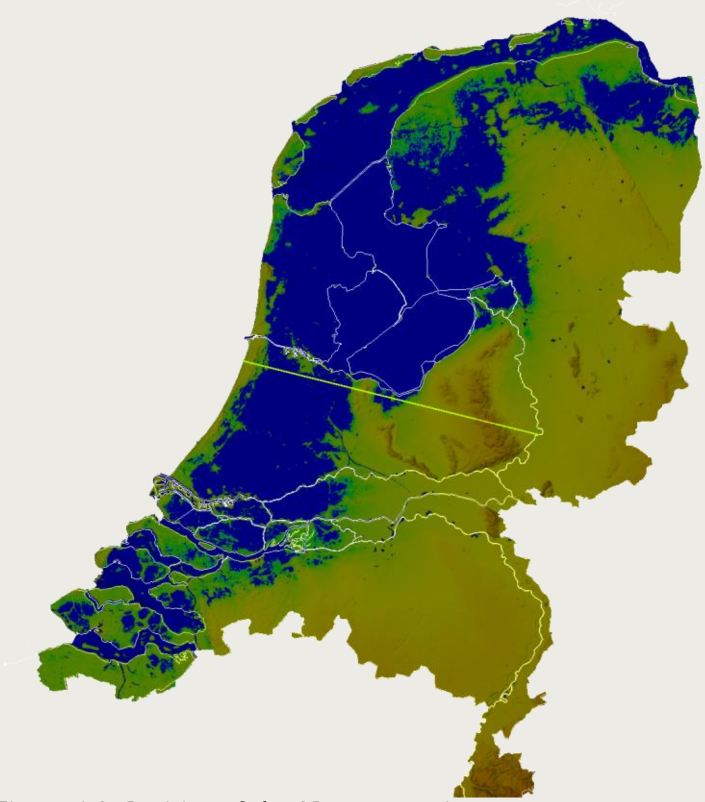

Figure 4.2: Position of the 2D cross section.

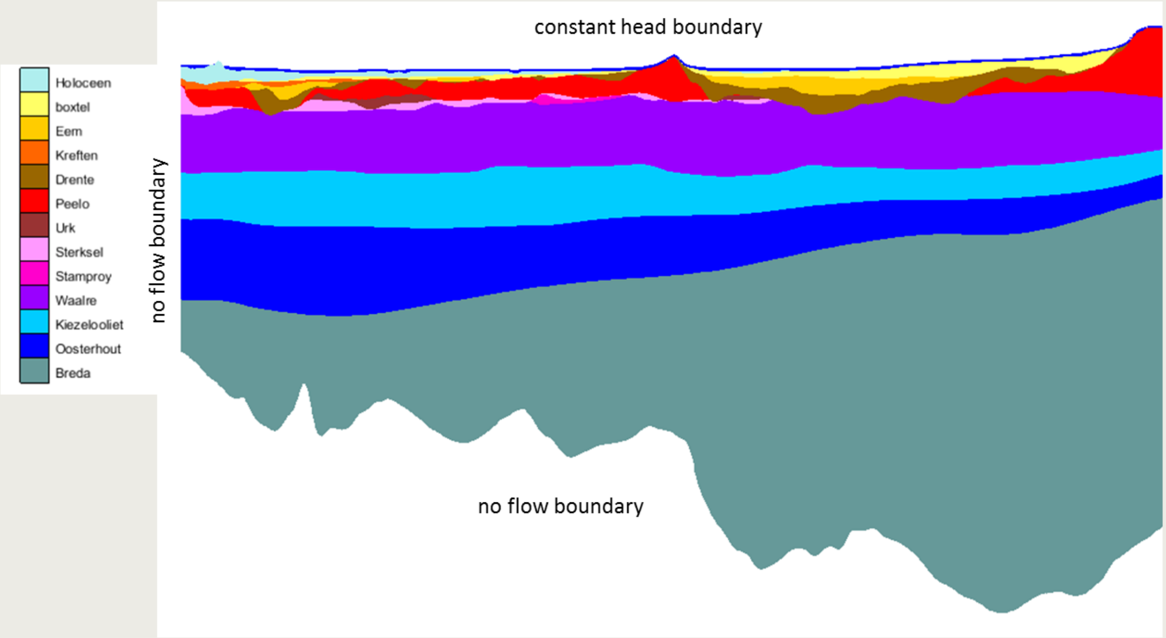

Figure 4.4: Geological model and boundary conditions implemented in the groundwater flow model. The blue line at the top indicates the simulated water table.

The boundary conditions for the model are chosen as follows (Figure 4.4):

- At the bottom and the sides of the model, a no flow boundary is assumed. The bottom of the model is considered an impermeable boundary. In the east, the model is cut off at the Veluwe, which is assumed a no-flow boundary. At the west, no outflow to the sea is assumed.
- At the top, a constant head boundary (constant water table) is assumed. The constant head values were acquired from a steady-state simulation where in each top cell, a drain was inserted in the model as well as an estimated recharge value of 290 mm/y. The simulated water table is indicated in Figure 4.4.

The stratigraphy is formed by a rather complex series of sandy and clayey sediments. Given this complexity of the hydrostratigraphic model and to avoid numerical problems which would occur if numerical layers follow the hydrostratigraphy (i.e. zero thicknesses at discontinuities), the hydrogeologic unit flow package (HUF) (Anderman and Hill, 2000) was used in the model. The HUF Package is an internal flow package that allows defining the geometry of the system hydrogeology explicitly using hydrostratigraphic units. The vertical hydrostratigraphic unit geometry can differ from the vertical geometry of the numerical model grid. The HUF package calculates (interpolates where necessary) the effective hydraulic properties (conductances) for the entire computational grid based on the hydraulic properties defined for the hydrostratigraphic units. The use of this package is particularly useful in a situation where several hydrostratigraphic units wedge out (e.g. exist only in a part of the area), as is the case here.

MODFLOW 2005 uses the finite differences method for solving a 3D groundwater flow problem. This method implies space discretization into rectangles of constant width/length along respectively columns and rows. In the vertical direction, the thickness of the cells may vary, although a large variation in thickness may result in computational instability. We chose a regular horizontal schematization with cell dimensions (column widths) of 100 m. In the vertical direction, the model includes 120 numerical layers. As we use the HUF package (Anderman and Hill, 2000) of MODFLOW-2005, the numerical grid is defined independently of the hydrostratigraphic unit geometry.

4.5.3. Results benchmark

For the MODFLOW simulations, we chose a regular horizontal schematization with cell dimensions (column widths) of 100 m. In the vertical direction, the model includes 20 numerical layers. The numerical layers have an unequal distance: at the top, the discretization is finer and progressively coarsens with depth (Figure 4.5). The number of active cells in the model equals 19040.

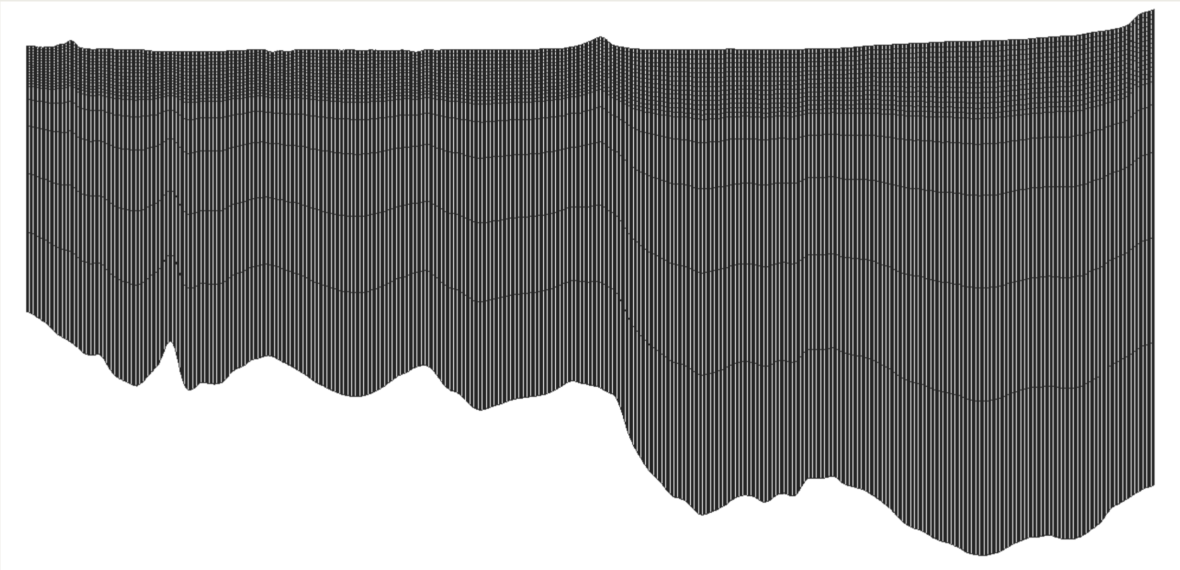

Figure 4.5: Spatial discretization of the MODFLOW model.

The COMSOL model is meshed more densely. As opposed to MODFLOW, the COMSOL grid needs to follow the irregular boundaries of the different formations. Furthermore, the coupled non-linear flow and heat transfer computations require a denser mesh in order to avoid numerical oscillations. This results in a mesh consisting of 600 000 finite elements.

Figure 4.6 shows the comparison of the logarithm of the Darcy velocity vector at a vertical cut line in the middle of the computational 2D domain. The agreement between both codes is reasonable as they show similar trends in the groundwater velocity. However, the absolute values are not completely similar. This can be attributed to the much coarser meshing of MODFLOW, the difference in numerical method (finite elements vs. finite differences) and the manner in which both codes deal with the strongly conflicting hydraulic conductivities at the boundaries of the formations.

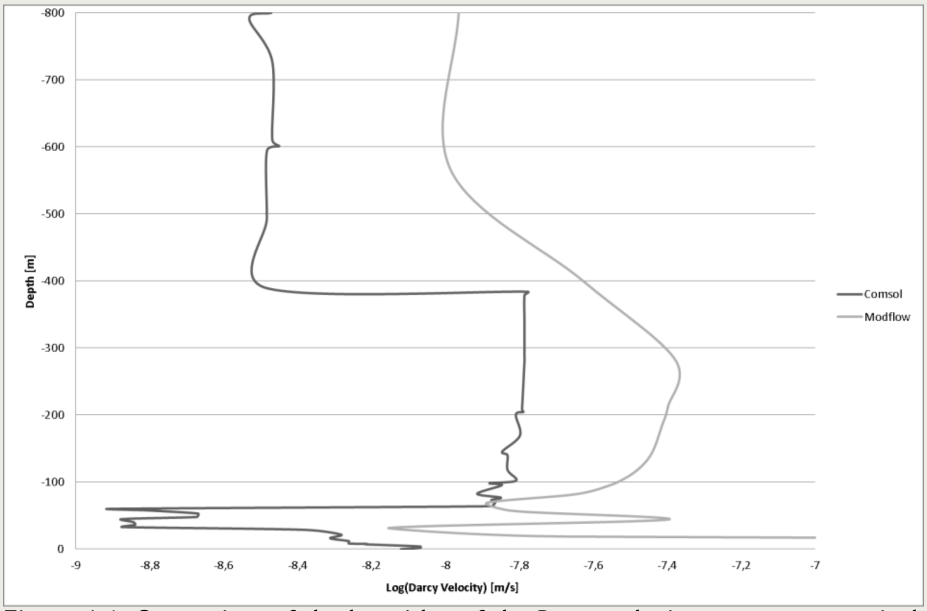

Figure 4.6: Comparison of the logarithm of the Darcy velocity vector at a vertical cut line in the middle of the domain.

4.6. Coupled groundwater and permafrost

4.6.1. Model setup and geometry

The model geometry is the same as depicted in Figure 4.4. As an extra feature, four rivers are added to the top of the domain. These rivers are 300m wide and the surface temperature at this location will follow the same temperature evolution as the rest of the surface albeit that temperatures will never drop below the freezing point there. This will allow the development of talik zones underneath the rivers which could influence the permafrost formation and recharge to the aquifers underlying the frozen topsoils. Through the transient simulation a constant head boundary (constant water table) is assumed. The constant head values were acquired from a steady-state simulation in MODFLOW2005 where in each top cell, a drain was inserted in the model as well as an estimated recharge value of 290 mm/y.

Location of the 4 rivers given as kilometers from the left (west) boundary.

Spaarne: (611541,5803124), 7.7 km
Amstel: (630075,5798510), 26.8 km
Vecht: (641520,5795656), 38.6 km
Eem: (657922,5791563), 55.5 km

4.6.2. Simulation cases

Series 1: Only Conductive heat transfer - sensitivity analysis by varying K_{res} = 1e-1, 1e-3, 1e-6, 1e-9.

It is known from lab scale test that the hydraulic conductivity of soil samples reduces to essentially zero during freezing. When this reduction of the conductivity is applied to the whole formation, recharge will also drop to almost zero except where surface waters maintain open taliks. It is not entirely certain that this assumption holds for the whole formation. Therefore, different values of the residual permeability are tested to investigate the effect of this assumption on the flow velocities in the formations above the Rupel clay. The first set of simulations considers the impact of a Weichselian temperature cycle on a transect of about 100 km wide and 1 km deep in which heat transfer only occurs by conduction (in order to speed up the simulations). In this way, the groundwater flow is influenced by the heat transfer and freezing processes (through conductivity reduction), but the flow does not influence the heat transfer.

Series 2: Advective and conductive heat transfer - sensitivity analysis by varying Kres = 1e-3, 1e-6.
Model setup and geometry are identical to series 1, only heat transfer can occur through conduction and advection.

4.6.3. Results

Permafrost depth

Series 1: Conductive heat transfer
The calculated permafrost depths are in the same range as the ones obtained from the one-dimensional simulations performed in (Ten Veen et al., 2015). Maximum permafrost depths (50% frozen) are in the range of 140 m (Figure 4.7). Differences can be attributed to the coarser meshing (due to the problem size) and the presence of the rivers and underlying taliks. As the water flow does not influence the heat transfer in this serie of calculations, the permafrost evolution is identical for all values of K_{res}.

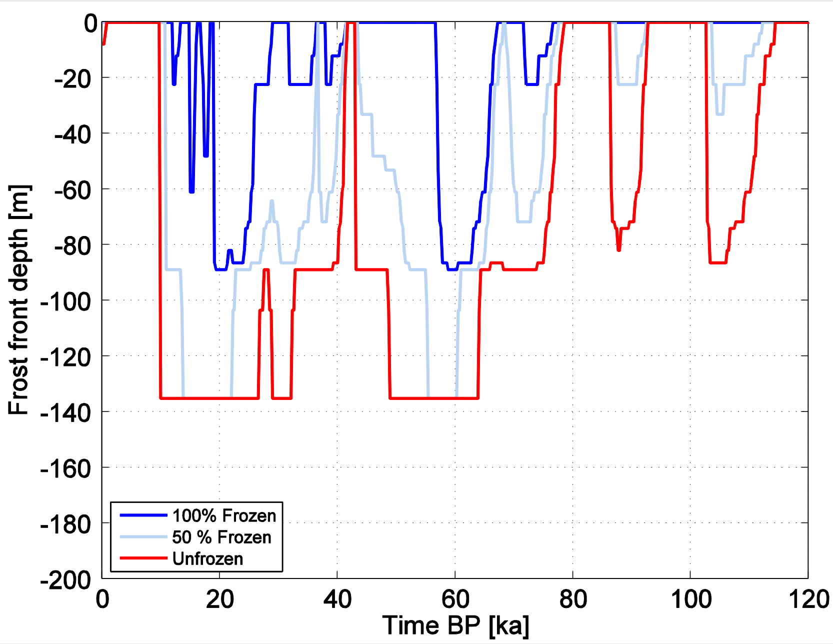

Figure 4.7: Permafrost progradation during a simulation of the Weichselian glaciation for series 1.

Series 2: advective heat transfer.
Figure 4.8 and Figure 4.9 show the results of the simulations in which advective heat transfer is taken into account, respectively for K_{res} = 1e-3 and 1e-6. The results are comparable to the case with only heat conduction. The main difference is the depth of the fully frozen front, which extends to about 100 m deep during the coldest periods. This can be explained by the fact that a strong downward flow exists in the first 100 m (see Figure 4.11). Due to the advective heat transport the first 100m will get cooled down more quickly as the surface temperature approaches 0°C. When the soil is completely frozen, the permeability drops considerably and furthermore advective heat transport is switched off in these cells *(1. As this is physically correct- permafrost ice does not flow - and 2. to avoid numerical problems)*. From then on, the cold must be transported by conduction, which limits the further progradation of the 100 % frozen front. Figure 4.12 shows a

snapshot of the fluid fraction and temperature isolines at a time of 20 ka BP (e.g. the time when the maximum permafrost depth occurs). Underneath the rivers, unfrozen zones still exist which connect the surface to the subpermafrost aquifers.

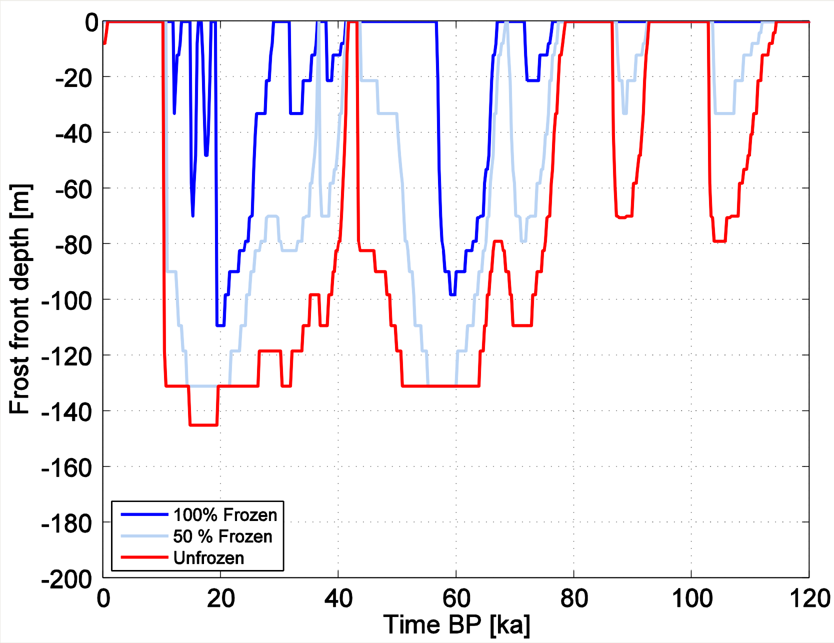

Figure 4.8: Permafrost progradation during a simulation of the Weichselian glaciation for series 2 (K_{res}=1e-3).

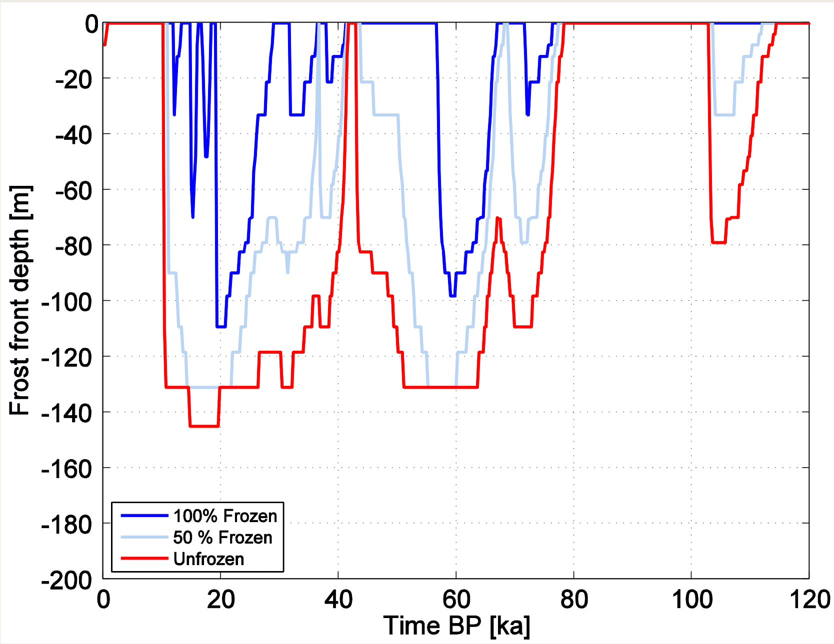

Figure 4.9: Permafrost progradation during a simulation of the Weichselian glaciation for series 2 (K_{res}=1e-6).

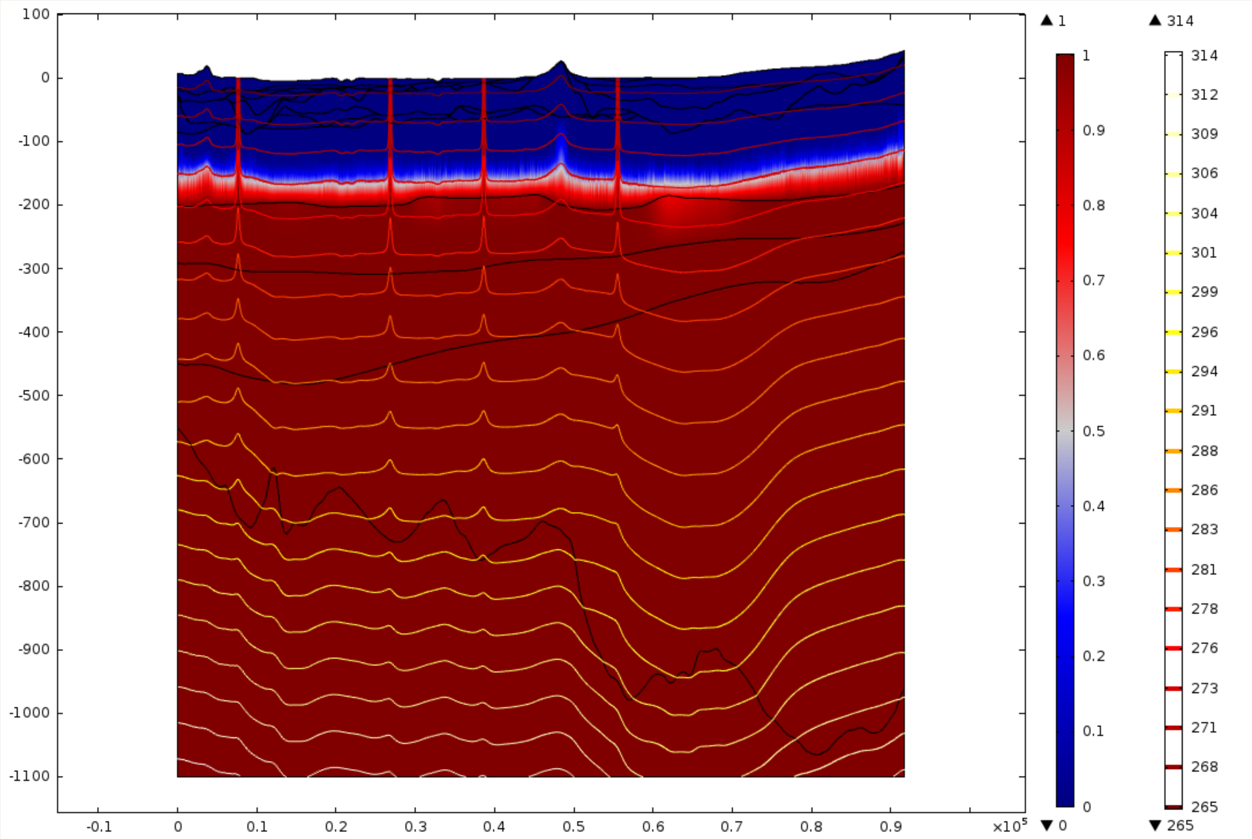

Figure 4.12: 2D view of Temperature (isolines) and fluid fraction (surface plot where 0= 100% frozen) for series 2 (K_{res}=1e-6) at 20 ka BP.

Flow velocities

Series 1

The initial flow profile is shown in Figure 4.11. The evolution of the flow velocities throughout the simulation of a Weichselian temperature cycle is monitored in three observation points within three formations (Breda, Oosterhout, Kiezeloöliet). Their locations are indicated using black dots.

Figure 4.14, Figure 4.15 and Figure 4.16 show the ratio of the temporal Darcy velocities to the initial velocity during the course of the simulation for each value of K_{res} and for each observation point.

It can be seen that during the coldest periods, which corresponds to deepest permafrost fronts, the velocity in these locations drops with several orders of magnitude. At these times the maximum velocity reduction scales relatively well with the value of K_{res} for the Breda and Oosterhout formations. This is expected as the hydraulic heads at the top are kept fixed and the flow velocities in these layer are determined completely by effective conductivity of the layers above it, which controls the vertical inflow into the aforementioned aquifers.

The situation in the Kiezeloöliet is slightly more complex. The permafrost front stops halfway in the formation. Due to the differences in thermal conductivities, porosities and flow velocities in the formations above it, the shape of the frozen front is more or less irregular. This will create a diverse pattern of hydraulic conductivities above and around the observation point.

Together with the nearby presence of a taliks, preferential flowpaths arise in the Kiezeloöliet. It could explain why the velocities at the observation point are more strongly reduced than what would be expected from the value of K_{res}. The close-up in Figure 4.17 shows that the water flow is diverted around the observation point.

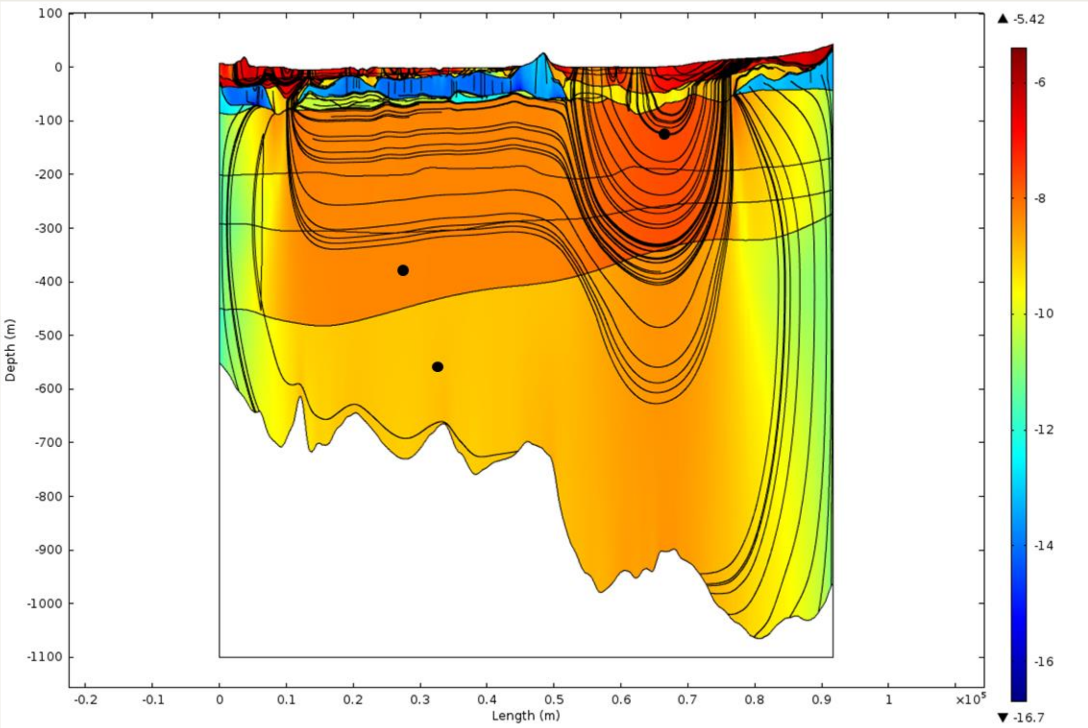

Figure 4.11: Initial steady state velocity field (logarithm of Darcy velocity and streamlines). Observation points are indicated as black dots.

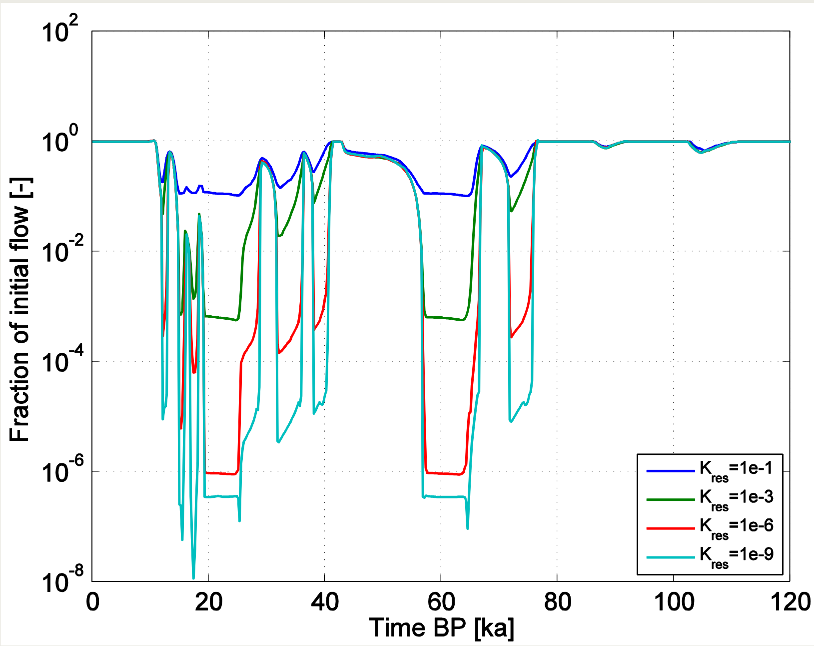

Figure 4.14: Evolution of the relative size of the flow velocity in the Breda Formation (series 1).

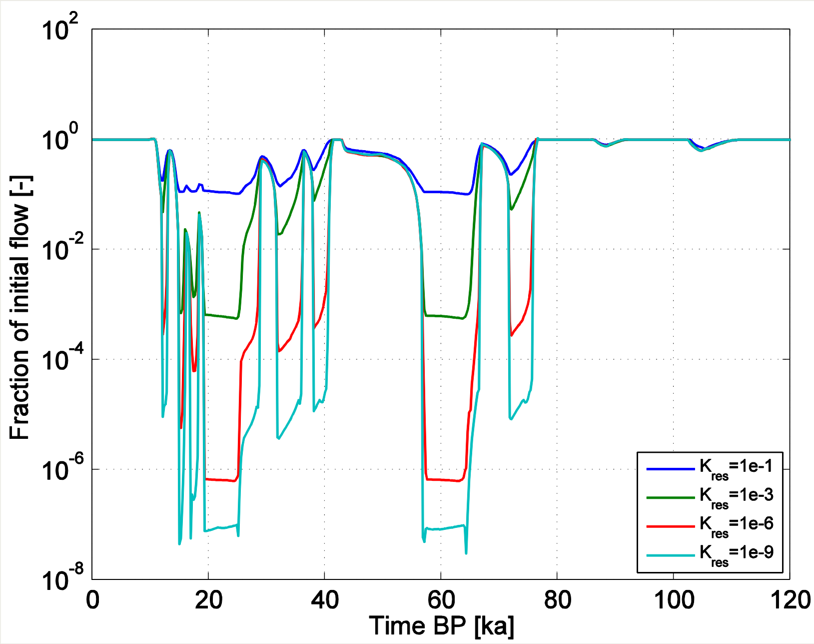

Figure 4.15: Evolution of the relative size of the flow velocity in the Oosterhout Formation (series 1).

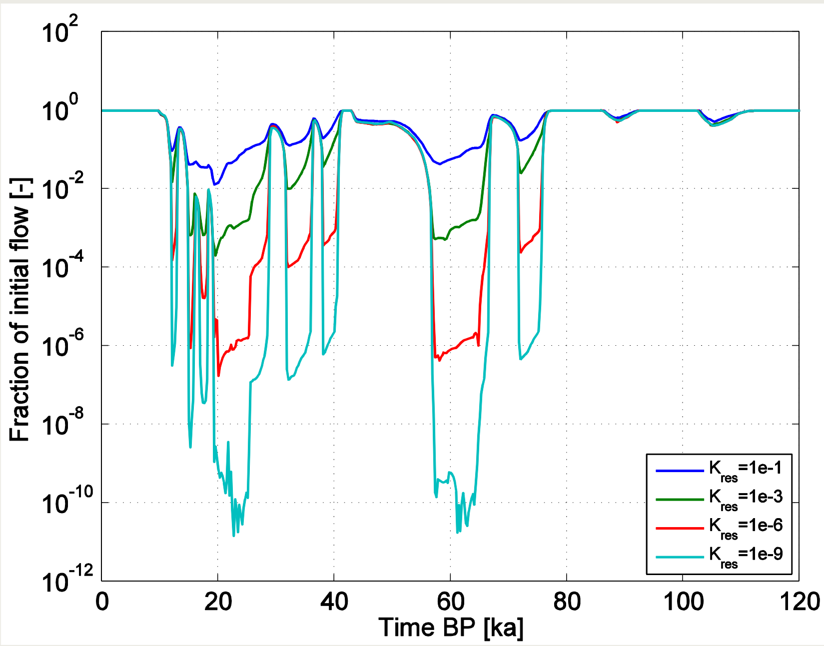

Figure 4.16: Evolution of the relative size of the flow velocity in the Kiezeloöliet Formation (series 1).

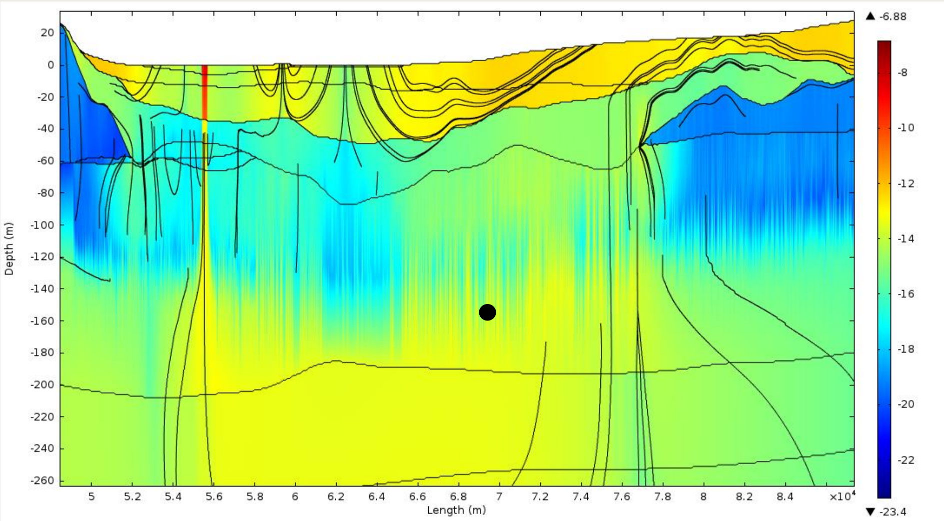

Figure 4.17: Velocity field in the Kiezeloöliet Formation at a time of 20 ka BP (logarithm of Darcy velocity and streamlines). The observation point is indicated as a black dot.

Series 2

Figure 4.18 and Figure 4.19 show the evolution of the relative velocity in the three aforementioned formations, this time for both simulations of series 2. The same conclusions can be drawn as from the series 1 simulations. The velocities in the lower two formations scale well with the reduction factor, while the velocities in the Kiezeloöliet observation point are even more reduced due to the deeper penetration of the fully frozen front.

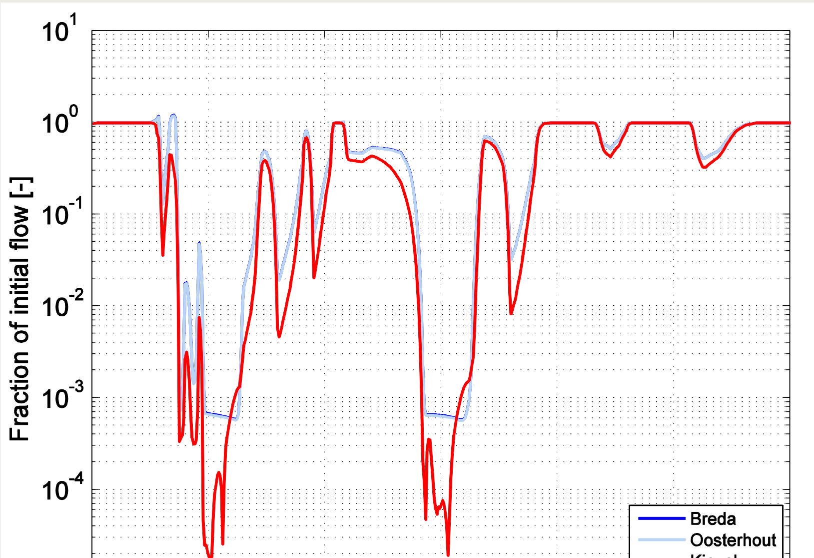

Figure 4.18: Evolution of the relative size of the flow velocity in the Breda, Oosterhout and Kiezeloöliet formations (series 2, K_{res}=1e-3).

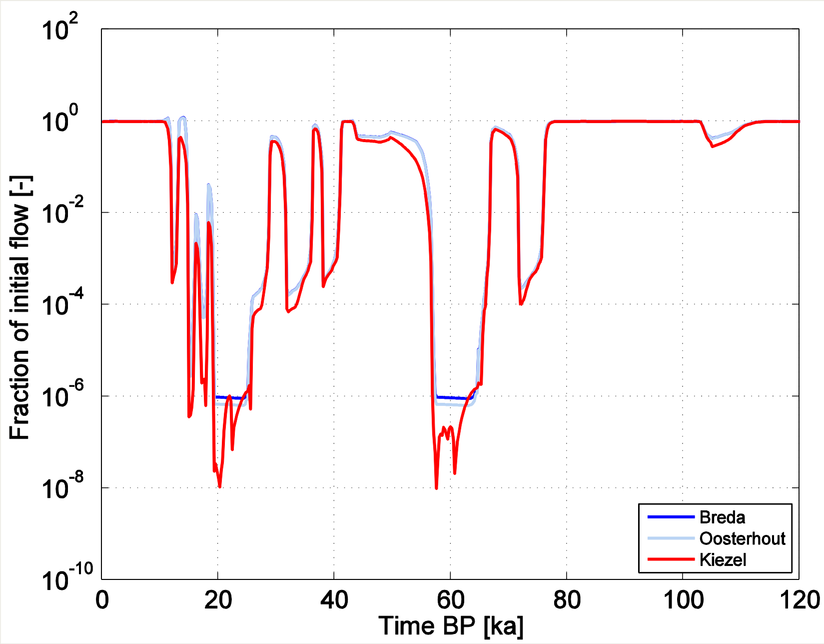

Figure 4.19: Evolution of the relative size of the flow velocity in the Breda, Oosterhout and Kiezeloöliet formations (series 2, K_{res}=1e-6).

4.7. Conclusions

The main conclusions resulting from the coupled groundwater and permafrost simulations are:

1. 2D simulation results for conductive heat transfer conditions show that the penetration of the permafrost (50% frozen) reaches a maximum depth of 140 m. This result is in the same range as the depths obtained from 1D simulations reported in Ten Veen et al. (2015).

2. 2D simulation results taking advective heat transport into account show that the penetration of the permafrost (50% frozen) front reaches maximum depths comparable to the ones resulting from the 2D conductive heat transfer simulations. The maximum depth of the fully frozen front (100%) extends to somewhat greater depths under advective flow conditions.

3. 2D simulations for both conductive and advective heat transfer conditions show that the groundwater flow velocities drop with several orders of magnitude in layers overlying the Rupel (Breda, Oosterhout and Kiezeloöliet) during the coldest periods, i.e. periods associated with the deepest permafrost.

The above conclusions indicate that permafrost will not reach the Rupel Clay Member at a generic depth of 500 m under Weichselian temperature conditions.

5. Future impact of ice sheet loading on pressure conditions

5.1. Introduction

The impact of advancement and retreat of continental ice sheets on hydraulic boundary conditions and hydraulic properties of subsurface layers results from the combined influence of changed hydraulic heads or water fluxes at the surface during glaciation (including ice sheets and permafrost conditions, and erosion and deposition related to glaciation), direct glacial loading by ice weight, flexural loading resulting from bending of the lithosphere by ice weight and to a minor extent to changes in thermal boundary conditions (Neuzil, 2012).

Chapters 3 and 4 describe the effects of glaciations and permafrost conditions on the groundwater flow system taking into account the influence of changed hydraulic boundary conditions. Chapter 3 included simulations of the influence on hydraulic head gradients over the Rupel Clay Member due to changed boundary conditions for glacial valley scenarios based on findings of Ten Veen et al. (2015). Ten Veen et al. (2015) also indicated that it is very unlikely that the Rupel Clay Member itself will be affected by subglacial erosional processes. Here focus is on investigating the effect of direct glacial loading and unloading on pressure conditions in the Rupel Clay Member at a generic depth of 500m. The influence of glacial erosion of the overburden of the Rupel Clay Member during glaciation cycles has not been taken into account, because at this time the quantitative estimations of such future erosion and its regional distribution are lacking.

The weight of an ice sheet adds vertical load at the ground surface, while the retreat of an ice sheet removes the load. This loading and unloading is comparable to loading by sedimentary deposition and unloading by erosion. The ice sheet and sedimentary loading and unloading will have comparable type of effects on pressure buildup and dissipation in the subsurface. When sedimentary loading is rapid and permeability poor, pore water cannot flow from the pores fast enough, and the pore water will support the ever increasing stress induced by the sedimentary load: increasing the pore pressures (creating overpressure). Lateral continuous permeable stratigraphic units (aquifers) allow dewatering in response to sedimentary loading and pore pressures remain relatively low to near hydrostatic in these units.

Basin modelling takes the impact of sedimentary loading and unloading on groundwater flow and pressure evolution into account. We use 3D basin modelling to investigate the impact of glacial loading and unloading.

5.2. Basin modelling

In order to study the impact of glacial loading on the pressure condition in the Rupel Clay Member we use the detailed 3D basin model of the northern part of the Netherlands. This model is described in detail in the report on Task 421_1 by Verweij and Nelskamp (2015). This basin model was modified to include glacial loading by ice sheets during the last two ice ages. The effects of these previous ice loading events are taken as analogues for future effects.

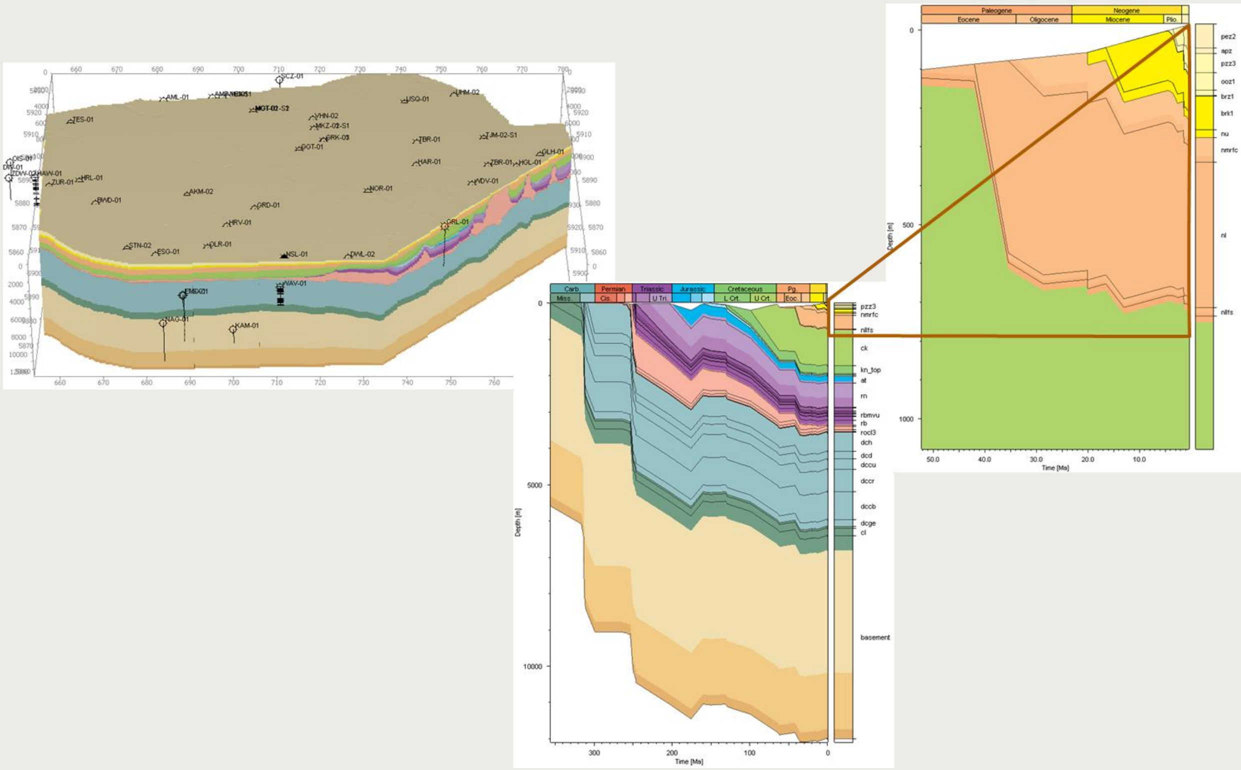

Figure 5.1: 3D basin model in northern part of the Netherlands.

The Elsterian (0.47-0.42 Ma) and Saalian (0.38-0.13 Ma) ice sheets reached the onshore area of the Netherlands (Figure 5.2). Figure 5.2 shows that the Elsterian ice sheet did not cover the whole of the area included in the 3D Basin model. The thickness of the ice sheets close to the ice margin are difficult to assess. Previous studies from the last ice age in North America suggest thicknesses along the ice margin of 100 to 1000 m, depending on the location and elevation of the ice margin (Figure 5.3; Dyke et al. 2002). Schokking (1998) estimated a 195 m thickness of the Saalian ice sheet based on his study on overconsolidation of the Pot Clay at shallow depths in the northern part of the Netherlands.

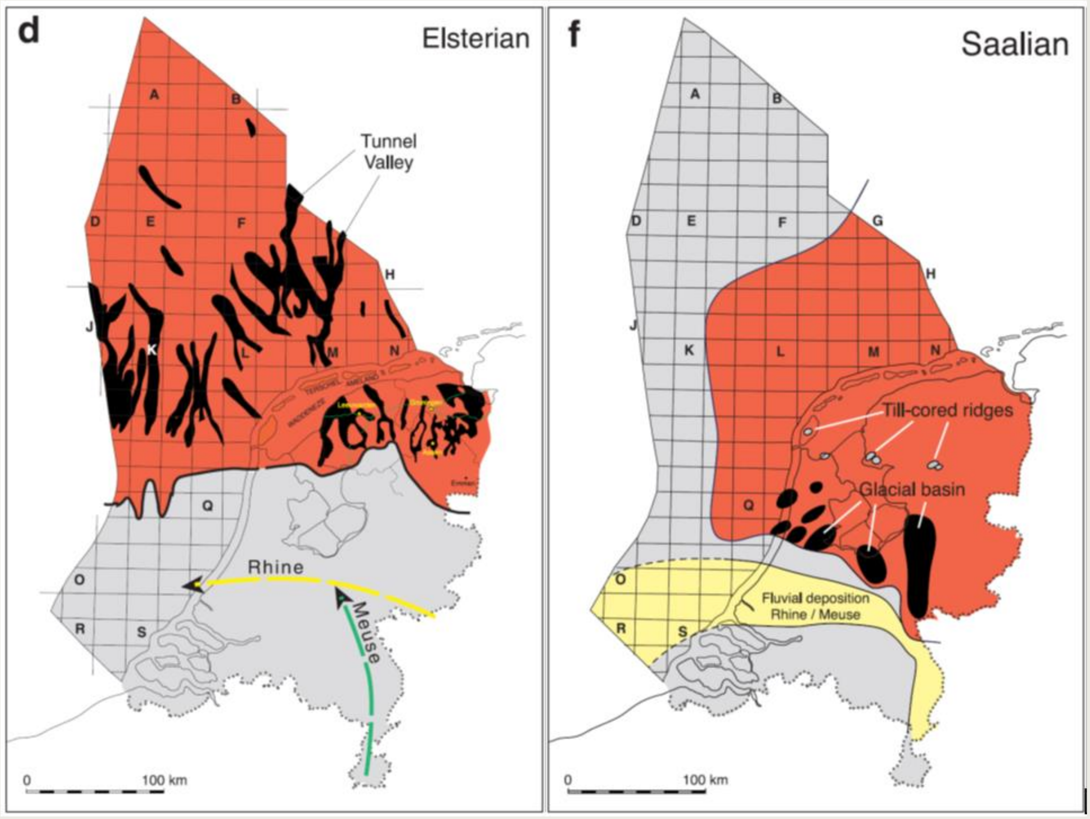

Figure 5.2: Paleogeographical maps of the extent of the Elsterian and Saalian ice sheets (From De Gans, 2007).

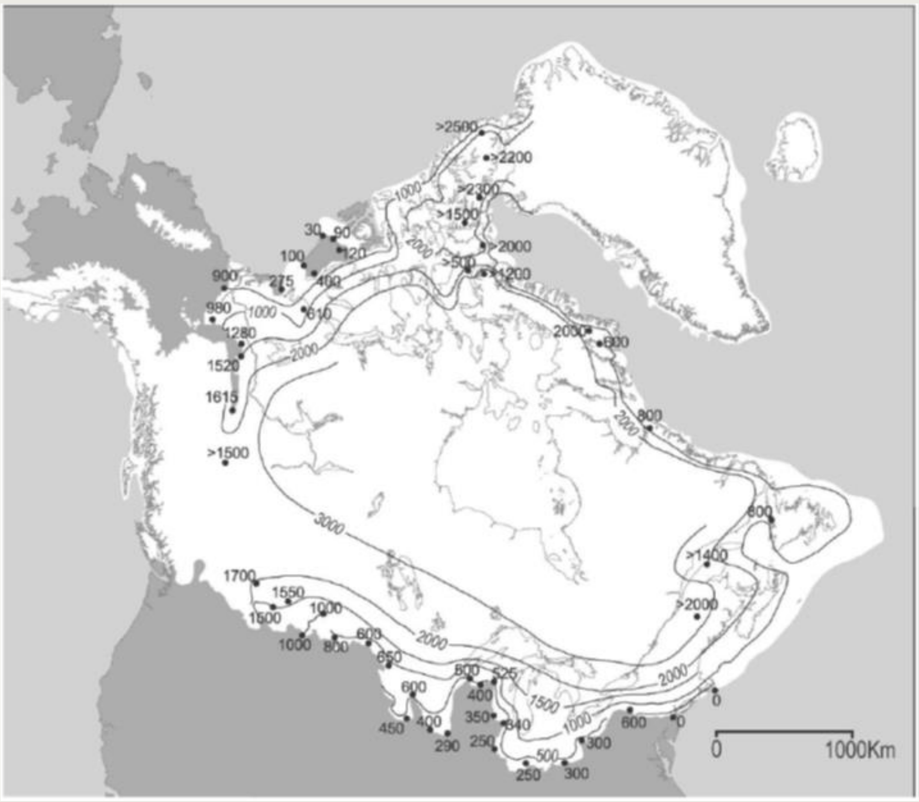

Figure 5.3: Ice surface contours based on elevations along the last glacial maximum ice margin and topographic high points overridden by ice in North America (From Dyke et al. 2002).

5.2.1. Basin modelling input

For the purpose of this study a uniform ice sheet thickness of 200 m was assumed for the Saalian glaciation. A uniform thickness of 100 m was assumed where the Elsterian ice sheet covered the study area, rapidly decreasing to 0 m for the area that was not covered by ice (Figure 5.4). The properties assigned to the ice sheet are taken from the default properties available in the basin modelling software package PetroMod (Table 5.1). The density of the ice sheet is water density.

Table 5.1: Properties assigned to the ice sheet.

	Thermal Conductivity	Heat Capacity	Mechanical Compaction	Chemical Compaction	Permeability	Seal Properties
0 oC	2.22	0.49	n/a	n/a	n/a	Perfect seal
-60 oC	2.90	0.40	n/a	n/a	n/a	

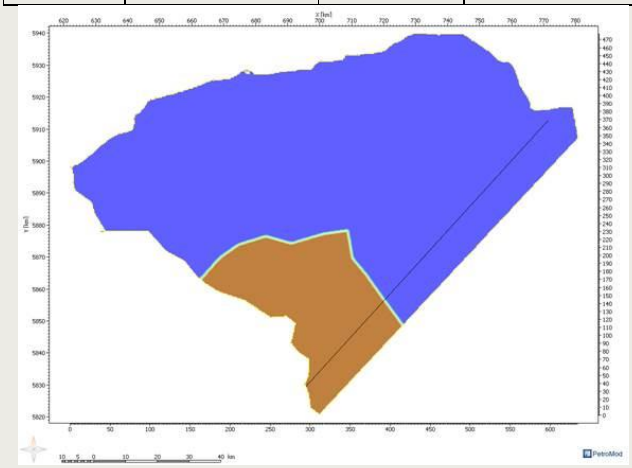

Figure 5.4: Distribution of Elsterian ice sheet in basin model: blue area is covered by Elsterian ice sheet with maximum thickness of 100 m; brown area is not covered by ice sheet.

The ice sheet loading is incorporated as a rapid loading event of increasing ice sheet thickness immediately followed by decreasing thickness. In the model the maximum height of the Elsterian ice sheet (100 m) is reached at 0.4 Ma and the maximum height of and the Saalian ice sheet (200 m) at 0.18 Ma. The accompanying change in topography is incorporated in the so-called paleo water depth boundary condition. From 1.5 Ma to Elsterian times the water depth is around 0 m and becomes negative during the periods of ice sheet coverage representing the increase in topography related to the elevation of the ice sheet.

Other input for the basin model is unchanged in comparison with the 3D basin model described in Verweij and Nelskamp (2015). The lithostratigraphic build-up of this 3D model consists of stratigraphic layers from Carboniferous age to present-day. Here focus is on the evolution of the shallower part of the subsurface during the last 1 million year of geological history. Table 5.2 shows the lithological composition of the model layers from the Rupel Clay Member to the ground surface. The lithological composition of the Breda Formation overlying the Rupel Clay Member varies laterally from 100% sand in the north-northwest to 100% clay in the southeastern part of the model.

Table 5.2: Input lithological composition of Rupel Clay Member and younger lithostratigraphic units; in the northern part of the model the input lithology of the Breda is 100% sand.

Lithostratigraphic units	New mixed lithologies
Holoceen	50% sand 50% clay
Boxtel	50% sand 50% clay
Kreftenheye	100% sand
Eem-Woudenberg	50% sand 50% clay
Kreftenheye-Zutphen	100% sand
Drente	25% sand 75% clay
Drachten	100% sand
Urk-Tynje	75% sand 25% clay
Peelo	50% sand 50% clay
Urk	75% sand 25% clay
Appelscha	100% sand
Peize-Waalre	75% sand 25% clay
Maassluis	50% sand 50% clay
Oosterhout	62,5% sand 37,5% clay
Breda	100% clay
Rupel	5% sand 86,5% clay 8,5% silt

Important general assumptions underlying the basin modelling are

- ice sheet loading and unloading is vertical
- the model is laterally constrained: no horizontal compression or extension of the basin fill is taken into account
- compaction of the subsurface is mechanical according to vertical effective stress-based rock property model (Athy's Law)
- solid rock is incompressible
- pore water is incompressible
- vertical deformation only of the basin fill/rock matrix
- density of pore water is constant
- heat flow is conductive

The side and bottom boundaries of the model are closed for ground water flow. The basin modelling includes compaction-driven groundwater flow and topography-driven groundwater flow. The model does not take the formation of glacial melt water or formation of permafrost into account.

5.2.2. Basin modelling results

Figure 5.5 shows a 1D time extraction of the basin modelling results for the northern part of the modelled area where both the Elsterian and Saalian ice sheet covered the ground surface. The periods of increase and decrease of the ice sheet thickness are indicated by the black line (topography). The present-day top of the Rupel Clay Member is at 575 m depth at the location of the 1D extraction. The red line in Figure 5.5 shows that from 1.5 Ma until the start of the Elsterian the burial depth of the Rupel Clay Member increased significantly and reached about its present-day burial depth at the start of the Elsterian glaciation. The blue line shows the impact of the rapid changes in loading during advance and retreat of the ice sheets on the changes in overpressure in the Rupel Clay Member.

At the beginning of the ice-sheet loading the model is in the state of stress and pore pressure resulting from the burial history before glaciation started. The excess pore pressure due to burial of the Rupel Clay Member at the start of the Elsterian glaciation (0.43 Ma) is 0.23 MPa. The excess pore pressure increases to a maximum of 0.55 MPa at the time of maximum thickness of the ice sheet (100 m) at 0.40 Ma. Only part of the ice sheet load is carried by the pore water at 0.40 Ma. The excess pore pressure decreases from 0.55 MPa to 0.43 MPa at the end of the ice sheet loading at 0.38 Ma. After the initial rapid decrease of excess pressure due to unloading, the rate of pressure decrease slows down. The Elsterian ice sheet did not reach the southern part of the model (Figure 5.4). Loading of the aquifers by the ice-sheet induces a lateral flow of groundwater towards the ice-free southern part of the model. The sandy Breda Formation is on top of the Rupel Clay Member and can be considered to be an aquifer in the northern part of the modelled area. Compaction-driven flow from the Rupel Clay to the dewatering Breda Formation limits the build-up of excess pressure in the Rupel Clay Member.

The advance of the Saalian ice sheet induces a rapid increase in overpressure reaching 2.08 MPa at the time of maximum ice-sheet thickness (200m) at 0.18 Ma. At this time the whole load of the Saalian ice sheet is carried by the pore water in the Rupel Clay Member. The excess pore pressure rapidly decreases in response to unloading during the retreat of the ice sheet. At the end of the glaciation (at 0.16 Ma) the excess pressure is reduced to 0.63 MPa. The unloading did not restore the pore pressures to the initial pre-glacial state. In stead the excess pore pressure slowly decreases after the end of glacial loading. The Saalian ice sheet covers the whole modelled area. The ice sheet is a perfect seal. Hence, all model boundaries (top, bottom and side boundaries) are no flow boundaries and the model can be considered to be a closed box during Saalian ice sheet loading: the groundwater in aquifers as well as in the low permeable units (clay) has no outflow possibilities and the excess pore pressures reach the maximum possible values related to ice sheet loading.

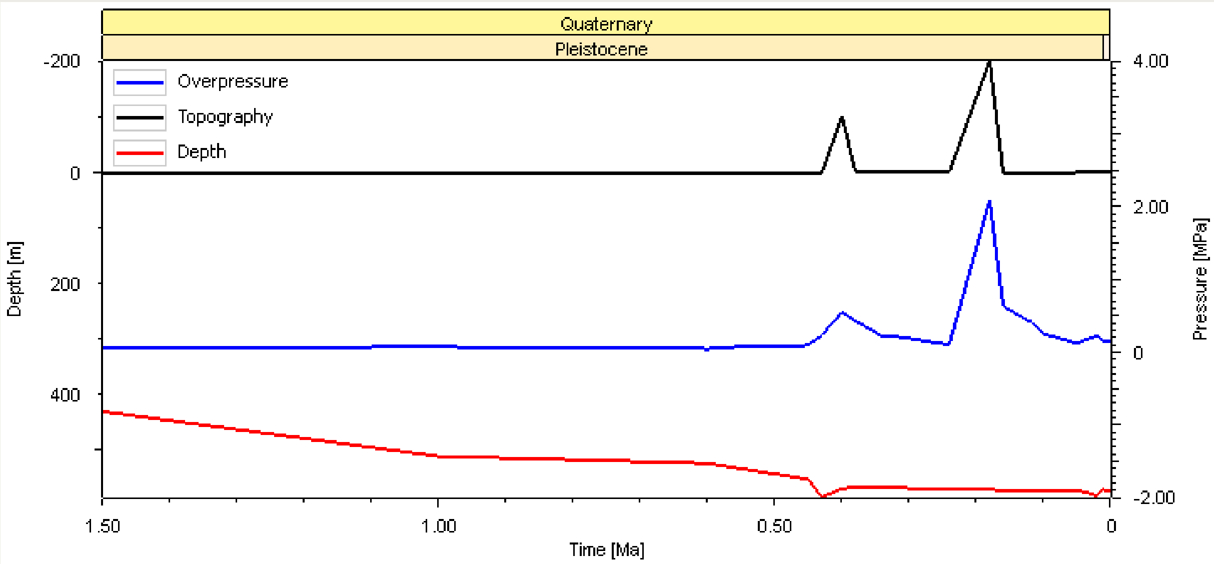

Figure 5.5: 1D extraction of the 3D basin model in northern part of the area showing: the change in surface topography related to the increase and decrease of the thickness of the Elsterian and Saalian ice sheets (black line at the top); the change in over pressure in the Rupel Clay Member at present-day depth of 575 m (blue line in the middle) related to the ice sheet loading and unloading; change in burial depth of the Rupel Clay Member (red line at the bottom).

Unlike changes in boundary pressure or water flux, changes in boundary stress (such as changes in stress induced by ice sheet loading and unloading) and their effects propagate almost instantaneously throughout the subsurface (Neuzil, 2012). The almost instantaneous increase and the initial decrease in excess pressure in the Rupel Clay Member is a direct response to the changes in stress induced by ice sheet loading and unloading.

In contrast, the slow dissipation of the excess pressures from the Rupel Clay Member after the initial almost instantaneous decrease in excess pressure is related to the slow flow of water from the Rupel Clay Member. The time required to dissipate an overpressure through a permeable unit is proportional to the square of its thickness and is inversely proportional to its hydraulic diffusivity. The decay time of excess pore pressure through a layer of thickness L (m) with uniform hydraulic properties is L^2/D_h. For example, the hydraulic diffusivity (D_h) for the Rupel Clay Member is in the order of 2.10^{-9} m^2/s, assuming a matrix compressibility of 10^{-7} (Pa^{-1}), a porosity of 0.3 and permeability of 10^{-19} m^2. For a thickness of the Rupel Clay of 100 m, the decay time is about 160 000 year; for a thickness of 50 m the decay time reduces to 40 000 year. Both permeability of the Rupel Clay and the thickness, that is the distance between the overpressuring in the Rupel Clay and an overlying or underlying aquifer with about hydrostatic pressure conditions determine the time it takes for the excess pressure to dissipate from the Rupel Clay Member by groundwater flow.

The Breda Formation on top of the Rupel Clay Member is composed of sand in the northern part of the model and of clay in the southeast. It can be expected that it will take more time for excess pressures to dissipate from the Rupel Clay Member in the southeastern part of the model because of the larger distance between the Rupel and a sandy formation. This is clearly demonstrated in Figure 5.6. The basin modelling results show that the overpressure in the Rupel Clay Member still persists until present-day.

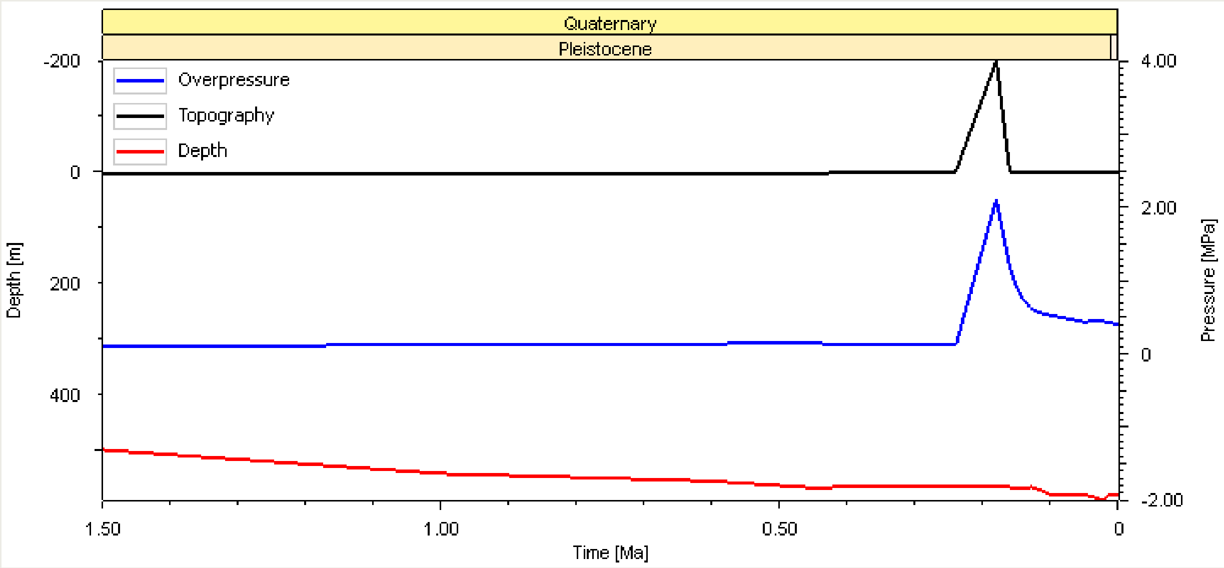

Figure 5.6: 1D extraction of the 3D basin model in southern part of the area showing: the change in surface topography related to the increase and decrease of the thickness of the Saalian ice sheet (black line at the top); the change in overpressure in the Rupel Clay Member at present-day depth of 575 m (blue line in the middle) related to the ice sheet loading and unloading; change in burial depth of the Rupel Clay Member (red line at the bottom).

Cross section (Figure 5.7) demonstrates that there is also a vertical difference in overpressure in the Rupel Clay Member below the Elsterian ice sheet: the overpressure decrease towards the top of the Rupel and overpressures are near hydrostatic in the overlying Breda and younger units. This is in contrast to the simulated situation at the maximum extent of the Saalian ice sheet: overpressure in the Rupel Clay Member and all units overlying it are overpressured. In the Saalian modelling scenario there is no escape way for the pore water: all boundaries are closed for water flow and all the stress induced by the ice sheet loading is carried by the pore water. This can be considered as an end member scenario for the development of overpressure in the Rupel Clay Member.

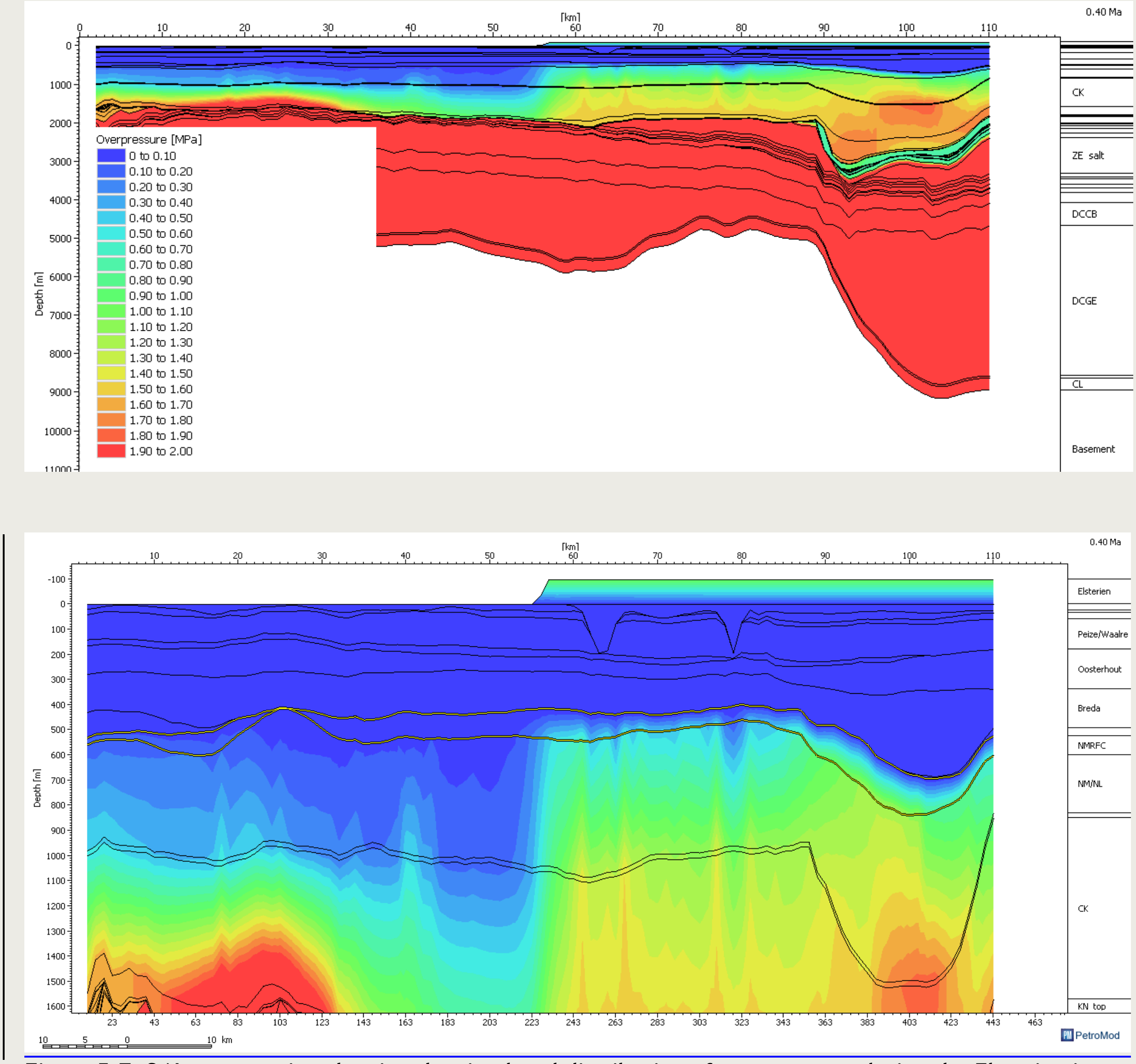

Figure 5.7: S-N cross section showing the simulated distribution of overpressure during the Elsterian ice coverage at 0.4 Ma. Figure at the top shows the overpressure distribution for the whole thickness of the basin model. The figure at the bottom clearly shows that overpressure has developed in the Rupel Clay Member below the ice sheet in the north and that pressures remain near hydrostatic in the south.

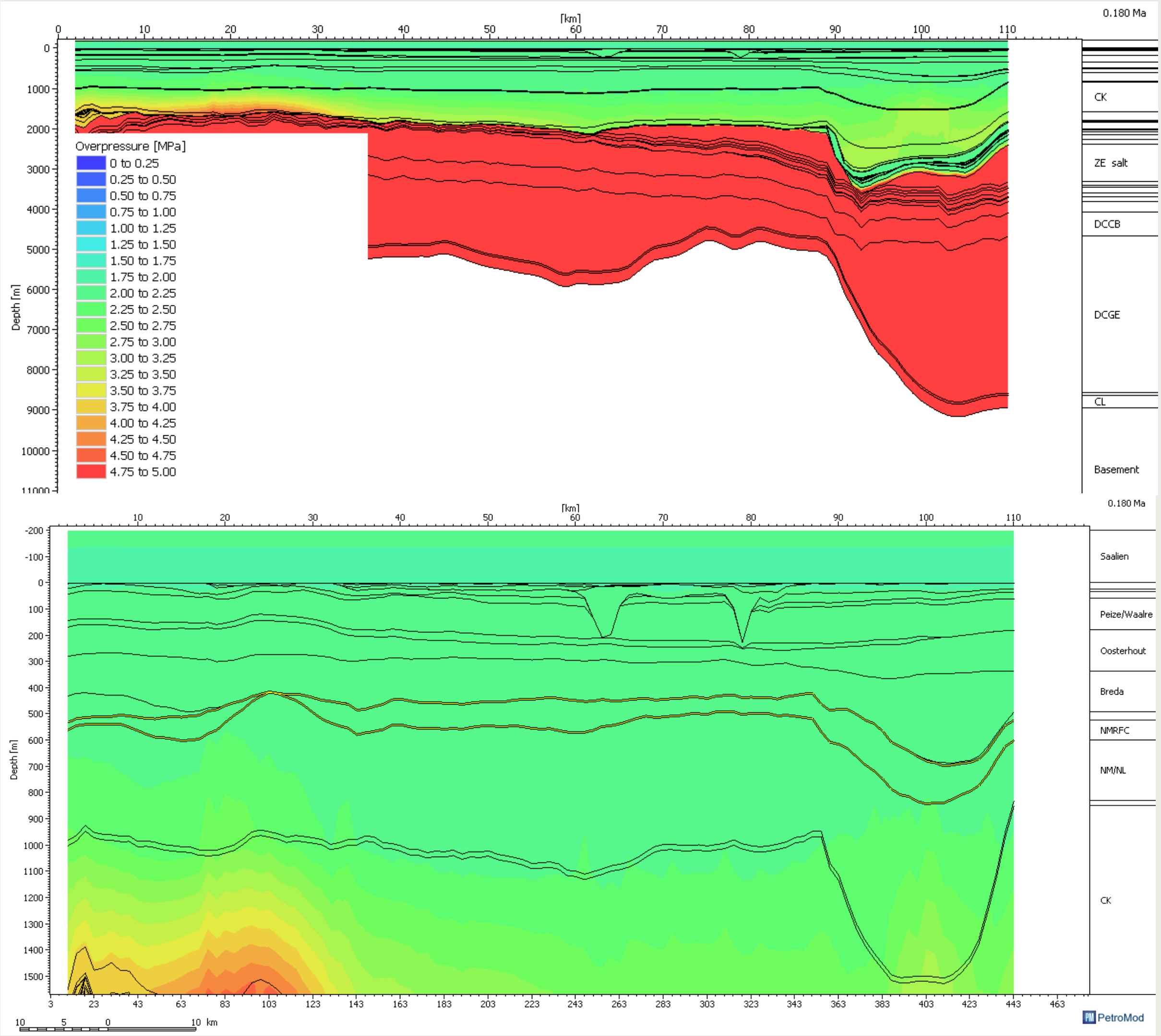

Figure 5.8: S-N cross section showing the simulated distribution of overpressure during the Saalian ice coverage at 0.18 Ma. The ice sheet - a perfect seal - covers the whole model. Figure at the top shows the overpressure distribution for the whole thickness of the basin model. The figure at the bottom clearly shows that overpressure has developed already directly below the ice sheet; in this modelling scenario there is no outflow possibility for the groundwater.

In reality, there will probably be lateral flow of water towards the front of the Saalian ice sheet to a greater or lesser extent, just as was demonstrated for the Elsterian ice sheet period. The occurrence of lateral flow through aquifers was also clearly demonstrated by Wildenborg et al. (2000). They used a hydromechanical model to simulate the effects of a potential future glaciation on Tertiary clays (including the Rupel Clay Member) along a simplified generic 2D cross-section considered to be representative of the Dutch subsurface. The initial geohydrological boundary conditions were based on a large scale groundwater model of NW Europe for glacial conditions (Van Weert and Leijnse, 1996, see Van Weert et al., 1997). Their modelling revealed that ice loading increases the pore pressures in aquifers and is accompanied by groundwater flow towards the ice margin and ahead of it. They also showed that a glaciation leads to amplified outflow of water from a clay layer to the aquifers above and below the clay. As expected such outflow increases with increase of permeability of the clay.

5.3. Conclusions

1. The 3D basin modelling results show that glacial loading may lead to maximum excess pore pressures in the Rupel Clay Member with magnitudes about equal to the stress caused by the weight of the ice sheet. This situation occurs when pore water cannot escape from the Rupel in response to the ice sheet loading.
2. The 3D basin modelling also indicates that during retreat of the ice sheet and associated glacial unloading the excess pressure in the Rupel Clay Member decreases again due to decrease in stress. However, the excess pressure has not returned to pre-glaciation values at the end of the glaciation. The remaining excess pressures will dissipate in time by outflow of groundwater from the Rupel Clay Member.

References

Anderman, E.R., Hill, M.C., 2000. *MODFLOW-2000, the U.S. Geological Survey Modular Ground-water model – documentation of the hydrogeologic-unit flow (HUF) package*. USGS Open file report 00-342, Denver, Colorado, 2000.

Beerten, K., 2011. *Permafrost in northwestern Europe during the Last Glacial*. External Report of the Belgian Nuclear Research Centre, Mol , Belgium, SCK•CEN-ER-138.

Bense V., Van Balen R., De Vries J., 2003. *The impact of faults on the hydrogeological conditions in the Roer Valley Rift System: an overview*. Netherlands Journal of Geosciences / Geologie en Mijnbouw 82 (1), 41-54.

Bense, V.F., Ferguson, G., Kooi, H., 2009. *Evolution of shallow groundwater flow systems in areas of degrading permafrost*. Geophysical Research Letters, 36.

Bintanja, R., Van de Wal, R.S.W., 2008. *North American ice-sheet dynamics and the onset of 100000 year glacial cycles*. Nature Vol.454, 869-872.

Bintanja, R., Van de Wal, R.S.W., 2011. Global 3Ma temperature, sea level, and ice volume reconstructions. IGBPpages/World Data Centre for Paleoclimatology Data Contribution series 2011-119. NOAA/NCDC Paleoclimatology Program, Boulder CO, USA.

Bonté, D., Van Wees, J.D., Verweij, H., 2012. *Subsurface temperature of the onshore Netherlands: new temperature dataset and modelling*. Netherlands Journal of Geosciences 91(4): 491-515.

Boulton G., Curle F., 1997. *Simulation of the effects of long-term climate change on groundwater flow and the safety of geological disposal sites*, Final report, contract no FI2W-CT90-0046, EUR 17793 EN, 308 p.

Busschers, F.S., Kasse, C., van Balen, R.T., Vandenberghe, J., Cohen, K.M., Weerts, H.J.T., Wallinga, J., Johns, C., Cleveringa, P., Bunnik, F.P.M., 2007. *Late Pleistocene evolution of the Rhine-Meuse system in the southern North Sea basin: imprints of climate change, sea-level oscillation and glacio-isostacy*. Quaternary Science Reviews 26, 3216-3248.

Buylaert, J. P., Ghysels, G., Murray, A. S., Thomsen, K. J., Vandenberghe, D., De Corte, F., Heyse, I., Van den haute, P., 2008. *Optical dating of relict sand wedges and composite-wedge pseudomorphs in Flanders, Belgium*. Boreas 38, 160–175.

Chen G., Sillen X., Verstricht J., Li X., 2010. *Revisiting a simple in situ heater test: the third life of ATLAS*.- Clays in Natural and Engineered Barriers for Radioactive Waste Confinement.- Nantes, France, 29 March - 1 April 2010.

COMSOL, 2014. *COMSOL Multiphysics 4.4, Earth Science Module*, COMSOL AB, Stockholm, Sweden.

Follestad, B., Fredin. O., 2011. *Geometry and vertical extent of the late Weichselian ice sheet in northwestern Oppland County, Norway*. Norges geologiske undersøkelse Bulletin, 451, 1–19.

Govaerts J., Beerten K., Ten Veen J., 2015. *Numerical simulation of Permafrost Depth in the Netherlands. SCK•CEN-R-5848, 44 p.* Appendix in OPERA-PU-TNO412.

Govaerts, J., Weetjens, E., Beerten, K., 2011. *Numerical simulation of permafrost depth at the Mol site*. External Report SCK•CEN-ER-148.

Guiot, J., Pons, A., De Beaulieu, J.L., Reille, M., 1989. *A 140,000-year continental climate reconstruction from two European pollen records*. Nature 338, 309–313.

Harbaugh, A.W., 2005. *MODFLOW-2005, the U.S. Geological Survey modular ground-water model—the Ground-Water Flow Process: U.S. Geological Survey Techniques and Methods 6-A16*. USGS.

Harbaugh, A.W., Banta, E.R., Hill, M.C., and McDonald, M.G., 2000. *MODFLOW-2000, the U.S. Geological Survey modular ground-water model -- User guide to modularization concepts and the Ground-Water Flow Process*. U.S. Geological Survey Open-File Report 00-92, 121 p.

Holmén, J., H. Benabderrahmane, A. Buoro, and J. Brulhet, 2011. *Modelling of Permafrost Freezing and Melting and the Impact of a Climatic Cycle on Groundwater Flow at the Meuse/Haute-Marne Site*. Physics and Chemistry of the Earth, Vol. 36, Nos. 17–18, pp. 1,531–1,538.

Kitover, D.T., van Balen, R.T., Roche, D.M., Vandenberghe, J., Renssen, H., 2013. *New Estimates of Permafrost Evolution during the Last 21 k Years in Eurasia using Numerical Modelling*. Periglacial Processes and Landforms 24, 286–303.

Kömle N.I., Bing H., Feng W.J., Wawrzaszek R., Hütter E.S., He Ping, Marczewski W., Dabrowski B., Schröer K., Spohn T., 2007. *Thermal conductivity measurements of road construction materials in frozen and unfrozen state*. Acta Geotechnica 2, 127–138.

Mallants, D., 2006. *Basic concepts of water flow, solute transport, and heat flow in soils and sediments, second edition*. SCK•CEN-BLG-991, 169-183.

Marivoet, J., Bonne, A., 1988. *PAGIS, disposal in clay formations*. SCK•CEN-R-2748.

Mottaghy, D., Rath, V., 2006. *Latent heat effects in subsurface heat transport modelling and their impact on palaeotemperature reconstructions*. International Journal of Geophysics 164, 236–245.

NGRIP – North Greenland Ice Core Project members, 22, 209-223.

Noetzli, J., Gruber, S., 2009. *Transient thermal effects in Alpine permafrost*. The Cryosphere 3, 85–99.

Renssen, H., Vandenberghe, J., 2003. *Investigation of the relationship between permafrost distribution in NW Europe and extensive winter sea-ice cover in the North Atlantic Ocean during the cold phases of the Last Glaciation*. Quaternary Science Reviews hydrogeological and palaeoenvironmental data set for large-scale groundwater flow model simulations in the northeastern Netherlands. Meded. Rijks Geol. Dienst 52, 105-134.

Schokking,F. 1998. *Anisotropic geotechnical properties of a glacially overconsolidated and fissured clay*. PhD thesis Delft University of Technology, 160 p.

Ten Veen J., Govaerts J., Beerten K., Ventra D., Vis G., 2015. *Future evolution of the geological and geohydrological properties of the geosphere*. OPERA-PU-TNO412, 114 p.

Ter Voorde, M., Van Balen, R., Luijendijk, E., Kooi, H., 2014. *Weichselian and Holocene climate histrory reflected in temperatures in the upper crust of the Netherlands*. Netherlands Journal of Geosciences 93 (3), 107-117.

Valstar, J., Goorden, N., 2016. *Hydrological transport in the rock formations surrounding the host rock*, OPERA-PU-DLT621, 55 p.

Van Gijssel, K., 1995. A 2004. *High-resolution record of Northern Hemisphere climate extending into the last interglacial period*. Nature 431, 147–151.

Van Weert, F.H.A., Van Gijssel, K., Leijnse, A., Boulton, G.S., 1997. The effects of Pleistocene glaciations on the geohydrological system of Northwest Europe. Journal of Hydrology 195, 137-159.

Verweij, H., Nelskamp, S., 2015. *Definition of the present day boundary conditions for the near-field model_1*. Report OPERA-PU-TNO421_1, 45 p.

Verweij, H., Nelskamp, S., Guaipo Sarmiento, M.A., 2013. *Timing and distribution of biogenic gas generation in the shallow gas play in the Dutch offshore*. Extended abstract. 75th EAGE Conference & Exhibition incorporating SPE EUROPEC 2013 London, UK, 10-13 June 2013, 4p.

Verweij, J.M., Vis, G-J., Imberechts, E., 2015. *Spatial variation in porosity and permeability of the Rupel Clay Member in the Netherlands*. Netherlands Journal of Geosciences (submitted).

Vis, G. J., Verweij, J.M., 2014, *Geological and geohydrological characterization of the Boom Clay and its overburden*. Report OPERA-PU-TNO411, 86 p.

Wildenborg, A.F.B., Orlic, B., De Lange, G., De Leeuw, C.S., Zijl, W., Van Weert, F., Veling , E.J.M., De Cock, S., Thimus, J.F., Lehnen-de Rooij, C., Den Haan, E.J., 2000. *Transport of Radionuclides disposed of in Clay of Tertiary Origin (TRACTOR)*. Netherlands Institute oif Applied geoscience TNO – National Geological Survey. TNO report NITG 00-223-B, 223 p.

OPERA

Meer informatie:

Postadres
Postbus 202
4380 AE Vlissingen

T 0113-616 666
F 0113-616 650
E info@covra.nl

www.covra.nl